8 Quenching of Fluorescence

Fluorescence quenching refers to any process that decreases the fluorescence intensity of a sample. A variety of molecular interactions can result in quenching. These include excited-state reactions, molecular rearrangements, energy transfer, ground-state complex formation, and collisional quenching. In this chapter we will be concerned primarily with quenching resulting from collisional encounters between the fluorophore and quencher, which is called collisional or dynamic quenching. We will also discuss static quenching, which can be a valuable source of information about binding between the fluorescent sample and the quencher. Static quenching can also be a complicating factor in the data analysis. In addition to the processes described above, apparent quenching can occur due to the optical properties of the sample. High optical densities or turbidity can result in decreased fluorescence intensities. This trivial type of quenching contains little molecular information. Throughout this chapter we will assume that such trivial effects are not the cause of the decreases in fluorescence intensity.

Fluorescence quenching has been widely studied both as a fundamental phenomenon, and as a source of information about biochemical systems. These biochemical applications of quenching are due to the molecular interactions that result in quenching. Both static and dynamic quenching require molecular contact between the fluorophore and quencher. In the case of collisional quenching, the quencher must diffuse to the fluorophore during the lifetime of the excited state. Upon contact, the fluorophore returns to the ground state, without emission of a photon. In general, quenching occurs without any permanent change in the molecules, that is, without a photochemical reaction. In static quenching a complex is formed between the fluorophore and the quencher, and this complex is nonfluorescent. For either static or dynamic quenching to occur the fluorophore and quencher must be in contact. The requirement of molecular contact for quenching results in the numerous applications of quenching. For example, quenching measurements can reveal the accessibility of fluorophores to quenchers. Consider a fluorophore bound either to a protein or a membrane. If the protein or membrane is impermeable to the quencher, and the fluorophore is located in the interior of the macromolecule, then neither collisional nor static quenching can occur. For this reason quenching studies can be used to reveal the localization of fluorophores in proteins and membranes, and their permeabilities to quenchers. Additionally, the rate of collisional quenching can be used to determine the diffusion coefficient of the quencher.

It is important to recognize that the phenomenon of collisional quenching results in the expansion of the volume and distance within the solution which affects the fluorophore. The root-mean-square distance $\sqrt{\overline{\Delta x^2}}$ that a quencher can diffuse during the lifetime of the excited state (τ) is given by $\sqrt{\overline{\Delta x^2}} = \sqrt{2D\tau}$, where D is the diffusion coefficient. Consider an oxygen molecule in water at 25°C. Its diffusion coefficient is 2.5 x 10^{-5} cm^2/s. During a typical fluorescence lifetime of 4 ns the oxygen molecule can diffuse 45 Å. If the lifetime is longer, diffusion over still larger distances can be observed. For example, for lifetimes of 20 and 100 ns the average distances for oxygen diffusion are 100 and 224 Å, respectively. With the use of longer-lived probes with microsecond lifetimes (Chapter 20), diffusion over still larger distances can be observed. Hence, fluorescence quenching can reveal the diffusion of quenchers over moderately large distances comparable to the size of proteins and membranes. This situation is different from solvent relaxation. Spectral shifts resulting from reorientation of the solvent molecules are due primarily to the solvent shell immediately adjacent to the fluorophore.

8.1. QUENCHERS OF FLUORESCENCE

A wide variety of substances act as quenchers of fluorescence. One of the best-known collisional quenchers is molecular oxygen,[1] which quenches almost all known fluorophores. Depending upon the sample under investigation, it is frequently necessary to remove dissolved oxygen to obtain reliable measurements of the fluorescence yields or lifetimes. The mechanism by which oxygen quenches has been a subject of debate. The most likely mechanism is that the paramagnetic oxygen causes the fluorophore to undergo intersystem crossing to the triplet state. In fluid solutions the long-lived triplets are completely quenched, so that phosphorescence is not observed. Aromatic and aliphatic amines are also efficient quenchers of most unsubstituted aromatic hydrocarbons. For example, anthracene fluorescence is effectively quenched by diethylaniline.[2] For anthracene and diethylaniline the mechanism of quenching is the formation of an excited charge-transfer complex. The excited-state fluorophore accepts an electron from the amine. In nonpolar solvents fluorescence from the excited charge-transfer complex (exciplex) is frequently observed, and one may regard this process as an excited state reaction rather than quenching. In polar solvents the exciplex emission is often quenched, so that the fluorophore–amine interaction appears to be that of simple quenching. While it is now known that there is a modest through-space component to almost all quenching reactions, this component is short range (<2 Å), so that molecular contact is a requirement for quenching.

Another type of quenching is due to heavy atoms such as iodide and bromide. Halogenated compounds such as trichloroethanol and bromobenzene also act as collisional quenchers. Quenching by the larger halogens such as bromide and iodide may be a result of intersystem crossing to an excited triplet state, promoted by spin–orbit coupling of the excited (singlet) fluorophore and the halogen.[3] Since emission from the triplet state is slow, the triplet emission is highly quenched by other processes. The quenching mechanism is probably different for chlorine-containing substances. Indole, carbazole, and their derivatives are uniquely sensitive to quenching by chlorinated hydrocarbons and by electron scavengers[4] such as protons, histidine, cysteine, NO_3^-, fumarate, Cu^{2+}, Pb^{2+}, Cd^{2+}, and Mn^{2+}. Quenching by these substances probably involves a donation of an electron from the fluorophore to the quencher. Additionally, indole, tryptophan, and its derivatives are quenched by acrylamide, succinimide, dichloroacetamide, dimethylformamide, pyridinium hydrochloride, imidazolium hydrochloride, methionine, Eu^{3+}, Ag^+, and Cs^+. Quenchers of protein fluorescence have been summarized in several insightful reviews.[5–7] Hence a variety of quenchers are available for studies of protein fluorescence, especially to determine the surface accessibility of tryptophan residues and the permeation of proteins by the quenchers.

Additional quenchers include purines, pyrimidines, N-methylnicotinamide and N-alkyl pyridinium, and picolinium salts.[8–9] For example, the fluorescence of flavin adenine dinucleotide (FAD) and reduced nicotinamide adenine dinucleotide (NADH) are both quenched by the adenine moiety. Flavin fluorescence is quenched by both static and dynamic interactions with adenine,[10] whereas the quenching of dihydronicotinamide appears to be primarily dynamic.[11] These aromatic substances appear to quench by formation of charge-transfer complexes. Depending upon the precise structure involved, the ground-state complex can be reasonably stable. As a result, both static and dynamic quenching are frequently observed. A variety of other quenchers are known. These are summarized in Table 8.1, which is intended to be an overview and not a complete list. Known collisional quenchers include hydrogen peroxide, nitric oxide (NO), nitroxides, BrO_4^-, and even some olefins.

Because of the variety of substances that act as quenchers, one can frequently identify fluorophore–quencher combinations for a desired purpose. It is important to note that not all fluorophores are quenched by all the substances listed above. This fact occasionally allows selective quenching of a given fluorophore. The occurrence of quenching depends upon the mechanism, which in turn depends upon the chemical properties of the individual molecules. Detailed analysis of the mechanism of quenching is complex. In this chapter we will be concerned primarily with the type of quenching, that is, whether quenching depends on diffusive collisions or formation of ground-state complexes. Later in this chapter we describe biochemical applications of quenching. The mechanisms of quenching will be discussed in the following chapter.

8.2. THEORY OF COLLISIONAL QUENCHING

Collisional quenching of fluorescence is described by the Stern-Volmer equation:

$$\frac{F_0}{F} = 1 + k_q\tau_0[Q] = 1 + K_D[Q] \qquad (8.1)$$

Table 8.1. Quenchers of Fluorescence

Quenchers	Typical fluorophore	References
Acrylamide	Tryptophan, pyrene, and other fluorophores	5–7, 176–180
Amines	Anthracene, perylene	2, 124, 181–186
Amines	Carbazole	187
Amine anesthetics	Perylene, anthroyloxy probes	188–190
Bromate	–	191
Bromobenzene	Many fluorophores	192
Carbon disulfide	Laser dyes, perylene	193
Carboxy groups	Indole	194
Cesium (Cs^+)	Indole	195
Chlorinated compounds	Indoles and carbazoles	196–199
Chloride	Quinolinium, SPQ	200–203
Cobalt (Co^{2+})	NBD, PPO, Perylene (Energy transfer for some probes)	204–210
Dimethylformamide	Indole	211
Disulfides	Tyrosine	212
Ethers	9-Arylxanthyl cations	213
Halogens	Anthracene, naphthalene, carbazole	214–229
Halogen anesthetics	Pyrene, tryptophan	230–232
Hydrogen peroxide	Tryptophan	233
Iodide	Anthracene	234–237
Imidazole, histidine	Tryptophan	238
Indole	Anthracene, pyrene, cyanoanthracene	239–241
Methylmercuric chloride	Carbazole, pyrene	242
Nickel (Ni^{2+})	Perylene	243–244
Nitromethane and nitro compounds	Polycyclic aromatic hydrocarbon	245–256
Nitroxides	Naphthalene, PAH, Tb^{3+}, anthroyloxy probes	257–266
NO (nitric oxide)	Naphthalene, pyrene	267–270
Olefins	Cyanonaphthalene, 2,3-dimethylnaphthalene, pyrene	271–273
Oxygen	Most fluorophores	274–290
Peroxides	Dimethylnaphthalene	291
Picolinium nicotinamide	Tryptophan, PAH	292–296
Pyridine	Carbazole	297
Silver (Ag^+)	Perylene	298
Succinimide	Tryptophan	299–300
Sulfur dioxide	Rhodamine B	301
Thallium (Tl^+)	Naphthylamine sulfonic acid	302
Thiocyanate	Anthracene, 5,6-benzoquinoline	303–304
Xenon		305

In this equation F_0 and F are the fluorescence intensities in the absence and presence of quencher, respectively; k_q is the bimolecular quenching constant; τ_0 is the lifetime of the fluorophore in the absence of quencher, and Q is the concentration of quencher. The Stern-Volmer quenching constant is given by $K_D = k_q\tau_0$. If the quenching is known to be dynamic, the Stern-Volmer constant will be represented by K_D. Otherwise this constant will be described as K_{SV}.

Quenching data are usually presented as plots of F_0/F versus $[Q]$. This is because F_0/F is expected to be linearly dependent upon the concentration of quencher. A plot of F_0/F versus $[Q]$ yields an intercept of one on the y-axis and a slope equal to K_D (Figure 8.1). Intuitively, it is useful to note that K_D^{-1} is the quencher concentration at which $F_0/F = 2$ or 50% of the intensity is quenched. A linear Stern-Volmer plot is generally indicative of a single class of fluorophores, all equally accessible to quencher. If two fluorophore populations are present, and one class is not accessible to quencher, then the Stern-Volmer plots deviate from linearity toward the x-axis. This result is frequently found

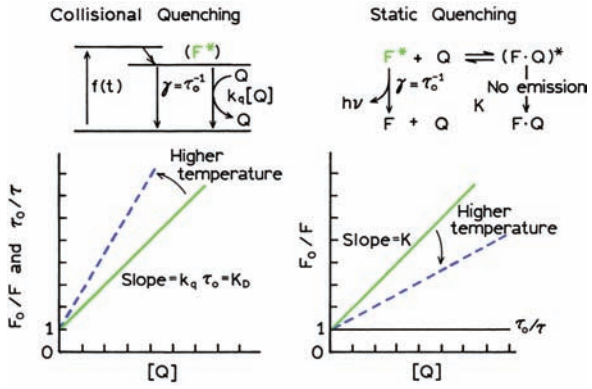

Figure 8.1. Comparison of dynamic and static quenching.

for the quenching of tryptophan fluorescence in proteins by polar or charged quenchers. These molecules do not readily penetrate the hydrophobic interior of proteins, and only those tryptophan residues on the surface of the protein are quenched.

It is important to recognize that observation of a linear Stern-Volmer plot does not prove that collisional quenching of fluorescence has occurred. In Section 8.3 we will see that static quenching also results in linear Stern-Volmer plots. Static and dynamic quenching can be distinguished by their differing dependence on temperature and viscosity, or preferably by lifetime measurements. Higher temperatures result in faster diffusion and hence larger amounts of collisional quenching (Figure 8.1). Higher temperature will typically result in the dissociation of weakly bound complexes, and hence smaller amounts of static quenching.

8.2.1. Derivation of the Stern-Volmer Equation

The Stern-Volmer equation can be derived by consideration of the fluorescence intensities observed in the absence and presence of quencher. The fluorescence intensity observed for a fluorophore is proportional to its concentration in the excited state, [*F**]. Under continuous illumination a constant population of excited fluorophores is established, and therefore $d[F^*]/dt = 0$. In the absence and presence of quencher the differential equations describing [F*] are

$$\frac{d[F^*]}{dt} = f(t) - \gamma[F^*]_0 = 0 \tag{8.2}$$

$$\frac{d[F^*]}{dt} = f(t) - (\gamma + k_q[Q])[F^*] = 0 \tag{8.3}$$

where $f(t)$ is the constant excitation function, and $\tilde{a} = \tau_0^{-1}$ is the decay rate of the fluorophore in the absence of quencher. In the absence of quenching the excited-state population decays with a rate $\tilde{a} = (\Gamma + k_{nr})$, where Γ is the radiative rate and k_{nr} is the non-radiative decay rate. In the presence of quencher there is an additional decay rate $k_q[Q]$. With continuous excitation the excited-state population is constant, so the derivatives in these equations can be set to zero. Division of eq. 8.3 by 8.2 yields

$$\frac{F_0}{F} = \frac{\gamma + k_q[Q]}{\gamma} = 1 + k_q\tau_0[Q] \tag{8.4}$$

which is the Stern-Volmer equation.

The Stern-Volmer equation may also be obtained by considering the fraction of excited fluorophores, relative to the total, which decay by emission. This fraction (F/F_0) is given by the ratio of the decay rate in the absence of quencher (γ) to the total decay rate in the presence of quencher ($\gamma + k_q[Q]$):

$$\frac{F}{F_0} = \frac{\gamma}{\gamma + k_q[Q]} = \frac{1}{1 + K_D[Q]} \tag{8.5}$$

which is again the Stern-Volmer equation. Since collisional quenching is a rate process that depopulates the excited state, the lifetimes in the absence (τ_0) and presence (τ) of quencher are given by

$$\tau_0 = \gamma^{-1} \tag{8.6}$$

$$\tau = (\gamma + k_q[Q])^{-1} \tag{8.7}$$

and therefore

$$\frac{\tau_0}{\tau} = 1 + k_q\tau_0[Q] \tag{8.8}$$

This equation illustrates an important characteristic of collisional quenching, which is an equivalent decrease in fluorescence intensity and lifetime (Figure 8.1, left). For collisional quenching

$$\frac{F_0}{F} = \frac{\tau_0}{\tau} \tag{8.9}$$

The decrease in lifetime occurs because quenching is an additional rate process that depopulates the excited state.

The decrease in yield occurs because quenching depopulates the excited state without fluorescence emission. Static quenching does not decrease the lifetime because only the fluorescent molecules are observed, and the uncomplex fluorophores have the unquenched lifetime τ_0.

8.2.2. Interpretation of the Bimolecular Quenching Constant

In papers on quenching one frequently encounters the bimolecular quenching constant (k_q), which reflects the efficiency of quenching or the accessibility of the fluorophores to the quencher. As shown below, diffusion-controlled quenching typically results in values of k_q near 1 x 10^{10} M^{-1} s^{-1}. Values of k_q smaller than the diffusion-controlled value can result from steric shielding of the fluorophore or a low quenching efficiency. Apparent values of k_q larger than the diffusion-controlled limit usually indicate some type of binding interaction.

The meaning of the bimolecular quenching constant can be understood in terms of the collisional frequency between freely diffusing molecules. The collisional frequency (Z) of a fluorophore with a quencher is given by

$$Z = k_0[Q] \tag{8.10}$$

where k_0 is the diffusion-controlled bimolecular rate constant. This constant may be calculated using the Smoluchowski equation:

$$k_0 = 4\pi RDN/1000 = \frac{4\pi N}{1000}(R_f + R_q)(D_f + D_q) \tag{8.11}$$

where R is the collision radius, D is the sum of the diffusion coefficients of the fluorophore (D_f) and quencher (D_q), and N is Avogadro's number. The collision radius is generally assumed to be the sum of the molecular radii of the fluorophore (R_f) and quencher (R_q). This equation describes the diffusive flux of a molecule with a diffusion coefficient D through the surface of a sphere of radius R. The factor of 1000 is necessary to keep the units correct when the concentration is expressed in terms of molarity. The term N/1000 converts molarity to molecules/cm^3.

The collisional frequency is related to the bimolecular quenching constant by the quenching efficiency f_Q:

$$k_q = f_Q k_0 \tag{8.12}$$

For example, if $f_Q = 0.5$ then 50% of the collisional encounters are effective in quenching and k_q will be half the diffusion-controlled value k_0. Since k_0 can be estimated with moderate precision, the observed value of k_q can be used to judge the efficiency of quenching. Quenchers like oxygen, acrylamide, and I^- generally have efficiencies near unity, but the quenching efficiency of weak quenchers like succinimide depends on the solvent and/or viscosity. The efficiency is generally less with the lighter halogens. The quenching efficiency depends upon the reduction potentials of the fluorophore and amine quencher, as expected for a charge-transfer reaction (Chapter 9).

The efficiency of quenching can be calculated from the observed value of k_q, if the diffusion coefficients and molecular radii are known. The radii can be obtained from molecular models, or from the molecular weights and densities of the quencher in question. Diffusion coefficients may be obtained from the Stokes-Einstein equation:

$$D = kT/6\pi\eta R \tag{8.13}$$

where k is Boltzmann's constant, η is the solvent viscosity, and R is the molecular radius. Frequently, the Stokes-Einstein equation underestimates the diffusion coefficients of small molecules. For example, quenching efficiencies of 2–3 were calculated for oxygen quenching of fluorophores dissolved in various alcohols.[12] These impossibly large efficiencies were obtained because the diffusion coefficient of oxygen in organic solvents is several fold larger than predicted by eq. 8.13. This equation describes the diffusion of molecules that are larger than the solvent molecules, which is not the case for oxygen in ethanol. As an alternative method, diffusion coefficients can be obtained from nomograms based upon the physical properties of the system.[13] Once the diffusion coefficients are known, the bimolecular quenching constant for $f_Q = 1$ can be predicted using Smoluchowski eq. 8.11.

It is instructive to consider typical values for k_q and the concentrations of quencher required for significant quenching. For example, consider the quenching of tryptophan by oxygen.[14] At 25°C the diffusion coefficient of oxygen in water is 2.5 x 10^{-5} cm^2/s and that of tryptophan is 0.66 x 10^{-5} cm^2/s. Assuming a collision radius of 5 Å, substitution into eq. 8.11 yields k_0 = 1.2 x 10^{10} M^{-1} s^{-1}. The observed value of the oxygen Stern-Volmer quenching constant was 32.5 M^{-1}. The unquenched lifetime of tryptophan is 2.7 ns, so that k_q = 1.2 x 10^{10} M^{-1} s^{-1}, which is in excellent agreement with the predicted value. This indicates that essential-

ly every collision of oxygen with tryptophan is effective in quenching, that is $f_Q = 1.0$. A bimolecular quenching constant near 1 x 10^{10} M^{-1} s^{-1} may be considered as the largest possible value in aqueous solution. Many quenchers are larger than oxygen. Smaller diffusion-limited quenching constants are expected because the larger molecules have smaller diffusion coefficients. For example, the acrylamide quenching efficiency of tryptophan fluorescence is also near unity,[15] but k_q = 5.9 x 10^9 M^{-1} s^{-1}. This somewhat smaller value of k_q is a result of the smaller diffusion coefficient of acrylamide relative to oxygen. Frequently data are obtained for fluorophores that are bound to macromolecules. In this case the fluorophore is not diffusing as rapidly. Also, the quenchers can probably only approach the fluorophores from a particular direction. In such cases the maximum bimolecular quenching constant is expected to be about 50% of the diffusion-controlled value.[16]

8.3. THEORY OF STATIC QUENCHING

In the previous section we described quenching that resulted from diffusive encounters between the fluorophore and quencher during the lifetime of the excited state. This is a time-dependent process. Quenching can also occur as a result of the formation of a nonfluorescent ground-state complex between the fluorophore and quencher. When this complex absorbs light it immediately returns to the ground state without emission of a photon (Figure 8.1).

For static quenching the dependence of the fluorescence intensity upon quencher concentration is easily derived by consideration of the association constant for complex formation. This constant is given by

$$K_S = \frac{[F - Q]}{[F][Q]} \tag{8.14}$$

where $[F - Q]$ is the concentration of the complex, $[F]$ is the concentration of uncomplexed fluorophore, and $[Q]$ is the concentration of quencher. If the complexed species is nonfluorescent then the fluorescence that remains (F/F_0) is given by the fraction of the total fluorophores that are not complexed: $f = F/F_0$. Recalling that the total concentration of fluorophore $[F]_0$ is given by

$$[F]_0 = [F] + [F - Q] \tag{8.15}$$

substitution into eq. 8.14 yields

$$K_S = \frac{[F]_0 - [F]}{[F][Q]} = \frac{[F_0]}{[F][Q]} - \frac{1}{[Q]} \tag{8.16}$$

We can substitute the fluorophore concentration for fluorescence intensities, and rearrangement of eq. 8.16 yields

$$\frac{F_0}{F} = 1 + K_S[Q] \tag{8.17}$$

Note that the dependence of F_0/F on $[Q]$ is linear, which is identical to that observed for dynamic quenching, except that the quenching constant is now the association constant. Unless additional information is provided, fluorescence quenching data obtained by intensity measurements alone can be explained by either dynamic or static processes. As will be shown below, the magnitude of K_S can sometimes be used to demonstrate that dynamic quenching cannot account for the decrease in intensity. The measurement of fluorescence lifetimes is the most definitive method to distinguish static and dynamic quenching. Static quenching removes a fraction of the fluorophores from observation. The complexed fluorophores are nonfluorescent, and the only observed fluorescence is from the uncomplexed fluorophores. The uncomplexed fraction is unperturbed, and hence the lifetime is τ_0. Therefore, for static quenching $\tau_0/\tau = 1$ (Figure 8.1, right). In contrast, for dynamic quenching $F_0/F = \tau_0/\tau$.

One additional method to distinguish static and dynamic quenching is by careful examination of the absorption spectra of the fluorophore. Collisional quenching only affects the excited states of the fluorophores, and thus no changes in the absorption spectra are expected. In contrast, ground-state complex formation will frequently result in perturbation of the absorption spectrum of the fluorophore. In fact, a more complete form of eq. 8.17 would include the possibility of different extinction coefficients for the free and complexed forms of the fluorophore.

8.4. COMBINED DYNAMIC AND STATIC QUENCHING

In many instances the fluorophore can be quenched both by collisions and by complex formation with the same quencher. The characteristic feature of the Stern-Volmer

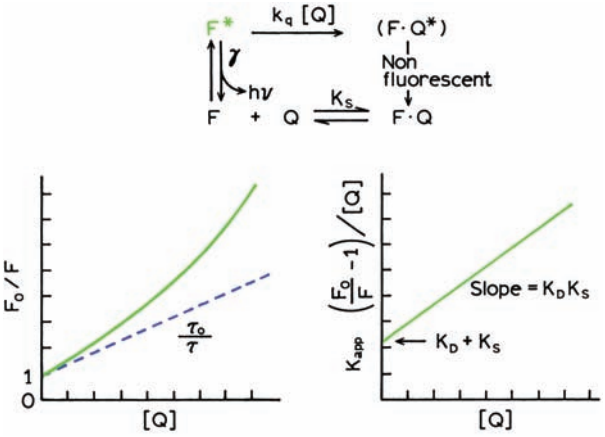

Figure 8.2. Dynamic and static quenching of the same population of fluorophores.

plots in such circumstances is an upward curvature, concave towards the *y*-axis (Figure 8.2). Then the fractional fluorescence remaining (F/F_0) is given by the product of the fraction not complexed (f) and the fraction not quenched by collisional encounters. Hence

$$\frac{F}{F_0} = f\frac{\gamma}{\gamma + k_q[Q]} \tag{8.18}$$

In the previous section we found that $f^{-1} = 1 + K_S[Q]$. Inversion of eq. 8.18 and rearrangement of the last term on the right yields

$$\frac{F_0}{F} = (1 + K_D[Q])(1 + K_S[Q]) \tag{8.19}$$

This modified form of the Stern-Volmer equation is second order in $[Q]$, which accounts for the upward curvature observed when both static and dynamic quenching occur for the same fluorophore.

The dynamic portion of the observed quenching can be determined by lifetime measurements. That is, $\tau_0/\tau = 1 + K_D[Q]$—the dashed line in Figure 8.2. If lifetime measurements are not available, then eq. 8.19 can be modified to allow a graphical separation of K_S and K_D. Multiplication of the terms in parentheses yields

$$\frac{F_0}{F} = 1 + (K_D + K_S)[Q] + K_D K_S[Q]^2 \tag{8.20}$$

$$\frac{F_0}{F} = 1 + K_{app}[Q] \tag{8.21}$$

where

$$K_{app} = \left[\frac{F_0}{F} - 1\right]\frac{1}{[Q]} = (K_D + K_S) + K_D K_S[Q] \tag{8.22}$$

The apparent quenching constant is calculated at each quencher concentration. A plot of K_{app} versus $[Q]$ yields a straight line with an intercept of $K_D + K_S$ and a slope of $K_S K_D$ (Figure 8.2). The individual values can be obtained from the two solutions of the quadratic equation (see eq. 8.23 below). The dynamic component can generally be selected to be the solution comparable in magnitude to the expected diffusion-controlled value, by the temperature or viscosity dependence of the values, or from other available information about the sample.

8.5. EXAMPLES OF STATIC AND DYNAMIC QUENCHING

Before proceeding with additional theories and examples of quenching it seems valuable to present some examples which illustrate both static and dynamic quenching. Data for oxygen quenching of tryptophan are shown in Figure 8.3.[14] The Stern-Volmer plot is linear, which indicates that only one type of quenching occurs. The proportional decrease in the fluorescence lifetime and yields proves that the observed quenching is due to a diffusive process. From the

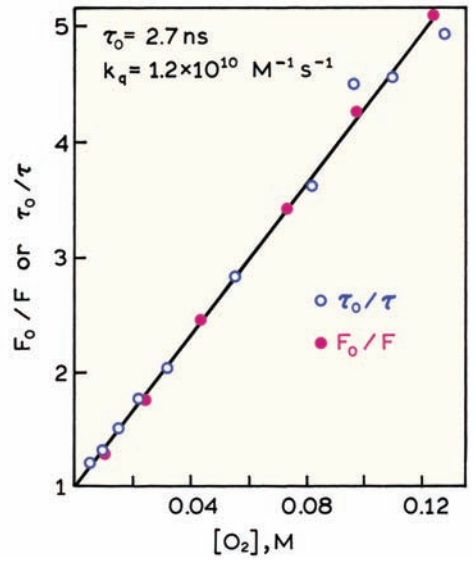

Figure 8.3. Oxygen quenching of tryptophan as observed by fluorescence lifetimes and yields. Revised and reprinted with permission from [14]. Copyright © 1973, American Chemical Society.

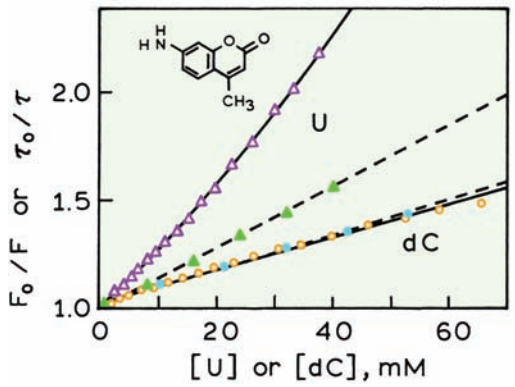

Figure 8.4. Quenching of coumarin C-120 by the nucleotides uridine (F_0/F, open triangle; τ_0/τ, solid triangle) or deoxycytosine (F_0/F, ○; τ_0/τ, ●). The sample was excited at the isoelectric point at 360 nm. Revised and reprinted with permission from [19]. Copyright © 1996, American Chemical Society.

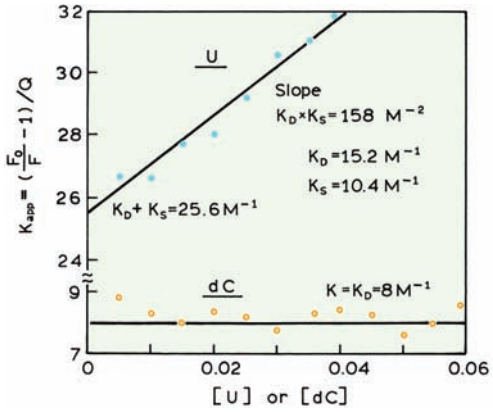

Figure 8.5. Separation of the dynamic and static quenching constants for quenching of C-120 by U or dC. Data from [19].

slope of the Stern-Volmer plot one can calculate that K_D = 32.5 M^{-1}, or that 50% of the fluorescence is quenched at an oxygen concentration of 0.031 M. The value of K_D and the fluorescence lifetime are adequate to calculate the bimolecular quenching constant, $k_q = 1.2 \times 10^{10}\ M^{-1}\ s^{-1}$. This is the value expected for the diffusion-controlled bimolecular rate constant between oxygen and tryptophan (eq. 8.11), which indicates efficient quenching by molecular oxygen.

Static quenching is often observed if the fluorophore and quencher can have a stacking interaction. Such interactions often occur between purine and pyrimidine nucleotides and a number of fluorophores.[17–19] One example is quenching of the coumarin derivative C-120 by the nucleotides uridine (U) and deoxycytosine (dC). The intensity Stern-Volmer plot for quenching by U (open triangles) shows clear upward curvature (Figure 8.4). The lifetime Stern-Volmer plot (solid triangles) is linear and shows less quenching than the intensity data. The larger amount of quenching seen from the intensity as compared to the lifetime indicates that C-120 is being decreased by both complex formation with uridine as well as collisional quenching by uridine. Contrasting data were obtained for quenching of C-120 by cytosine (dC). In this case the Stern-Volmer plots are linear for both intensities and lifetimes, and $F_0/F = \tau_0/\tau$. Hence quenching of C-120 by dC is purely dynamic.

For quenching of C-120 by uridine, the static and dynamic quenching constants can be determined by a plot of K_{app} versus [nucleotide] (see Figure 8.5). The slope (S) and intercept (I) were found to be 158 M^{-2} and 25.6 M^{-1}, respectively. Recalling $I = K_D + K_S$ and $S = K_D K_S$, rearrangements yields

$$K_S^2 - K_S I + S = 0 \tag{8.23}$$

The solutions for this quadratic equation are K_S = 15.2 or 10.4 M^{-1}. From the lifetime data we know K_D is near 13.5 M^{-1}. The lower value of 10.4 M^{-1} was assigned as the static quenching constant. At a uridine concentration of 96 mM, 50% of the ground-state C-120 is complexed and thus nonfluorescent.

It is interesting to mention why the interactions of nucleotides and C-120 were studied. The goal was to develop a method for DNA sequencing using a single electrophoretic lane for all four nucleotides.[19] This would be possible if coumarin derivatives could be identified that display different lifetimes when adjacent to each nucleotide. In this case the DNA sequence would be determined from the lifetimes observed for each band on the sequencing gel. For this fluorophore–quencher pair the quenching mechanism is a charge-transfer interaction. This mechanism is well understood, which could facilitate a rational approach to selection of the fluorophore for lifetime-based sequencing. The use of lifetime measurements in fluorescence sensing is Chapter 19 and DNA sequencing is described in Chapter 21.

8.6. DEVIATIONS FROM THE STERN-VOLMER EQUATION: QUENCHING SPHERE OF ACTION

Positive deviations from the Stern-Volmer equation are frequently observed when the extent of quenching is large. Two examples of upward-curving Stern-Volmer plots are shown for acrylamide quenching of NATA (Figure 8.6) and of the fluorescent steroid dihydroequilenin (DHE) (Figure

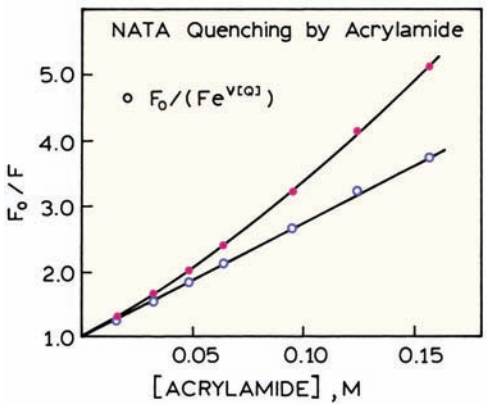

Figure 8.6. Acrylamide quenching of NATA in water (●). The open circles show the values of $F_0/(F\ e^{V[Q]})$ where V = 2.0 M^{-1}. Revised from [20].

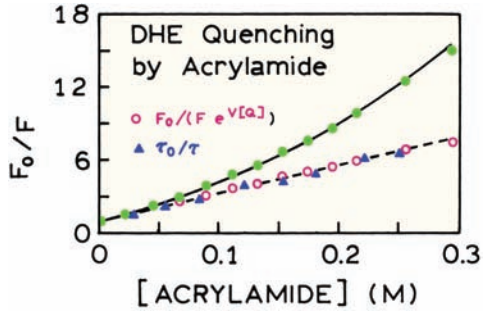

Figure 8.7. Acrylamide quenching of dihydroequilenin (DHE) in buffer containing 10% sucrose at 11°C. The value of V was 2.4 M^{-1}. Revised and reprinted with permission from [21]. Copyright © 1990, American Chemical Society.

8.7). The upward-curving Stern-Volmer plots could be analyzed in terms of the static and dynamic quenching constants (eq. 8.19). This analysis yields K_S values near 2.8 and 5.2 M^{-1} for acrylamide quenching of NATA and DHE, respectively. These values imply that quencher concentrations near 0.3 M are required to quench half of the fluorophores by a static process. Such a weak association suggests that the fluorophores and quenchers do not actually form a ground-state complex. Instead it seems that the apparent static component is due to the quencher being adjacent to the fluorophore at the moment of excitation. These closely spaced fluorophore–quencher pairs are immediately quenched, and thus appear to be dark complexes.

This type of apparent static quenching is usually interpreted in terms of a "sphere of action" within which the probability of quenching is unity. The modified form of the Stern-Volmer equation that describes this situation is

$$\frac{F_0}{F} = (1 + K_D[Q])\ \exp([Q]VN/1000) \qquad (8.24)$$

where V is the volume of the sphere.[22] The data in Figures 8.6 and 8.7 are consistent with a sphere radius near 10 Å, which is only slightly larger than the sum of the radii of the fluorophore and quencher. When the fluorophore and quencher are this close, there exists a high probability that quenching will occur before these molecules diffuse apart. As the quencher concentration increases, the probability increases that a quencher is within the first solvent shell of the fluorophore at the moment of excitation.

8.6.1. Derivation of the Quenching Sphere of Action

Assume the existence of a sphere of volume V within which the probability of immediate quenching is unity. Intuitively, if a fluorophore is excited when a quencher is immediately adjacent, then this fluorophore is quenched and is therefore unobservable. The only observable fluorophores are those for which there are no adjacent quenchers. The modified form of Stern-Volmer eq. 8.24 is derived by calculating the fraction of fluorophores that does not contain a quencher within its surrounding sphere of action.[22]

The probability of finding a number (n) of quenchers molecules in a given volume can be calculated from the Poisson distribution:

$$P(n) = \frac{\lambda^n}{n!}e^{-\lambda} \qquad (8.25)$$

where λ is the mean number of quenchers per volume V. The average concentration in molecules/cm^3 is given by $[Q]$N/1000, so the average number of molecules in the sphere is $\lambda = V[Q]N/1000$. Only those fluorophores without nearby quenchers are fluorescent. The probability that no quenchers are nearby is

$$P(0) = e^{-\lambda} \qquad (8.26)$$

Thus, the existence of the sphere of action reduces the proportion of observable fluorophores by the factor $\exp(-V[Q]N/1000)$, which in turn yields eq. 8.24. Division

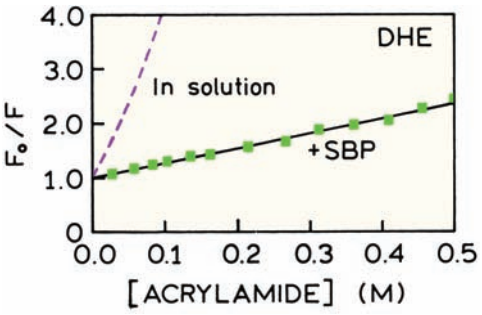

Figure 8.8. Acrylamide quenching of DHE when free in solution (dashed). and when bound to steroid-binding protein (SBP, – ■ –). Revised and reprinted with permission from [21]. Copyright © 1990, American Chemical Society.

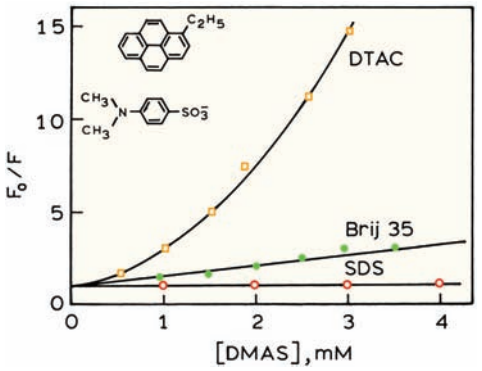

Figure 8.9. Quenching of 1-ethylpyrene (EP) by dimethyaniline sulfonate (DMAS) in positively charged micelles of dodecyltrimethylammonium chloride (DTAC), neutral micelles of Brij 35, or negatively charged micelles of sodium dodecylsulfate (SDS). Revised from [27].

of the values of F_0/F by exp(V[Q]N/1000) corrects the steady-state intensities for this effect and reveals the dynamic portion of the observed quenching (Figures 8.6 and 8.7). For simplicity, the static term is often expressed in terms of reciprocal concentration.

8.7. EFFECTS OF STERIC SHIELDING AND CHARGE ON QUENCHING

The extent of quenching can be affected by the environment surrounding the fluorophore. One example is the quenching of the steroid dihydroequilenin (DHE) by acrylamide. When free in solution, DHE is readily quenched by acrylamide. However, when bound to a steroid-binding protein (SBP) much less quenching occurs (Figure 8.8). In fact, the modest amount of quenching was attributed to dissociation of DHE from the protein.[21] Protection against quenching is frequently observed for probes bound to macromolecules,[23–24] and even cyclodextrins.[25] In fact, binding of probes to cyclodextrin has been used as a means to obtain room temperature phosphorescence.[26] The macromolecules or cyclodextrins provide protection from the solvent, but usually not complete protection from diffusing quenchers. Such solutions are usually purged to remove dissolved oxygen in order to observe phosphorescence.

The electronic charge on the quenchers can have a dramatic effect on the extent of quenching (Figure 8.9). This is illustrated by quenching of 1-ethylpyrene (EP) in micelles, where the detergent molecules have different charges.[27] The quencher was p-N,N-dimethylaniline sulfonate (DMAS) which is negatively charged. The micelles were positively charged (DTAC), neutral (Brij35), or negatively charged (SDS). There is extensive quenching of EP in the positively charged DTAC micelles, and essentially no quenching in the negatively charged SDS micelles. In general, one can expect charge effects to be present with charged quenchers such as iodide, and to be absent for neutral quenching like oxygen and acrylamide.

8.7.1. Accessibility of DNA-Bound Probes to Quenchers

The most dramatic effects of charge and shielding on quenching have been observed for fluorophores bound to DNA. The extent of quenching is decreased by intercalation of probes into the DNA double helix. For instance, ethidium bromide (EB) bound to DNA was found to be protected from oxygen quenching by a factor of 30 as compared to EB in solution.[14] Given the high negative charge density of DNA, one can expect the quenching to be sensitive to the charge of the quencher, the ionic strength of the solution, and the rate of quencher diffusion near the DNA helix.[28–29]

Collisional quenching by oxygen was used to study quenching of several DNA-bound probes.[30–31] Oxygen was chosen as the quencher because it is neutral, and should thus be unaffected by the charge on the DNA. The probes were selected to have different sizes and different modes of binding to DNA (Figure 8.10). Proflavin intercalates into double-helical DNA, and was expected to be protected from quenching. The bimolecular quenching constant for intercalated proflavin was less than 10% of the diffusion-controlled rate (Table 8.2). The k_q value for proflavin may be smaller than shown, as there was little quenching under these experimental conditions. Hoechst 33258 is known to

Table 8.2. Decay Times and Oxygen Quenching Constants of Probes Bound to DNA[31]

Fluorophore	Type of complex	τ_0 (ns)	k_q (M^{-1} sec^{-1})
Proflavine	Intercalation	6.3	$<0.1 \times 10^{10}$
Coronene	Partial intercalation	225	0.17×10^{10}
Hoechst 33258	Minor groove	3.5	1.1×10^{10}

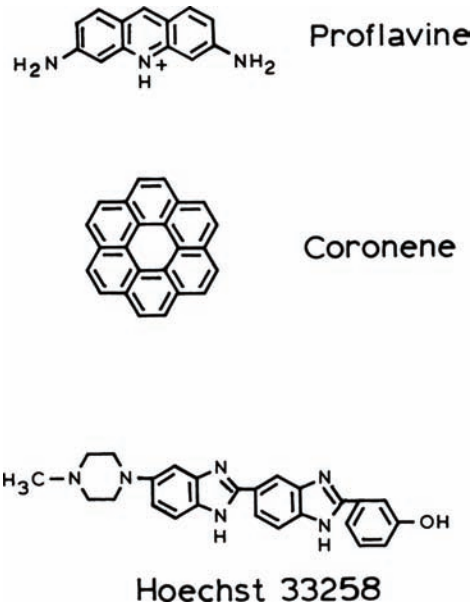

Figure 8.10. Structure of three probes bound to DNA (Table 8.2). Reprinted with permission from [31]. Copyright © 1988, American Society for Photobiology.

bind to the minor groove of DNA. Surprisingly, the k_q values for Hoechst DNA is near the diffusion-controlled limit, suggesting complex accessibility by oxygen. The behavior of coronene was intermediate. Coronene is rather large, and not able to fully fit into a DNA helix. The intermediate value of k_q was explained as due to partial intercalation of coronene, with the value of k_q reflecting partial exposure to water. These results illustrate how the extent of probe exposure can be correlated with the bimolecular quenching constant. The values of the unquenched fluorescence lifetimes were needed to calculate the values of k_q from the Stern-Volmer quenching constants.

The extent of quenching can also be affected by the charge on the quenchers. This is illustrated by iodide quenching of Hoechst 33258 when free in solution and

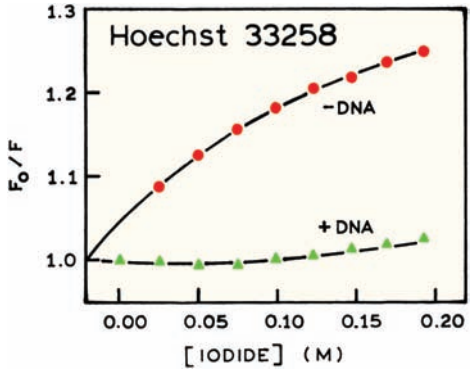

Figure 8.11. Iodide quenching of Hoechst 33258 in the absence and presence of calf thymus DNA. The ionic strength was kept constant using KCl. Revised from [32].

when bound to DNA (Figure 8.11). Hoechst 33258 is readily quenched by iodide when free in solution, but is not quenched when bound to DNA. In the previous paragraph we saw that Hoechst 33258 bound to DNA was completely accessible to the neutral quencher oxygen. Apparently, the negative charges on DNA prevent iodide from coming into contact with Hoechst 33258 when bound to the minor groove of DNA.

8.7.2. Quenching of Ethenoadenine Derivatives

The nucleotide bases of DNA are mostly nonfluorescent. A fluorescent analogue of adenine has been created by addition of an etheno bridge, the so called ε-ATP derivatives (Chapter 3). Depending on the pH and extent of phosphorylation, the charge on the ethenoadenine nucleotides ranges from –3 for ε-ATP to 0 for ethenoadenosine. Hence one expects the extent of quenching to depend on the charge of the quencher.

Stern-Volmer plots for the various ε-Ad nucleotides are shown in Figure 8.12. For the neutral quencher acrylamide there is no effect of charge (right). For the positively charged quencher Tl^+ the largest Stern-Volmer constant was observed for ε-ATP, with progressively smaller values as the number of negatively charged phosphates decreased (left). The opposite trend was observed for iodide quenching where the extent of quenching was lowest for ε-ATP with three negative charges (middle). Such effects of charge on quenching can be used to determine the local charge around fluorophores on proteins based on quenching by positive, neutral, and negatively charged quenchers.[33–35]

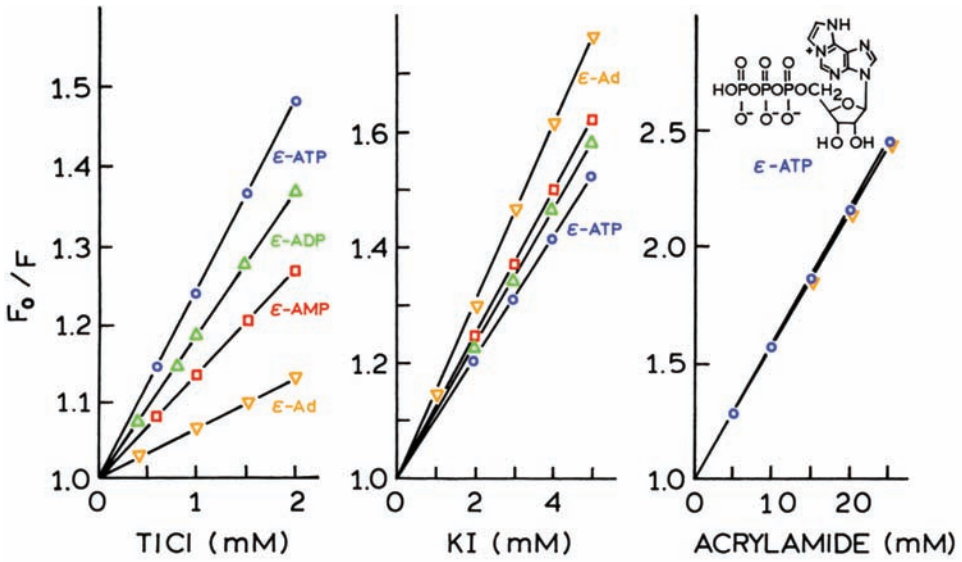

Figure 8.12. Quenching of etheno-ATP (ε-ATP, ○), ε-ADP (Δ), ε-AMP (□) and ε-Ad (∇) by thallium, iodide, and acrylamide in 10 mM phosphate buffer, 0.1 M KCl, 20°C, pH 7.0. Revised from [33].

8.8. FRACTIONAL ACCESSIBILITY TO QUENCHERS

Proteins usually contain several tryptophan residues that are in distinct environments. Each residue can be differently accessible to quencher. Hence one can expect complex Stern-Volmer plots, and even spectral shifts due to selective quenching of exposed versus buried tryptophan residues. One example is quenching of lysozyme. This protein from egg white has six tryptophan residues, several of which are known to be near the action site. Lysozyme fluorescence was observed with increasing concentrations of trifluoroacetamide (TFA), which was found to be a collisional quencher of tryptophan fluorescence.[36] The Stern-Volmer plot curves downward towards the *x*-axis. As will be described below, this is a characteristic feature of two fluorophore populations, one of which is not accessible to the quencher. In the case of lysozyme the emission spectrum shifts progressively to shorter wavelengths with increasing TFA concentrations (Figure 8.13, right). This indicates that those tryptophan residues emitting at larger wavelengths are quenched more readily than the shorter wavelength tryptophans.

The emission spectrum of the quenched residues can be calculated from taking the difference between the unquenched and quenched emission spectra. This spectrum shows that the quenched residues display an emission maxima at 348 nm. The protected residues display an emission maxima at 333 nm. Similar results were obtained for quenching of lysozyme by iodide.[37]

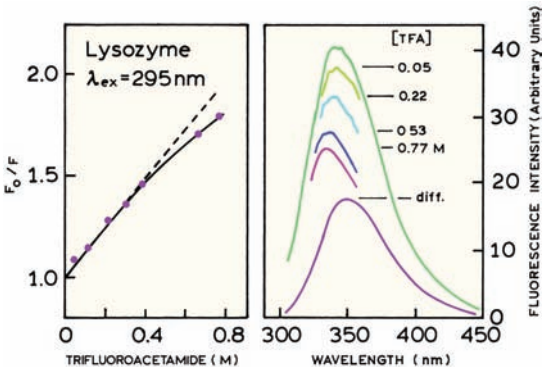

Figure 8.13. Quenching of lysozyme by trifluoroacetamide (TFA). **Left**: Stern-Volmer plot. **Right**: Emission spectra with increasing concentrations of TFA. Also shown is the difference spectrum (diff), 0.0–0.77 M TFA. Revised and reprinted from [36]. Copyright © 1984, with permission from Elsevier Science.

8.8.1. Modified Stern-Volmer Plots

The differing accessiblities of tryptophan residues in proteins has resulted in the frequent use of quenching to resolve the accessible and inaccessible residues.[37] Suppose there are two populations of fluorophores, one of which is accessible (*a*) to quenchers and the other being inaccessible or buried (*b*). In this case the Stern-Volmer plot will display

downward curvature (Figure 8.13). The total fluorescence in the absence of quencher (F_0) is given by

$$F_0 = F_{0a} + F_{0b} \tag{8.27}$$

where the subscript 0 once again refers to the fluorescence intensity in the absence of quencher. In the presence of quencher the intensity of the accessible fraction (f_a) is decreased according to the Stern-Volmer equation, whereas the buried fraction is not quenched. Therefore, the observed intensity is given by

$$F = \frac{F_{0a}}{1 + K_a[Q]} + F_{0b} \tag{8.28}$$

where K_a is the Stern-Volmer quenching constant of the accessible fraction, and $[Q]$ is the concentration of quencher. Subtraction of eq. 8.28 from eq. 8.27 yields

$$\Delta F = F_0 - F = F_{0a}\left(\frac{K_a[Q]}{1 + K_a[Q]}\right) \tag{8.29}$$

Inversion of eq. 8.29 followed by division into eq. 8.27 yields

$$\frac{F_0}{\Delta F} = \frac{1}{f_a K_a[Q]} + \frac{1}{f_a} \tag{8.30}$$

where f_a is the fraction of the initial fluorescence that is accessible to quencher:

$$f_a = \frac{F_{0a}}{F_{0b} + F_{0a}} \tag{8.31}$$

This modified form of the Stern-Volmer equation allows f_a and K_a to be determined graphically (Figure 8.14). A plot of $F_0/\Delta F$ versus $1/[Q]$ yields f_a^{-1} as the intercept and $(f_a K)^{-1}$ as the slope. A y-intercept of f_a^{-1} may be understood intuitively. The intercept represents the extrapolation to infinite quencher concentration ($1/[Q] = 0$). The value of $F_0/(F_0 - F)$ at this quencher concentration represents the reciprocal of the fluorescence that was quenched. At high quencher concentration only the inaccessible residues will be fluorescent.

In separation of the accessible and inaccessible fractions of the total fluorescence it should be realized that there may be more than two classes of tryptophan residues.

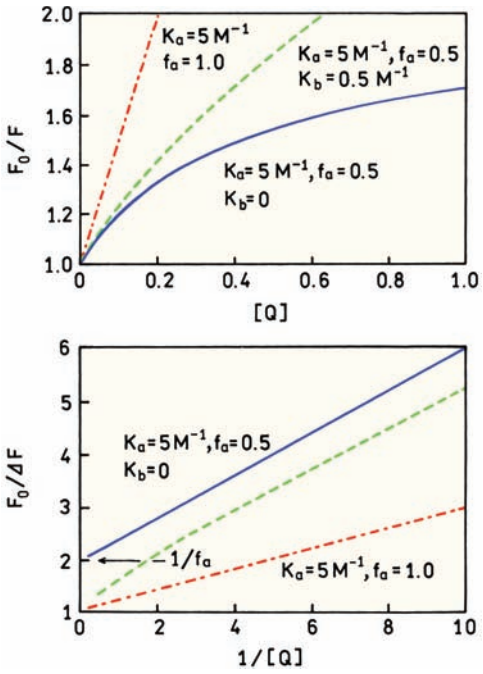

Figure 8.14. Stern-Volmer and modified Stern-Volmer plots for two populations of fluorophores, an accessible fraction with K_a = 5 M^{-1} and f_a = 0.5, and an inaccessible fraction with K_b = 0. The dashed line shows the effect of the "inaccessible" population being quenched with a K value one-tenth of the accessible population, K_b = 0.5 M^{-1}.

Also, even the presumed "inaccessible" fraction may be partially accessible to quencher. This possibility is illustrated by the dashed lines in Figure 8.14, which show the expected result if the Stern-Volmer constant for the buried fraction (K_b) is one-tenth that of the accessible fraction (K_b = 0.1 K_a). For a limited range of quencher concentrations, the modified Stern-Volmer plot can still appear to be linear. The extrapolated value of f_a would be larger than seen with K_b = 0. Hence, the modified Stern-Volmer plots provide a useful but arbitrary resolution of two assumed classes of tryptophan residues.

8.8.2. Experimental Considerations in Quenching

While quenching experiments are straightforward, there are several potential problems. One should always examine the emission spectra under conditions of maximum quenching. As the intensity is decreased the contribution from background fluorescence may begin to be significant. Quenchers are often used at high concentrations, and the quenchers themselves may contain fluorescent impurities. Also, the intensity of the Raman and Rayleigh scatter peaks from water is independent of quencher concentration. Hence the

relative contribution of scattered light always increases with quenching.

It is also important to consider the absorption spectra of the quenchers. Iodide and acrylamide absorb light below 290 nm. The inner filter effect due to absorption can decrease the apparent fluorescence intensity, and thereby distort the quenching data.[38–39] Regardless of the quencher being used, it is important to determine if the inner filter effects are significant. If inner filter effects are present the observed fluorescence intensities must be corrected. The lifetime measurements are mostly independent of inner filter effects because the lifetime measurements are relatively independent of total intensity.

When using iodide or other ionic quenchers it is important to maintain a constant ionic strength. This is usually accomplished by addition of KCl. When using iodide it is also necessary to add a reducing agent such as $Na_2S_2O_3$. Otherwise, I_2 is formed, which is reactive and can partition into the nonpolar regions of proteins and membranes.

8.9. APPLICATIONS OF QUENCHING TO PROTEINS

8.9.1. Fractional Accessibility of Tryptophan Residues in Endonuclease III

There have been numerous publications on determining the fraction of protein fluorescence accessible to quenchers.[40–47] In Section 13.5 we show that proteins in the native state often display a fraction of the emission that is not accessible to water-soluble quenchers, and that denaturation of the proteins usually results in accessibility of all the tryptophan residues to quenchers. The possibility of buried and exposed residues in an apurinic single protein is illustrated by endonuclease III. Endo III is a DNA repair enzyme that displays both N-glycosylase and apurinic/apyrimidinic lyase activities. The structure of Endo III shows two domains, with the DNA binding site in the cleft region. Endo III contains two tryptophan residues.[42] Trp 132 is exposed to the solvent, and trp 178 is buried in one of the domains (Figure 8.15). Hence one expects these residues to be differently accessible to water-soluble quenchers.

The Stern-Volmer plot for iodide quenching of Endo III shows clear downward curvature (Figure 8.16, top). The modified iodide Stern-Volmer plot for Endo III shows clear evidence for a shielded fraction (bottom). Extrapolation to high iodide concentrations yields an intercept near 2, indicating that only half of the emission can be quenched by

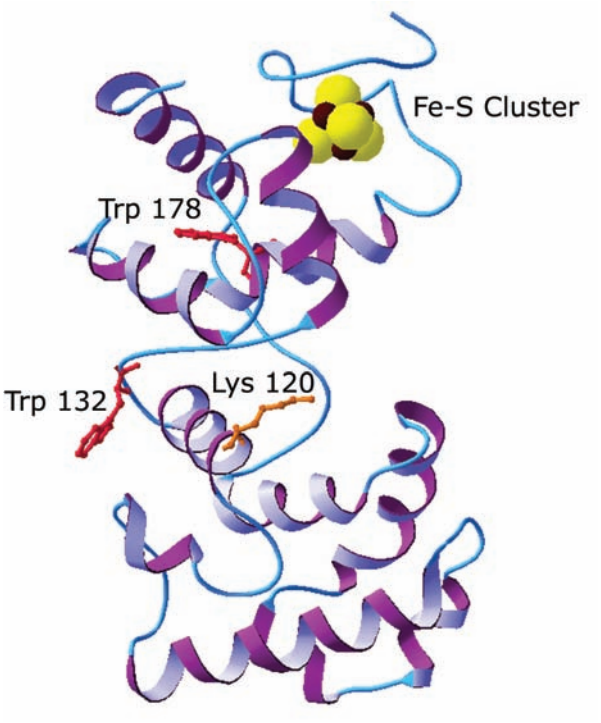

Figure 8.15. Structure of Endo III showing the exposed residue trp 132 and the buried residue trp 178 near the iron-sulfur cluster.

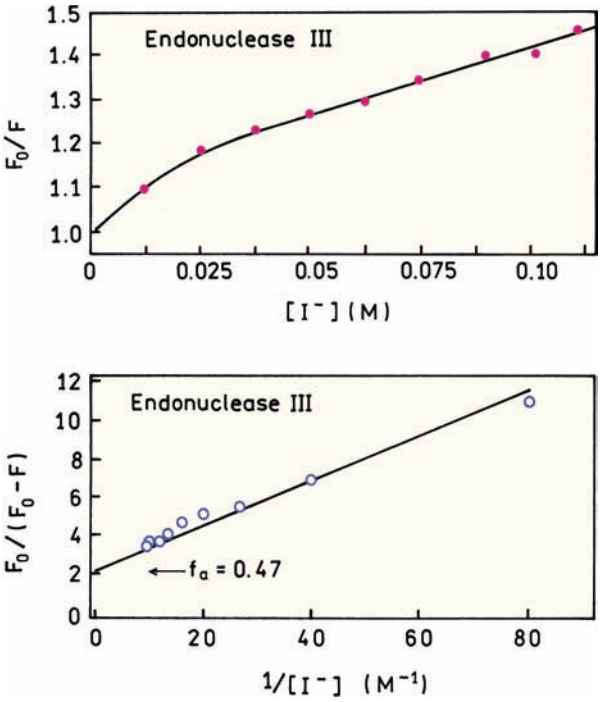

Figure 8.16. Stern-Volmer plot and modified Stern-Volmer plot for iodide quenching of Endo III showing evidence for two types of tryptophan residues. The inaccessible fraction is f_a = 0.47. Revised and reprinted with permission from [42]. Copyright $©$ 1995, American Chemical Society.

iodide. This suggests that both trp residues in Endo III are equally fluorescent, and that only one residue (trp 132) can be quenched by iodide. Similar results have been obtained for a large number of proteins, and the extent of quenching is known to depend on the size and polarity of the quenchers.[6,7] Quenching of solvent-exposed residues in proteins is now a standard tool in the characterization of proteins.

8.9.2. Effect of Conformational Changes on Tryptophan Accessibility

The conformational state of a protein can have an influence on the exposure of its tryptophan residues to solvent. This is illustrated by the cyclic AMP (cAMP) receptor protein (CRP) from *E. coli*.[44] This protein regulates the expression of more than 20 genes in *E. coli*. CRP consists of two identical polypeptide chains, each containing 209 amino acids. CRP contains two nonidentical trp residues at positions 13 and 85.

Acrylamide Stern-Volmer plots for CRP are shown in Figure 8.17, in the absence and presence of bound cAMP. In the absence of cAMP the Stern-Volmer plot shows obvious downward curvature, indicating that one of the trp residues is inaccessible or only slightly accessible to acrylamide. Binding of cAMP results in a dramatic change in the Stern-Volmer plot, which becomes more linear and even displays some upward curvature. Apparently, binding of cAMP to the CRP causes a dramatic conformational change that results in exposure of the previously shielded trp residue. Changes in accessibility due to conformational changes have been reported for other proteins.[48–49] Binding of substrates to proteins can also result in shielding of tryptophan, as has been observed for lysozyme[37] and for wheat-germ agglutinin.[36]

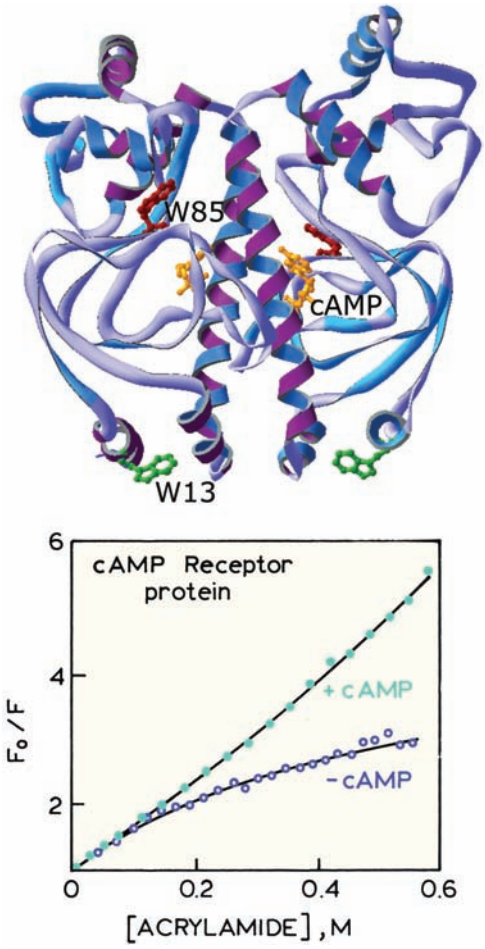

Figure 8.17. Acrylamide Stern-Volmer plot for cAMP receptor protein in the absence and presence of cAMP. Revised from [44].

8.9.3. Quenching of the Multiple Decay Times of Proteins

The intensity decays of proteins are typically multi-exponential. Hence, it is natural to follow the individual decay times as the protein is exposed to increasing concentrations of quencher. One example is the CRP protein we just described.[44] Frequency-domain data of its intrinsic tryptophan emission yield decay times near 1.5 and 6.8 ns. Similar decay times were observed in the absence and presence of bound cAMP. For the protein without bound cAMP, the shorter decay time did not change with increasing iodide concentration (Figure 8.18, top), whereas the long lifetime decreased. This decrease in lifetime indicates that the 6.8-ns component is due to the exposed trp residue. The 1.5-ns component is not quenched by iodide and is assigned to the buried trp residue. In the presence of bound cAMP both decay times are seen to decrease in the presence of iodide, indicating both are quenched (bottom). These results agree with the linear Stern-Volmer plot found for CRP with bound cAMP (Figure 8.17).

While the results shown in Figure 8.18 show a clear separation of decay times, caution is needed when interpreting decay times in the presence of quenchers. For many proteins the decay times will be closer than 1.5 and 6.8 ns, and the decay time for each trp residue can depend on emission wavelength. Hence, it may not be possible to assign a unique decay time to each tryptophan residue. Additionally, collisional quenching results in non-exponential decays,

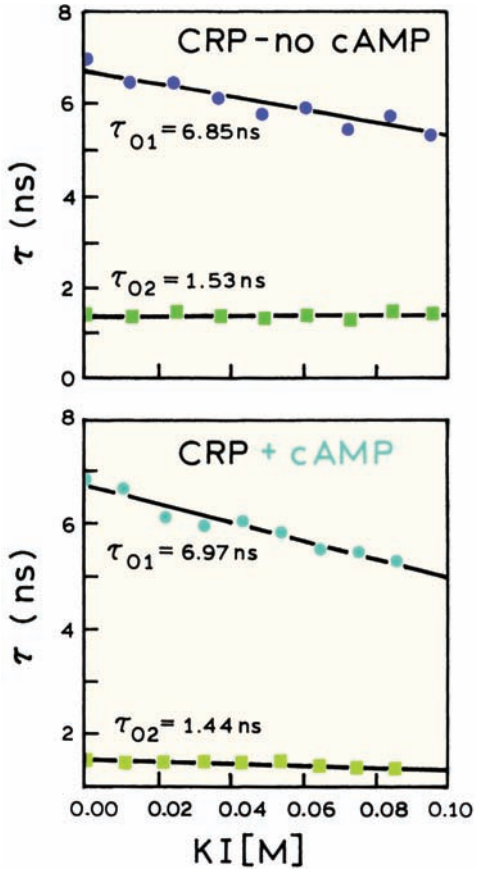

Figure 8.18. Iodide-dependent decay times of cAMP receptor protein (CRP) in the absence (top) and presence (bottom) of bound cAMP. Revised from [44].

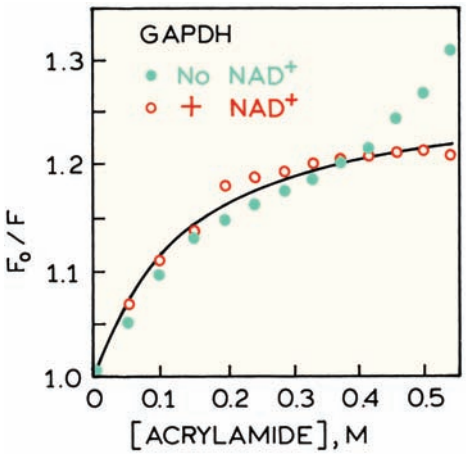

Figure 8.19. Acrylamide quenching of GAPDH in the absence (●) and presence (○) of the cofactor NAD^+. Revised and reprinted with permission from [54]. Copyright $©$ 1992, American Society for Photobiology.

even if the fluorophore shows a single decay time in the absence of quencher. This change in the intensity decay is due to transient effects in quenching, which are due to the rapid quenching of closely spaced *F–Q* pairs, followed by a slower quenching rate due to quencher diffusion. The presence of transient effects results in additional ns decay time components, which, depending on the method of measurement, can affect the apparent lifetimes for each residue. The assignment of decay times to trp residues in the presence of quenching can be ambiguous. Transient effects in quenching are described in the following chapter.

8.9.4. Effects of Quenchers on Proteins

When performing quenching experiments it is important to consider whether the quencher has an adverse effect on the protein. Some quenchers such as 2,2,2-trichloroethanol are known to bind to proteins and induce conformational changes.[50] For a time it was thought that acrylamide bound to proteins, but it is now accepted that such binding does not occur outside of several specific cases.[51–53] However, even the non-perturbing quencher acrylamide can affect certain proteins, as was found for glyceraldehyde-3-phosphate dehydrogenase (GAPDH).[54] This protein contains three tryptophan residues in each subunit of the tetrameric enzyme. For the apoenzyme, which lacks NAD^+, the acrylamide Stern-Volmer plot is highly unusual. The extent of quenching increases rapidly above 0.4 M acrylamide (Figure 8.19). This effect is not seen for the holoenzyme that contains bound NAD^+. Acrylamide also caused a slow loss of activity and reduction in the number of thiol groups. Acrylamide appears to bind to GAPDH, to react with the protein and destroy its activity, while at the same time increasing the exposure of the tryptophan residues to the aqueous phase.

8.9.5. Correlation of Emission Wavelength and Accessibility: Protein Folding of Colicin E1

Colicin E1 is a 522 residue polypeptide that is lethal to *E. coli* strains that do not contain the resistance plasmid. Colicin E1 exerts its toxic effects by forming a channel in the cytoplasmic membrane that depolarizes and deenergizes the cell. The active channel-forming domain consists of about 200 residues from the carboxy terminus, which form ten α-helices spanning the membrane.

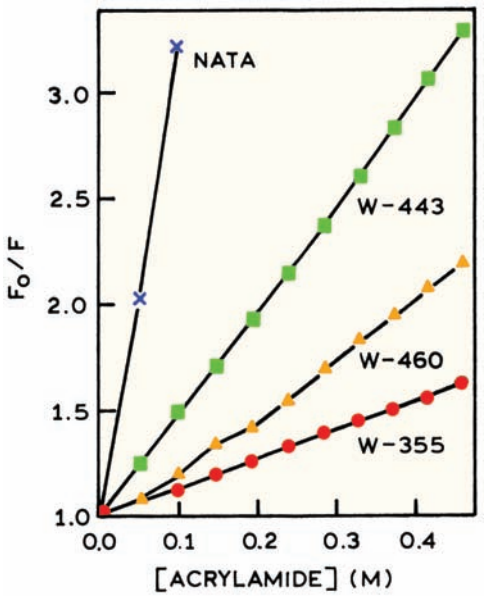

Figure 8.20. Acrylamide Stern-Volmer plot for NATA (*x*), and three single-tryptophan mutants of the channel-forming peptide of Colicin E1 at pH 3.5, W-355 (●), W-460 (▼), and W-443 (■). Revised and reprinted with permission from [55]. Copyright © 1993, American Chemical Society.

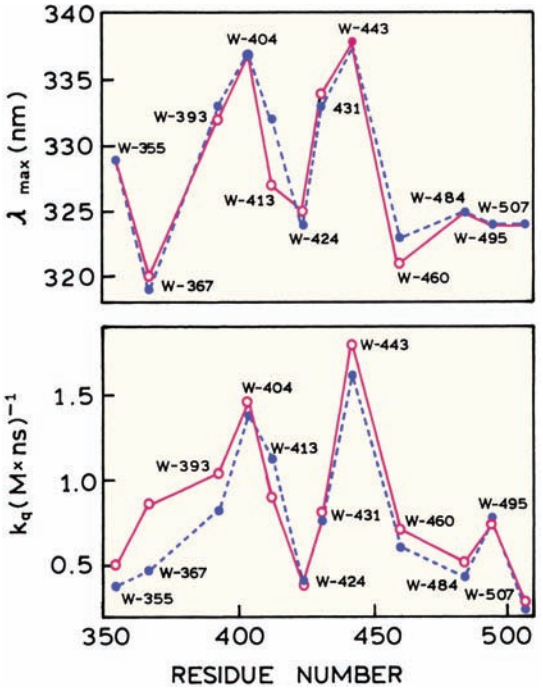

Figure 8.21. Emission maxima (top) and bimolecular quenching constants (bottom) of the twelve single-tryptophan mutants of the channel-forming peptide of Colicin E1 at pH 3.5. Revised and reprinted with permission from [55]. Copyright © 1993, American Chemical Society.

The conformation of the membrane-bound form of the colicin E1 channel peptide was studied by acrylamide quenching.[55] Twelve single tryptophan mutants were formed by site-directed mutagenesis. The tryptophan residues were mostly conservative replacements, meaning the trp residues were placed in positions previously containing phenylalanine or tyrosine. Acrylamide Stern-Volmer plots of three of these mutant proteins are shown in Figure 8.20. The accessibility to acrylamide quenching is strongly dependent on the location of the residue, and all residues are shielded relative to NATA. Depending on position, the trp residues also showed different emission maxima (Figure 8.21, top). The acrylamide bimolecular quenching constants were found to closely follow the emission maxima, with lower values of k_q for the shorter-wavelength tryptophans (bottom). Such data can be used to suggest a folding pattern for the channel-forming peptide, and to reveal conformational changes that occur upon pH activation of colicin E1.

8.10. APPLICATION OF QUENCHING TO MEMBRANES

8.10.1. Oxygen Diffusion in Membranes

Quenching by oxygen has been used to determine the apparent diffusion coefficient of oxygen in membranes. This can be accomplished using probes that partition into the lipid bilayers or are covalently bound to the lipids. Figure 8.22 shows oxygen Stern-Volmer plots for 2-methylanthracene in vesicles of DMPC and DPPC, which have phase-transition temperatures (T_c) near 24 and 37°C, respectively.[56] At the experimental temperature near 31°C the DPPC bilayers are below the phase transition, and the DMPC bilayers are above the phase transition. While anisotropy measurement on such a bilayer suggests a large change in viscosity at the transition temperature (Chapter 10), the effect on oxygen diffusion is only modest: near twofold. This surprisingly small change in the oxygen diffusion coefficient has been confirmed by other fluorescence[57–59] and ESR experiments.[60] These experiments even suggest that cholesterol, which generally makes membranes more rigid, results in increased rates of oxygen transport. This can be seen by quenching of pyrene dodecanoic acid (PDA) in erythrocyte ghost membranes (Figure 8.23). In this case, the ghost membranes were modified by addition of endogenous cholesterol. The apparent bimolecular quenching constant increases with increasing amounts of cholesterol, except for the highest membrane concentration

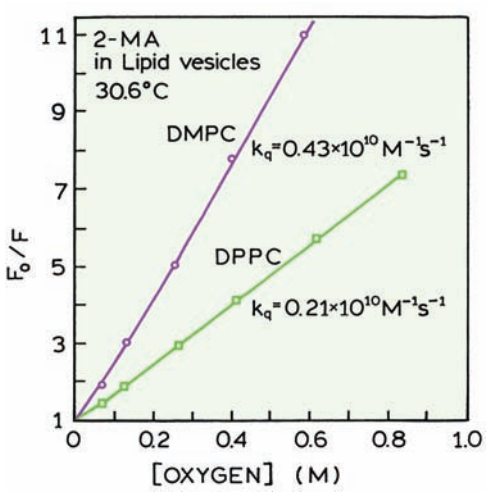

Figure 8.22. Oxygen quenching of 2-methylanthracene (2-MA) at 30.6°C, in DMPC (T_c = 24°C) and DPPC (T_c = 37°C) bilayers.

of cholesterol where the amount of quenching decreases (Figure 8.23, ●).

In order to calculate the bimolecular quenching constants it is necessary to know the oxygen concentration in the membranes. Unfortunately, precise values are not known, particularly for membranes with different lipid compositions. The oxygen solubility in membranes is usually taken as equal to that in nonpolar solvents, and thus approximately fourfold larger than in water. Assuming a lifetime of PDA near 120 ns, one can use the data in Figure 8.23 to calculate k_q = 0.22 x 10^{10} M^{-1} s^{-1}. The permeability (P) of a membrane can be approximated by $P = k_q D/\Delta x$, where D is the oxygen diffusion coefficient and Δx is the membrane thickness. Given that the diffusion coefficient of oxygen is about 1/5 of that in water, and the lipid–water partition coefficient is near 5, this equation suggests that biological membranes do not pose a significant diffusive barrier to oxygen.

8.10.2. Localization of Membrane-Bound Tryptophan Residues by Quenching

Collisional quenching is a short-range interaction, so that the extent of quenching can be used to indicate the amount of molecular contact between the fluorophore and quencher. This concept has been used to study the location of tryptophan residues in membrane-spanning peptides.[61] A series of peptides were synthesized that contained a single tryptophan residue. These peptides were roughly of the form $K_qL_kWL_mK_m$, where K is a charged amino acid lysine, L is a nonpolar amino acid leucine, and W is tryptophan. The number of nonpolar residues on each side of the tryptophan was varied to position the trp at various distances from the center of the DOPC bilayers. Figure 8.24 shows acrylamide quenching of the peptides when bound to DOPC vesicles. The extent of quenching depends strongly

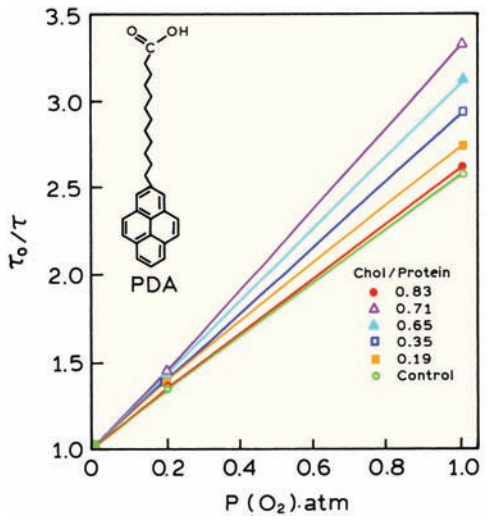

Figure 8.23. Oxygen quenching of pyrene dodecanoic acid in erythrocyte ghost membranes with various cholesterol/protein ratios: ○, control, no added cholesterol; Chol/Protein ratios: ■, 0.19; □, 0.35; ▲, 0.65; △, 0.71; ●, 0.83. Revised from [59].

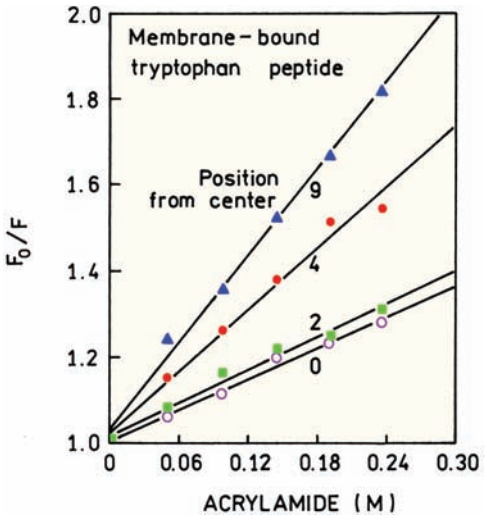

Figure 8.24. Acrylamide quenching of tryptophan residues in a membrane-spanning peptide. Revised and reprinted with permission from [61]. Copyright © 2003, American Chemical Society.

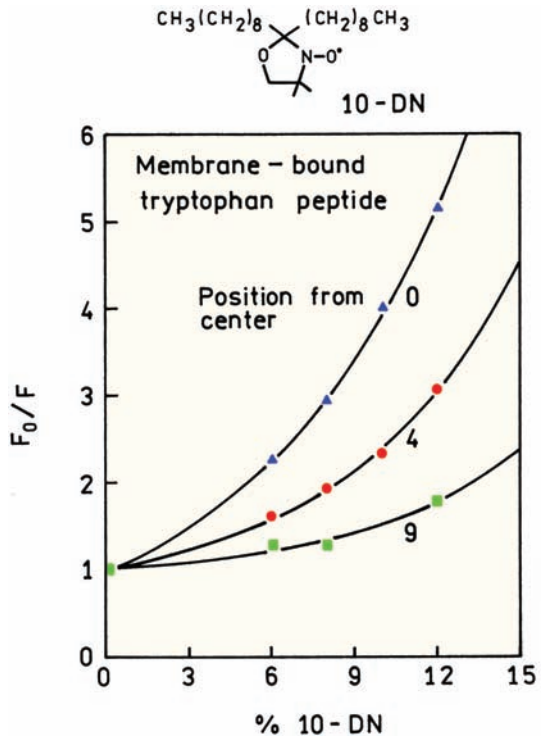

Figure 8.25. Quenching of tryptophan residues in a membrane-spanning peptide by a hydrophobic nitroxide. Revised and reprinted with permission from [61]. Copyright © 2003, American Chemical Society.

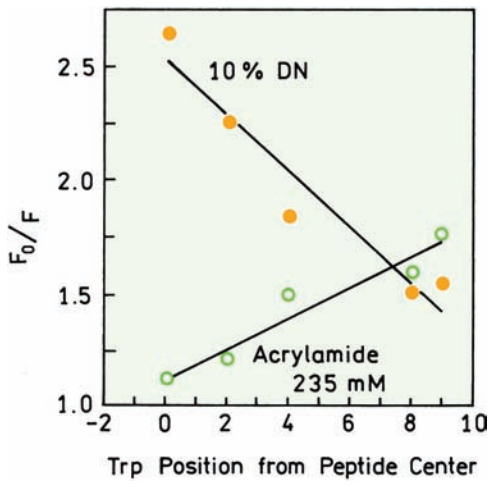

Figure 8.26. Comparison of acrylamide and nitroxide quenching of tryptophan residues in a membrane-spanning peptide. Revised and reprinted with permission from [61]. Copyright © 2003, American Chemical Society.

on the position of the trp residue relative to the center of the bilayer. The most accessible trp residue is located 9 positions from the center, and is the most protected residue in the center of the bilayer.

These membrane-bound peptides were also studied with hydrophobic quencher 10-doxylnonadecane (10-DN). This quencher (19 carbons in total length) should be able to bind to the DOPC bilayer without folding back on itself. The alkyl chains on each side of the doxyl group are equivalent in length. Hence the doxyl group was expected to localize at the center of the bilayer. Figure 8.25 shows quenching of the trp peptides in DOPC bilayers by 10-DN. 10-DN is not significantly soluble in water and the Stern-Volmer plot is presented in terms of the mole% of 10-DN in the bilayers. The Stern-Volmer plots curve upward but it is still clear that the trp residue at the center of the bilayer is most strongly quenched, and the extent of quenching by 10-DN decreases as the trp residue is displaced from the center of the bilayer. The effect of trp position on quenching is summarized in Figure 8.26. The extent of quenching by acrylamide, which is water soluble, decreases as the trp residue is displaced from the center of the bilayer. The extent of trp quenching by 10-DN shows the opposite dependence. Such experiments can be used to determine the location of tryptophan or other fluorophores in membranes when the structures are not known.

8.10.3. Quenching of Membrane Probes Using Localized Quenchers

The previous example showed that accessibility of a fluorophore to a quencher can be used to roughly indicate its position in a membrane. However, this approach did not provide an estimate of its actual location. A somewhat more advanced approach is to use quenchers that are covalently linked to the phospholipids and thus restricted to particular depths in the lipid bilayers. Typical lipid quenchers are the brominated phosphatidylcholines (bromo-PCs) and nitroxide-labeled PCs or fatty acids (Figure 8.27). This approach was used to determine the locations of the fluorenyl groups in a series of fluorenyl fatty acids when bound to erythrocyte ghosts (Figure 8.28). The term "ghosts" refers to the red-blood-cell membranes following removal of hemoglobin by cell lysis. The fluorenyl probes were quenched by 9,10-dibromostearate that partitioned into the membrane.[62] Since the bromine atoms are rather small, they are expected to be localized according to their position on the fatty-acid chain. The bromine atoms are located near the center

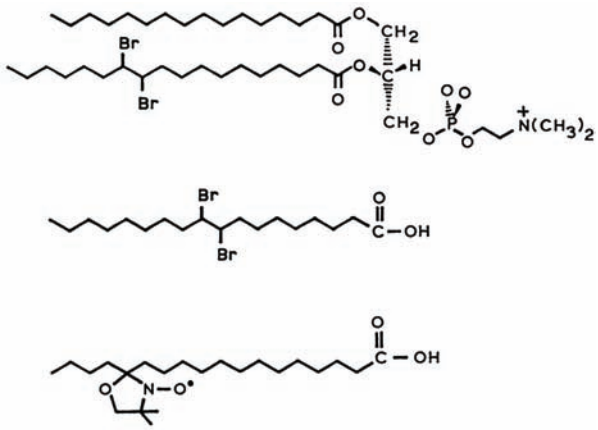

Figure 8.27. Structures of a bromo-PC (top), 9,10-dibromostearic acid (middle), and a nitroxide labeled fatty acid (bottom), which act as localized quenchers in membranes.

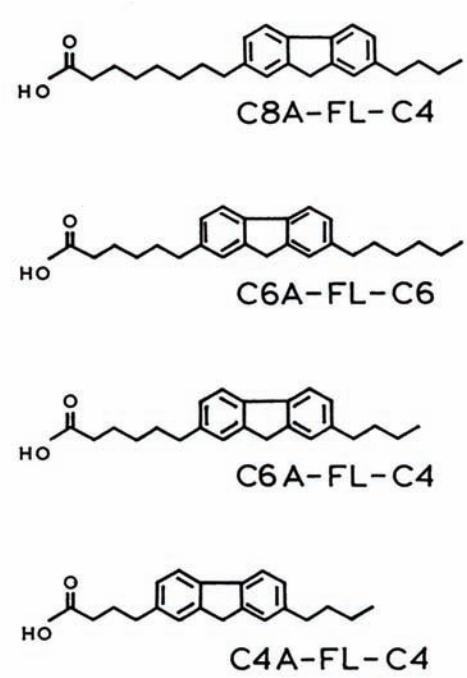

Figure 8.28. Structures of the fluorenyl fatty acids. Revised from [62].

of the fatty acid (Figure 8.27, middle), so one expects maximal quenching for those fluorenyl groups located as deep as the bromine atoms. The quenching data reveal larger amounts of quenching when the fluorenyl groups are placed more deeply in the bilayer by a longer methylene chain between the fluorenyl and carboxyl groups (Figure 8.29). Hence, the fluorenyl probes are located as expected from

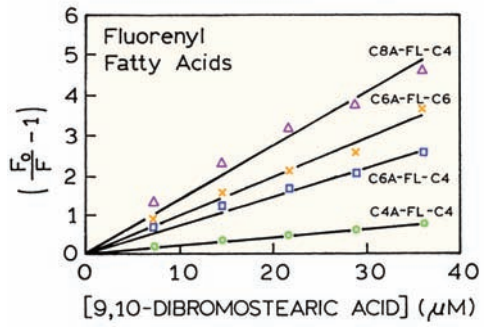

Figure 8.29. Quenching of fluorenyl fatty acids (Figure 8.28) by 9,10-dibromostearic acid in erythrocyte ghost membranes. Revised and reprinted with permission from [62]. Copyright © 1992, American Chemical Society.

their structure. For these fluorenyl fatty acids a continuing alkyl chain beyond the fluorenyl group was important for probe localization.

Another example of using localized quenchers is provided by studies of pyrene-labeled lipids.[63] A number of pyrene PCs were used that had a different number of methylene groups (n) between the glycerol backbone and the pyrene. This localizes the pyrene groups at different depths in the bilayers (Figure 8.30). Three different bromo-PCs with the bromides at position 6 and 7, 9 and 10, or 11 and 12 were used as quenchers. The apparent Stern-Volmer quenching constants were measured for each pyrene PC and each quencher (Figure 8.31). The largest quenching constant was observed for the smallest number of methylene groups in the pyrene PC (n) when using $Br_{6,7}$PC, in which the bromides are located just beneath the membrane surface. For larger values of n, maximum quenching was observed for $Br_{11,12}$PC, where the bromides are located more deeply in the membrane. In this case the fluorophores were localized in bilayer as would be predicted from their structure. Bromo-PCs are known to quench the fluorescence of membrane-bound proteins,[64–66] and have been used to study lateral phase separations in membranes.[67–68]

8.10.4. Parallax and Depth-Dependent Quenching in Membranes — Advanced Topic

The use of quenching to determine the location of fluorophores in membranes has been formalized using two similar methods: parallax quenching[69–75] and depth-dependent quenching.[76–78] The basic idea is to compare the amount of quenching observed for quenchers that are located at two

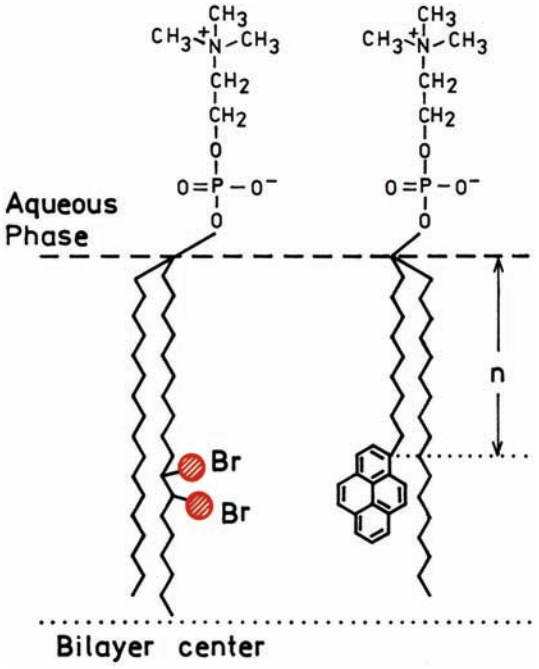

Figure 8.30. Schematic representation of the structures of Pyr_nPC and $Br_{x,y}PC$ species used to study depth-dependent quenching of the pyrene moiety. Revised and reprinted with permission from [63]. Copyright © 1995, American Chemical Society.

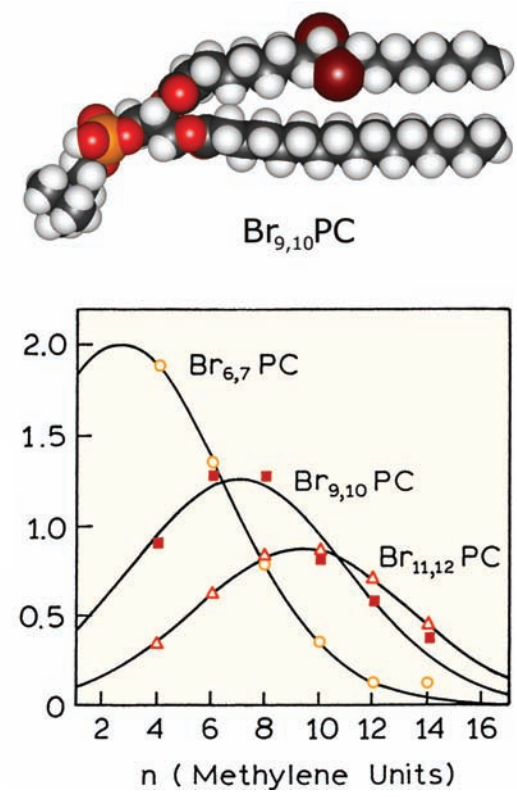

Figure 8.31. Dependence of K_{SV}^{app}, the apparent Stern-Volmer quenching constant, on n, the number of methylene units in the pyrenylacyl chains, for bilayers with different $Br_{x,y}PC$ quenchers. The subscripts x and y indicate the location of the bromine atoms. The bilayers consisted of 1-palmitoyl-2-oleoylphosphatidylcholine (POPC) with 50 mole% cholesterol. Revised and reprinted with permission from [63]. Copyright © 1995, American Chemical Society. Structure courtesy of Dr. Alexey S. Ladokhin from University of Kansas.

different depths in the bilayer. The distance of the fluorophore from the center of the bilayer (Z_{CF}) is then calculated from[79]

$$Z_{CF} = L_{cl} + \{[-\ln(F_1/F_2)/\pi C] - L_{21}\}/2L_{21} \quad (8.32)$$

where L_{21} is the difference in depth between the shallow and deep quenchers. The shallow quencher is located at a distance L_{cl} from the center of the bilayer. C is the concentration of quenchers in molecules per unit area. F_1 and F_2 are the relative intensities of the fluorophore in the presence of the shallow and deep quencher, respectively. This model was derived by assuming complete quenching within a critical distance of the quencher, and that quenching does not occur across the bilayer. This model also assumes there is no diffusion in the membrane. In principle the location of the fluorophore can be determined using two quenchers. This analysis yields a single distance and will not reveal a distribution of fluorophore depths if such a distribution is present.

An alternative method is depth-dependent quenching.[79] In this case the fluorophore is assumed to be present at a distribution of depths. For a quencher at a depth h the extent of quenching is given by

$$\ln\frac{F_0}{F(h)} = G(h) + G(-h) \quad (8.33)$$

$$G(h) = \frac{S}{\sigma\sqrt{2\pi}}\exp\left[-\frac{(h-h_m)^2}{2\sigma^2}\right] \quad (8.34)$$

where in this expression h_m is the most probable depth for the fluorophore, and σ is the width of the distribution of fluorophore depth. Two distributions are used to account for both sides of bilayers. If more than two quenchers are used the distribution is overdetermined and the values of h_m and

σ are found by least-squares or other filtering procedures. Depth-dependent quenching was used for the analysis shown in Figure 8.31.

8.10.5. Boundary Lipid Quenching

Advanced Topic

Quenching in membranes can also be used to study boundary lipids, which are the lipid molecules surrounding a fluorophore or a membrane-bound protein.[80–86] Suppose a protein is surrounded by a discrete number of lipid molecules, and that the tryptophan fluorescence is accessible to quenchers in the membrane phase. Then the number of boundary lipid molecules can be estimated from

$$\frac{F - F_{\min}}{F_0 - F_{\min}} = (1 - [Q])^n \qquad (8.35)$$

where F_0 is the intensity in the absence of quencher and $F_{\min}$ is the intensity when the probe is in pure quencher lipid. F is the intensity at a given mole fraction of quencher lipid.

This model was tested using small probes in membranes, and for Ca^{2+}-ATPase, which is a large membrane-bound protein containing 11 to 13 tryptophan residues. For tryptophan octyl ester, the intensity decreased according to $n = 6$, indicating that each tryptophan was surrounded by 6 lipid molecules (Figure 8.32). For the Ca^{2+}-ATPase, the intensity decreased with $n = 2$. This does not indicate that only two lipid molecules surrounded this protein, but that only two lipid molecules are in contact with tryptophan residues in the Ca^{2+}-ATPase. Similar results of two boundary quenchers were found for the Ca^{2+}-ATPase using 1,2-bis(9,10-dibromooleoyl)phosphatidylcholine.[82]

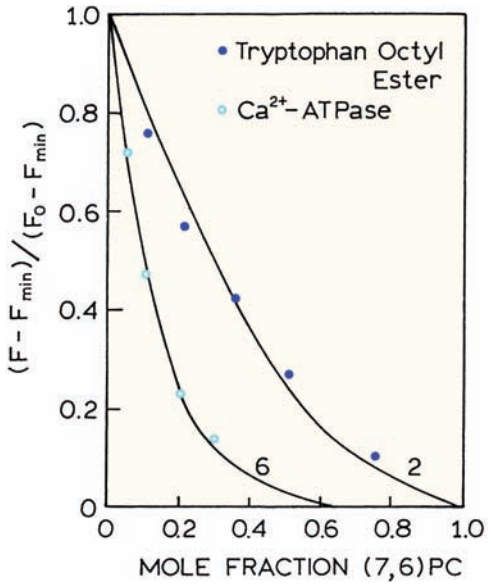

Figure 8.32. Quenching of tryptophan octyl ester (○) and the Ca^{2+}-ATPase (●) by a spin labeled (7,6)PC in egg PC vesicles. (7,6)-PC in a phosphatidylcholine in which the spin label is located on the 8th carbon atom chain of the 2-position fatty acyl group. The structure of the nitroxide spin label is shown in Figure 8.27. The solid lines are for the indicated values of n (eq. 8.35). The dashed lines show the theoretical curves for $n = 10$ or 2 in (eq. 8.35). Revised and reprinted with permission from [80]. Copyright © 1981, American Chemical Society.

8.10.6. Effect of Lipid–Water Partitioning on Quenching

In the preceding examples of quenching in membranes the quenchers were not soluble in water. Hence, the quencher concentrations in the membrane were known from the amount of added quencher. However, there are many instances where the quencher partitions into the membranes, but some fraction of the quencher remains in the aqueous phase. Consequently, the quencher concentration in the membrane is not simply determined by the amount of quencher added, but also by the total lipid concentration in the sample. In these cases it is necessary to determine the lipid–water partition coefficient in order to interpret the observed quenching.

Consider a quencher that distributes between the membrane and aqueous phases. At non-saturating concentrations of quencher the concentrations in the water (w) and membrane (m) phases are related by the partition coefficient

$$P = [Q]_m / [Q]_w \qquad (8.36)$$

The total (T) concentration of quencher added ($[Q]_T$) partitions between the water and membrane phases according to

$$[Q]_T V_T = [Q]_m V_m + [Q]_w V_w \qquad (8.37)$$

where V_m and V_w represent the volume of the membrane and water phases, respectively. By defining

$$\alpha_m = V_m / V_T \qquad (8.38)$$

to be the volume fraction of membrane phase, one obtains[87]

$$[Q]_m = \frac{P[Q]_T}{P\alpha_m + (1 - \alpha_m)} \quad (8.39)$$

Substitution of this expression for the membrane concentration of quencher into the Stern-Volmer equation yields

$$\frac{1}{\tau} = \frac{1}{\tau_0} + \frac{k_m P[Q]_T}{P\alpha_m + (1 - \alpha_m)} = \frac{1}{\tau_0} + k_{app}[Q]_T \quad (8.40)$$

where k_m is the bimolecular quenching constant for the membrane-bound fluorophore. The apparent quenching constant is given by

$$\frac{1}{k_{app}} = \alpha_m\left(\frac{1}{k_m} - \frac{1}{k_m P}\right) + \frac{1}{k_m P} \quad (8.41)$$

When the fluorophore is present in the membrane phase, the apparent quenching constant is dependent upon P, α_m and k_m. A plot of k_{app}^{-1} vs. α_m allows P and k_m to be determined. Thus, the quenching method allows simultaneous quantitation of both the extent to which a quencher partitions into a bilayer and its diffusion rate (D_q) in this bilayer. The successful determination of the quencher diffusion and partition coefficients requires that the range of lipid concentrations results in a range of fractional partitioning of the quencher. The fraction of the quencher partitioned in the membrane (f_m) is given by

$$f_m = \frac{P\alpha_m}{P\alpha_m + (1 - \alpha_m)} \quad (8.42)$$

To calculate the volume fraction of the lipid, the usual assumption is equal densities for the water and membrane phases. In this case a 10-mg/ml membrane suspension corresponds to $\alpha_m = 0.01$. The above method of determining the lipid–water partition coefficient only applies when the quencher molecules are present in the bilayer at the moment of excitation. If the diffusional encounters involve molecules in the aqueous phase, which diffuse into the lipid phase during the lifetime of the excited state, then no dependence of the apparent quenching on lipid concentration is expected. The situation is more complex when the quenching results from quenchers in both the lipid phase and in the water phase.

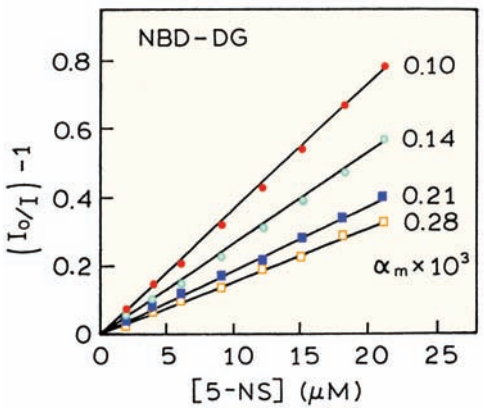

Figure 8.33. Quenching of 1-oleoyl-2-hexanoyl-NBD-glycerol (NBD-DG) by 5-doxylstearate (5-NS). α_m refers to the volume fraction of the egg PC phase. Revised from [92]. Copyright © 1994, with permission from Elsevier Science.

A number of publications have appeared on the effect of partitioning and quenching.[87–92] One example is quenching of a NBD-labeled lipid by the nitroxide fatty acid 5-doxylstearate (5-NS). In contrast to the nitroxide-labeled PCs, the fatty acids have a low but significant solubility in water. When NBD-labeled vesicles are titrated with 5-NS the Stern-Volmer plots are dependent on lipid concentration (Figure 8.33). At lower lipid concentrations addition of the same total amount of 5-NS results in larger amounts of quenching than observed at higher lipid concentrations. At low lipid concentrations, the added quencher results in a higher quencher concentration in the membrane. This is because there is less lipid into which the quencher can partition. It is this dependence of the apparent quenching constant on lipid concentration that allows the partition coefficient to be determined. This is done by a plot of k_{app}^{-1} vs. α_m (Figure 8.34). The data indicate that 5-NS partitions almost 10,000-fold into the lipid phase, and that the bimolecular quenching constant is 1.1×10^9 M^{-1} s^{-1}. Use of the Smoluchowski equation yields a mutual diffusion coefficient for the probe and quencher near 3×10^{-6} cm^2/s. This value is larger than expected for a quencher in a membrane, and 100-fold larger than the diffusion coefficient of lipid in membranes determined by fluorescence recovery after photobleaching (FRAP). This difference is probably the result of different diffusion coefficients for short- and long-range diffusion in membranes, the so-called anomalous sub-diffusion (Chapter 24).

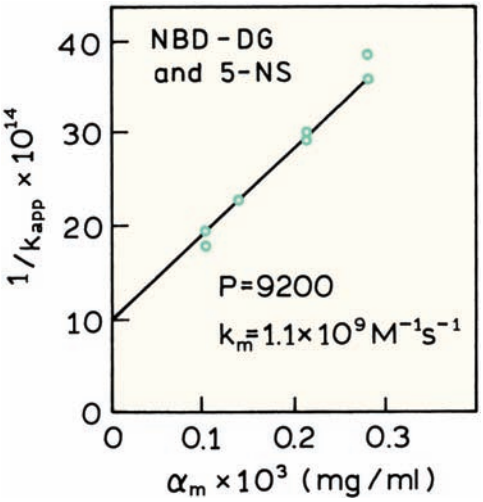

Figure 8.34. Dependence of the apparent quenching (NBD-DG and 5-NS) on lipid concentration (α_m). Revised from [92].

8.10.7. Quenching in Micelles

Quenching of fluorescence in micelles can also be complex (Figure 8.35). The top panel shows quenching of pyrene in methanol by a lipid-soluble pyridinium derivative, which probably quenches by a charge-transfer mechanism (Chapter 9). When the quencher $C_{16}PC$ is added to a methanol solution of pyrene the lifetimes decrease but remain a single exponential. When pyrene is bound to micelles, and lipid solubles quenchers are added, the decays become strongly multi-exponential. These decays are not typical of collisional quenchers in solution, as seen from the decay at long times above 200 ns. The decay time of this component is the same as pyrene in micelles without quenchers.

The complex pyrene intensity decays seen in Figure 8.35 are due to Poisson statistics in quencher binding to the micelles. Under the conditions of these experiments there was an average of less than one quencher per micelle. Hence some of the micelles contained a quencher, and some did not. The micelles without bound quencher display the lifetime of unquenched pyrene. The micelles with quenchers display a shorter lifetime. For such a system the intensity decay is given by[93–96]

$$I(t) = I_0 \exp(-t/\tau_0 + \bar{n}[\exp(-k_q t) - 1]) \quad (8.43)$$

where τ_0 is the unquenched lifetime, $\bar{n}$ is the mean number of quenchers per micelle, and k_q is the decay rate due to a single quencher molecule in the micelle.

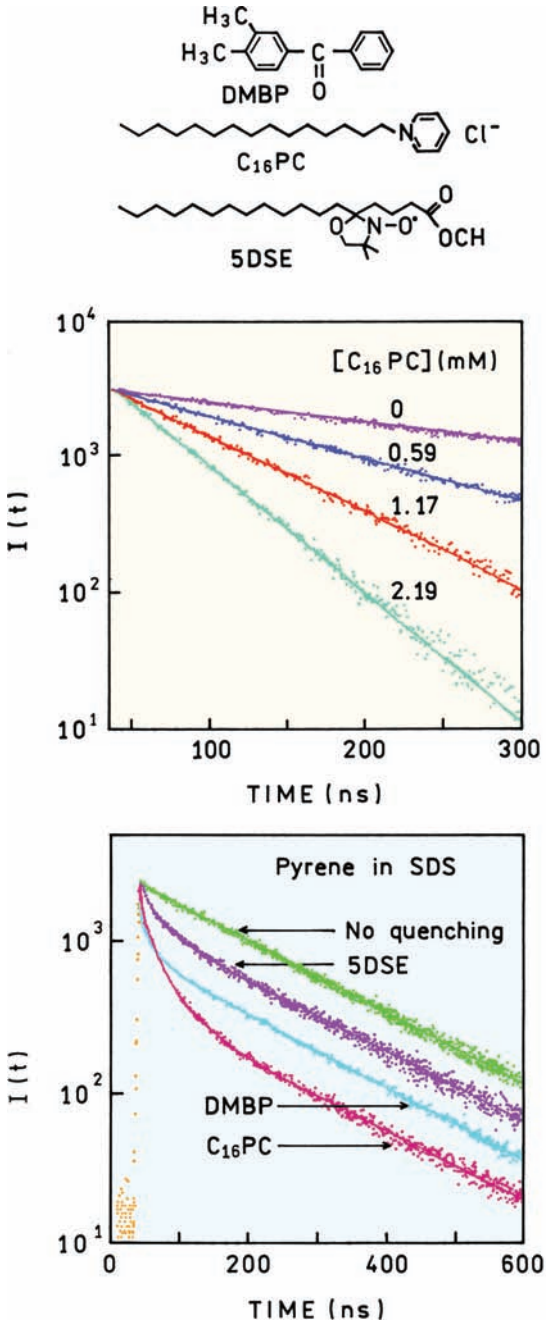

Figure 8.35. Quenching of pyrene in methanol solution (top) and in SDS micelles (bottom). Revised and reprinted with permission from [93]. Copyright © 2003, American Chemical Society.

8.11. LATERAL DIFFUSION IN MEMBRANES

Advanced Topic

In the preceding section on localization (except for oxygen) of probes in membranes, we did not consider diffusion of

the quenchers in the membranes. Diffusion in membranes is a complex topic, and the appropriate model depends on the chemical structure of the quencher. For small nonpolar quenchers, the membrane can be considered to be a three-dimensional system with the quencher diffusing freely. The situation changes if the quencher is a lipid, such as the bromo-PCs (Figure 8.27). In this case the quencher will be limited to lateral diffusion within a plane, which requires a different theory.

The theory for two-dimensional diffusion in membranes is complex. Analytical expressions are now available for the time-dependent decays of fluorophores in membranes, with the quenchers constrained to lateral diffusion in two dimensions.[97–102] The time-dependent decays expected for Smoluchowski quenching in two dimensions, and for the radiation model, have been reported.[97–100] For the usual assumption of instantaneous quenching on fluorophore-quencher contact, the intensity decay is given by

$$\ln\frac{I(t)}{I_0(t)} = -\gamma t - \frac{1}{2}R^2[Q]Q(t/\tau_q) \qquad (8.44)$$

where

$$Q(t/\tau_q) = \frac{16}{\pi}\int_0^\infty \frac{1-\exp(-(t/\tau_q)x^2)}{J_0^2(x)+Y_0^2(x)}\frac{dx}{x^3} \qquad (8.45)$$

In these expressions γ is the reciprocal of the unquenched decay time, $[Q]$ is the quencher concentration in molecules/Å^2, R is the interaction radius, and $\tau_q = R^2/D$, where D is the mutual diffusion coefficient. $J_0(x)$ and $Y_0(x)$ are zero-order Bessel functions of the first and second kinds, respectively. Even more complex expressions are needed for the radiation model. Because of the difficulties in evaluating eqs. 8.44–8.45, several approximate analytical expressions have been proposed.[98-99]

8.12. QUENCHING-RESOLVED EMISSION SPECTRA

8.12.1. Fluorophore Mixtures

The emission spectra of proteins often shift in the presence of quenching. This effect occurs because the various trp residues are differently exposed to the aqueous phase and thus differently accessible to quenchers. Alternatively, if a solution contains two fluorophores with different Stern-Volmer quenching constants, it will show different amounts of quenching at each wavelength depending on the relative amplitudes of the emission spectra. This concept of wavelength-dependent quenching has been extended to calculation of the underlying emission spectra from the quenching constant at each wavelength.[103–106] This is accomplished by measuring a Stern-Volmer plot of each emission wavelength (λ). For more than one fluorophore the wavelength-dependent data can be described by

$$\frac{F(\lambda)}{F_0(\lambda)} = \sum_i \frac{f_i(\lambda)}{1+K_i(\lambda)[Q]} \qquad (8.46)$$

where $f_i(\lambda)$ is the fractional contribution of the ith fluorophore to the steady-state intensity at wavelength λ to the unquenched emission spectrum, and $K_i(\lambda)$ is the Stern-Volmer quencher constant of the ith species at λ. For a single fluorophore the quenching constant is usually independent of emission wavelength, $K_i(\lambda) = K_i$.

In order to resolve the individual emission spectra the data are analyzed by nonlinear least squares. Typically one performs a global analysis in which the K_i values are global, and the $f_i(\lambda)$ values are variable at each wavelength. By global we mean that the quenching constant is the same for each fluorophore irrespective of the emission wavelength. The result of the analysis is a set of K_i values, one for each component, and the fractional intensities $f_i(\lambda)$ at each wavelength with $\Sigma f_i(\lambda) = 1.0$. The values of $f_i(\lambda)$ are used to calculate the emission spectrum of each component:

$$F_i(\lambda) = f_i(\lambda)F(\lambda) \qquad (8.47)$$

where $F(\lambda)$ is the steady-state emission spectrum of the sample.

The use of quenching to resolve emission spectra is illustrated by a sample containing both 1,6-diphenyl-1,3,5-hexatriene (DPH) and 5-((((2-iodoacetyl)amino)ethyl)-amino)naphthalene-1-sulfonic acid (I-AEDANS). DPH is not soluble in water, so the DPH is expected to be dissolved in the SDS micelles (Figure 8.36). I-AEDANS is water soluble and negatively changed, so it is not expected to bind to the negatively charged SDS micelles. Hence, I-AEDANS is expected to be quenched by the water soluble quencher acrylamide, and DPH is not expected to be accessible to acrylamide quenching.

Acrylamide Stern-Volmer plots for the separate solution of DPH-SDS and I-AEDANS are shown in Figure 8.37. As predicted from the low solubility of DPH in water

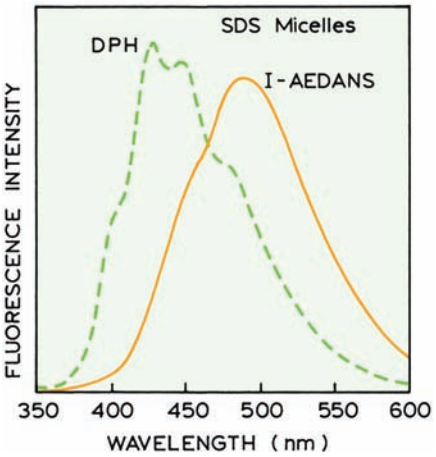

Figure 8.36. Steady-state emission spectra of (dashed) diphenylhexatriene (DPH) and (solid) I-AEDANS in 1.2 mM SDS micelles at 23°C. The concentration of diphenylhexatriene was 2 μM, that of I-AEDANS 170 μM. The excitation wavelength was 337 nm. Revised from [103].

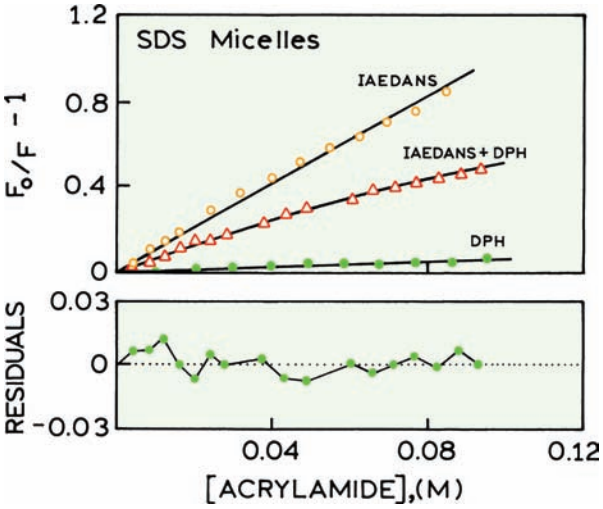

Figure 8.37. Stern-Volmer plots for acrylamide quenching of I-AEDANS, DPH, or I-AEDANS and DPH, in SDS micelles. For the mixture the solid line represents the fit with calculated parameters K_1 = 9.9 M^{-1}, K_2 = 0 M^{-1}, f_1 = 0.69, f_2 = 0.31. The lower panel shows the residuals for these values. Revised from [103].

and the high solubility of acrylamide in water, DPH is weakly quenched by acrylamide. In contrast, I-AEDANS is strongly quenched. The extent of quenching for the mixture is intermediate between that observed for each probe alone. As expected for a mixture of fluorophores, the Stern-Volmer plots curve downward due to the increasing fractional contribution of the more weakly quenched species at higher quencher concentrations.

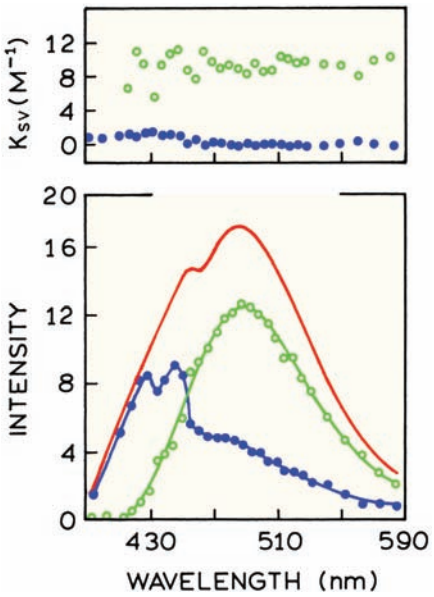

Figure 8.38. Quenching resolved emission spectra of the DPH-I-AEDANS mixture (bottom). The solid line shows the emission spectrum of the mixture. The upper panel shows the wavelength-dependent quenching constant, with average values of K_1 = 9.6 M^{-1} and K_2 = 0.47 M^{-1}. Revised from [103].

The curvature in the Stern-Volmer plots are used to recover the values of $K_i(\lambda)$ and $f_i(\lambda)$ at each wavelength. In this case the $K_i(\lambda)$ values were not used as global parameters, so that $K_1(\lambda)$ and $K_2(\lambda)$ were obtained for each wavelength. At wavelengths above 420 nm there were two values of 0.47 and 9.6 M^{-1}, representing the quenching constants of DPH and I-AEDANS, respectively. At the shortest wavelength below 420 nm there is only one $K_i(\lambda)$ value because only DPH emits. The recovered values of $f_i(\lambda)$ were used to calculate the individual spectra from the mixture (Figure 8.38). In Chapters 4 and 5 we showed how the component spectra for heterogeneous samples could be resolved using the time-domain or the frequency-domain data. The use of wavelength-dependent quenching provides similar results, without the use of complex instrumentation. Of course, the method depends on the probes being differently sensitive to collisional quenching, which requires that the decay times and/or accessibility to quenchers be different.

8.12.2. Quenching-Resolved Emission Spectra of the E. Coli Tet Repressor

The tet repressor from *E. coli* is a DNA-binding protein that controls the expression of genes that confer resistance to

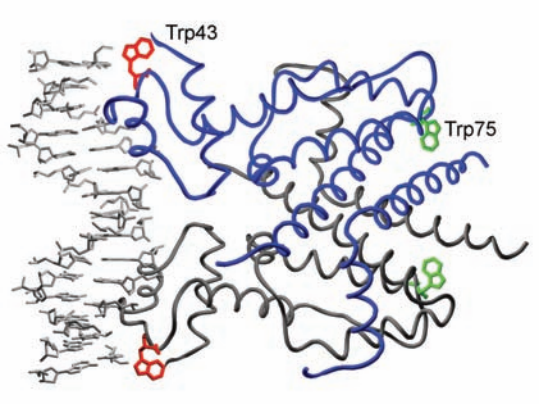

Figure 8.39. Three-dimensional structure of the *E. coli* tet repressor. The position of a bound DNA oligomer is shown for Problem 8.10. Figure courtesy of Dr. Oliver Scholz from the Friedrich-Alexander University of Erlangen-Neuremberg, Germany.

tetracycline. This protein is a symmetrical dimer that contains two tryptophan residues in each subunit at positions 43 and 75 (Figure 8.39). W43 is thought to be an exposed residue, and W75 is thought to be buried in the protein matrix.[107] Earlier studies of single-tryptophan mutants of the tet repressor confirmed the accessibility of W43 to iodide and the shielding of W75 from iodide quenching.[108] Hence, this protein provided an ideal model protein to attempt quenching resolution of the individual emission spectra of two tryptophan residues in a protein.

Iodide Stern-Volmer plots for the tet repressor were measured for various emission wavelengths[107] (Figure 8.40). A larger amount of quenching was observed at longer wavelengths. When analyzed in terms of two components, one of these components was found to be almost inaccessible to iodide. At 324 nm the recovered values for the more accessible fractions are $f_1 = 0.34$ and $K_1 = 16.2$ M^{-1}. For the inaccessible fraction the values are $f_2 = 0.66$ and $K_2 = 0$. The wavelength-dependent data were used to calculate the individual spectra (Figure 8.41). The blue-shifted emission with a maximum of 324 nm corresponds to the inaccessible fraction, and the red-shifted spectrum at 349 nm is the fraction accessible to iodide quenching. These emission spectra are assigned to W75 and W43, respectively. The results in Figure 8.41 (top) illustrate one difficulty often encountered in determination of quenching-resolved spectra. The quenching constant for a single species can be dependent on emission wavelength. In this case the quenching constant of the accessible tryptophan changed about twofold across its emission spectrum. When this occurs the values of $K_i(\lambda)$ cannot be treated as global parameters.

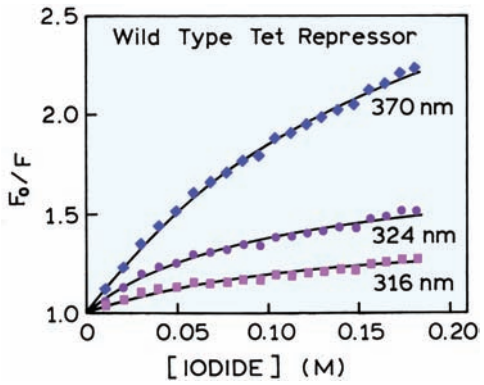

Figure 8.40. Iodide Stern-Volmer plots for the wild type tet repressor. The solution contained 1 mM sodium thiosulfate to prevent formation of I_2. From [107].

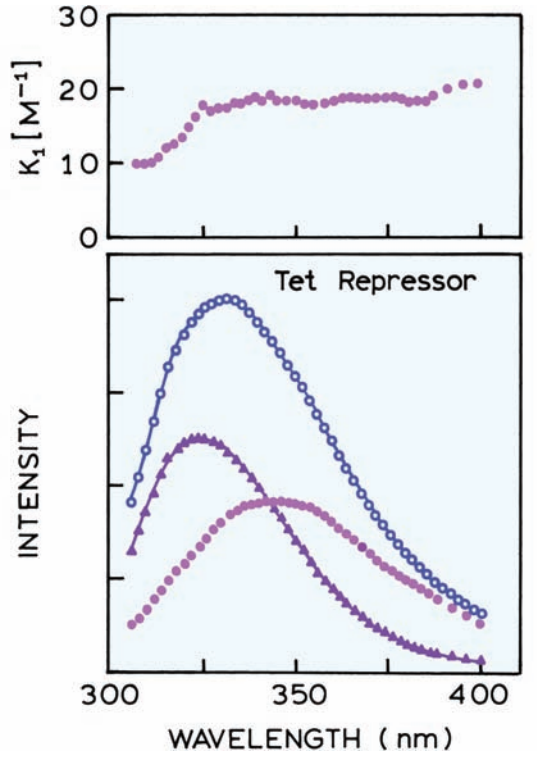

Figure 8.41. Fluorescence quenching-resolved spectra of wild-type tet repressor using potassium iodide as the quencher. The solid line is the unquenched emission spectrum. Top: wavelength-dependent values of K_1. From [107].

Single-tryptophan mutants of the tet repressor were used to study the accessibility of each trp residue to iodide quenching (Figure 8.42). Little if any quenching was observed for the protein containing only tryptophan 75, and tryptophan 43 was readily quenched by iodide.[109] Iodide

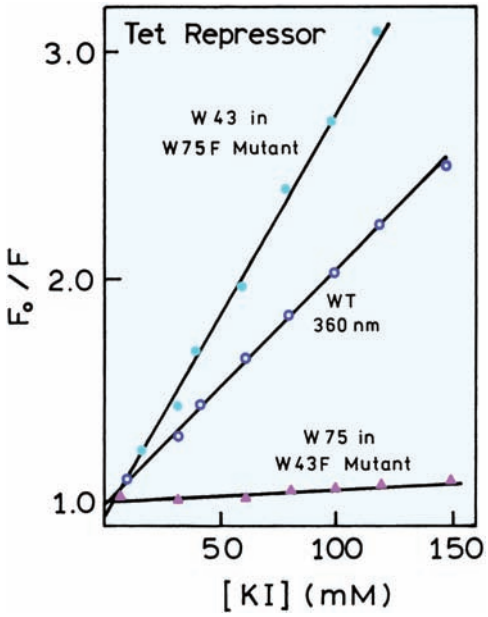

Figure 8.42. Stern-Volmer plots for the iodide quenching of *E. coli* tet repressor (wild type, WT) and its mutants (W75F and W43F). Revised from [108].

quenching of the wild-type protein is intermediate between the two single-tryptophan mutants. These results are consistent with those obtained from the quenching-resolved emission spectra. While the same information is available from the mutant proteins, the use of quenching provided the resolved spectra using only the wild-type protein.

It is valuable to notice a difference in the method of data analysis for the modified Stern-Volmer plots (Section 8.8.1) and for the quenching-resolved emission spectra. In a modified Stern-Volmer plot one assumes that a fraction of the fluorescence is totally inaccessible to quenchers. This may not be completely true because one component can be more weakly quenched, but still quenched to some extent. If possible, it is preferable to analyze the Stern-Volmer plots by nonlinear least squares, when the f_i and K_i values are variable. This approach allows each component to contribute to the data according to its fractional accessibility, instead of forcing one to be an inaccessible fraction. Of course, such an analysis is more complex, and the data may not be adequate to recover the values of f_i and K_i at each wavelength.

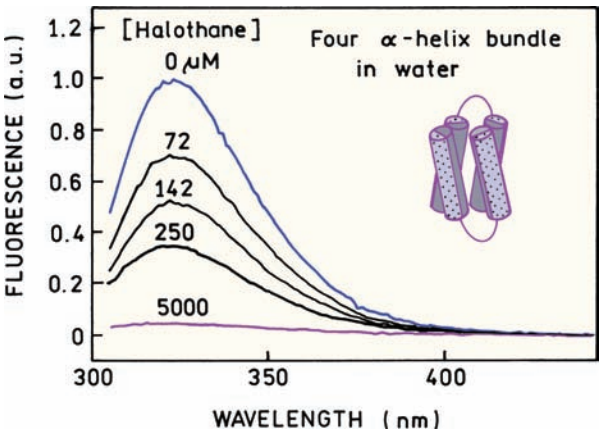

Figure 8.43. Emission spectra of a four α-helix bundle in water in the presence of halothane. Each peptide chain contains one tryptophan residue. Revised from [114].

8.13. QUENCHING AND ASSOCIATION REACTIONS

8.13.1. Quenching Due to Specific Binding Interactions

In the preceding sections we considered quenchers that were in solution with the macromolecule but did not display any specific interactions. Such interactions can occur, and often appear to be of static quenching.[110–115] One example is provided by a synthetic peptide which spontaneously forms a four α-helical bundle in aqueous solution (Figure 8.43). The bundle consists of two peptide chains. Each peptide chain contains two α-helical regions and a single tryptophan residue.[114] The general anesthetics are nonpolar and were expected to bind to the central nonpolar region of the four helix bundles.

The effects of halothane on the emission intensity of the four-helix bundle are shown in Figure 8.43. The emission is strongly quenched by even low concentrations of halothane. Quenching of the trp residues was also examined in the presence of 50% trifluoroethanol (TFE). Halothane quenching is much less efficient in this solvent (Figure 8.44). TFE is known to disrupt hydrophobic interactions but to enhance helix formation in peptides. In 50% TFE the peptide is expected to exist as two separate α-helical peptides that are not bound to each other. These results show that the trp residues are buried in a nonpolar region in the four-helix bundle and become exposed to the solvent phase when the two peptides dissociate.

How can one determine whether the quenching seen for the helix bundle in water is due to halothane binding, or to collisional quenching? One method is to calculate the apparent bimolecular quenching constant (k_q^{app}). Assume the decay time of trp residues in the bundle is near 5 ns. The

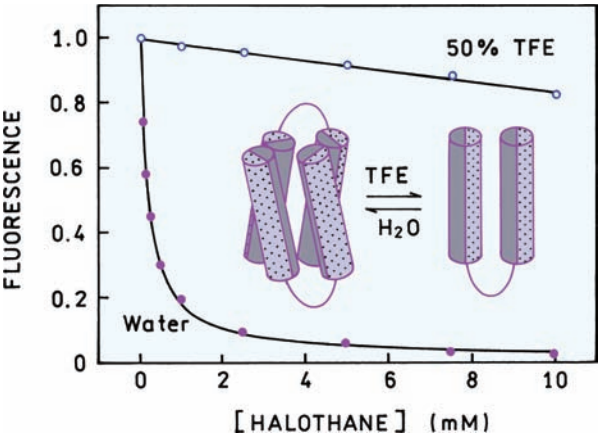

Figure 8.44. Tryptophan fluorescence intensities of the four α-helix bundle in the presence of halothane. Revised from [114].

data in Figure 8.43 indicate that the trp residues are about 50% quenched at 142 μM halothane. This corresponds to a Stern-Volmer quenching constant of K_{SV} = 7042 M^{-1}, which is two to three orders of magnitude larger than possible for diffusion-limited quenching in water. These results show that hydrophobic interactions of halothane result in the appearance of static quenching of the trp residues. These interactions result in an increase in the local concentration of halothane near the trp residues, as shown in the molecular dynamics snapshot of this system (Figure 8.45).

At a more microscopic level there may still be a dynamic component to the quenching. There is no reason to expect the formation of ground-state complexes between the trp and halothane. Hence the quenching may be dynamic but due to diffusion motions of halothane within the hydrophobic region of the bundle. There is not always a clear distinction between static and dynamic quenching. Actual and apparent complex formation may be distinguished from the absorption spectra, which is only expected to change for actual formation of ground-state complexes.

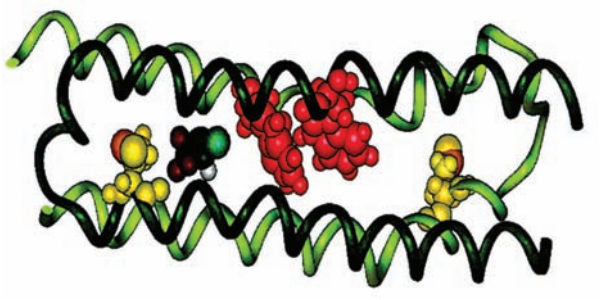

Figure 8.45. Molecular dynamic snapshot of the four α-helix bundle with one bound halothane molecule. The two peptides are shown in light and dark green, the tryptophans are red and the methionines are yellow-orange. The halothane molecule contains the multicolor spheres. Reprinted from [114]. Courtesy of Dr. Jonas Johansson from the University of Pennsylvania, USA.

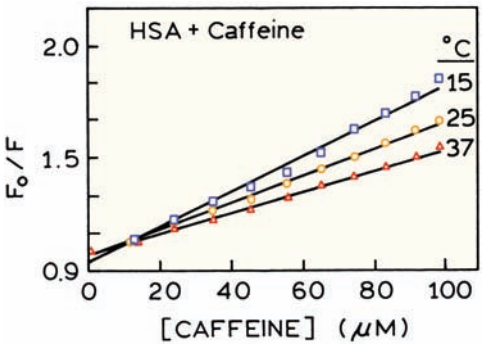

Figure 8.46. Quenching of HSA by caffeine. Revised from [113].

Another example of quenching due to a specific binding interaction is shown for binding of caffeine to HSA, an experiment most of us start each morning (Figure 8.46). The Stern-Volmer plots show a value of K_{SV} = 7150 M^{-1}. This value is obviously too large to be due to collisional quenching, especially for a lifetime near 5 ns. The apparent value of k_q^{app} is 1.4 x 10^{12}, over 100-fold larger than the maximum diffusion limited rate. Hence, the caffeine must be bound to the HSA. Caffeine is an electron-deficient molecule, and may form ground-state complexes with indole. This possibility could be tested by examination of the absorption spectra of HSA in the absence and presence of caffeine. If ground-state association with indole occurs, then the trp absorption spectrum is expected to change. Another indicator of complex formation is the temperature dependence of the Stern-Volmer plots. For diffusive quenching one expects more quenching at higher temperatures. In the case of HSA and caffeine there is less quenching at higher temperatures (Figure 8.46), which suggests the complex is less stable at higher temperatures.

8.14. SENSING APPLICATIONS OF QUENCHING

Fluorescence quenching has been used for sensing of a wide variety of analytes including oxygen, NO, and heavy metals. Fluorescence sensing is discussed in more detail in Chapter 19. The use of collisional quenching for sensing is illustrated by chloride-sensitive fluorophores.

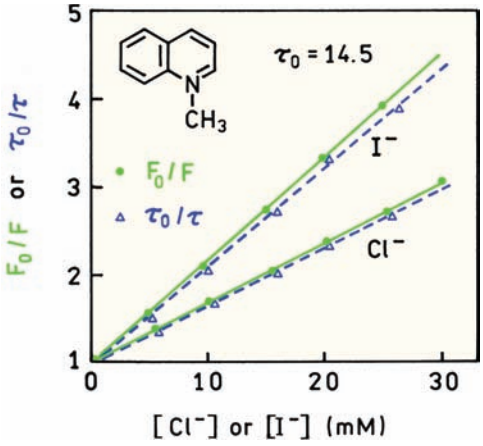

Figure 8.47. Chloride and iodide quenching of N-methylquinolinium iodide. The amount of iodide from the fluorophore is not significant. Revised from [123].

8.14.1. Chloride-Sensitive Fluorophores

Chloride is an important biological anion that plays a role in fluid adsorption, neuronal processes, and cellular pH. There has been extensive development of chloride-sensitive fluorophores for analytical and biochemical applications.[116–122] These chloride-sensitive fluorophores are usually based on a quinolinium or acridinium structure, with additional groups to modify the solubility or sensitivity of the fluorophore to quenching. Chloride quenching is usually collisional, as can be seen in Figure 8.47. This figure shows Stern-Volmer plots for quenching of N-methylquinolinium iodide (MAI) by chloride or iodide.[123] The equivalent decrease in intensity and lifetime shows that the quenching is collisional and complex formation does not occur.

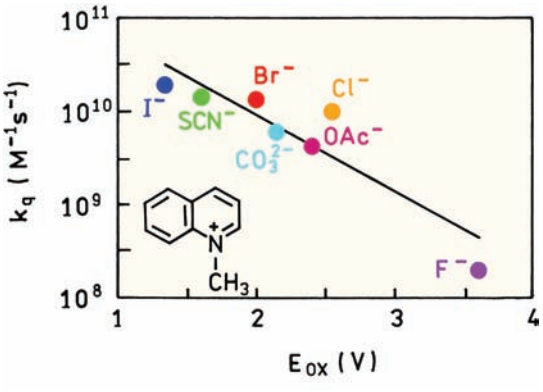

Figure 8.48. Bimolecular quenching constants for N-methylquinolinium iodide. Revised from [123].

Iodide appears to quench more strongly than chloride. Since the diffusion coefficients of chloride and iodide are similar, this result indicates that iodide is a more efficient quencher. The mechanism of quenching is most probably electron transfer from the anion to the fluorophore, which suggests the quenching efficiency should depend on the oxidation potential of the quencher. Figure 8.48 shows bimolecular quenching constants for MAI and several quenchers. The quenching efficiency is highest for iodide, which is easily oxidized. Quenching by fluoride is much less efficient because it is more difficult to remove an electron from the highly electronegative fluoride ion.

The quenching efficiencies for a charge-transfer mechanism is expected to depend on the free energy charge for the reaction (Chapter 9). For a charge-transfer process the free energy change is given by[124]

$$\Delta G \text{ (eV)} = E_{ox}(D^+/D) - E_{red}(A/A^-) - E_{00} + C \quad (8.48)$$

where E_{ox} is the oxidation potential of the electron donor, which in this case is the quencher. E_{red} is the reduction potential of the electron acceptor, which is the fluorophore. E_{00} is the singlet energy of the fluorophore, and C is a constant that accounts for the energy release due to the charge separation interaction of the charges with the solvent. As the oxidation potential increases, the value of ΔG becomes less negative and quenching becomes less efficient. The quenching efficiencies do not correlate precisely with eq. 8.48, because electron exchange and heavy atom effects are also present, but for this class of probes charge-transfer is the dominant mechanism for quenching by halides. Knowledge of the quenching mechanism is valuable because it allows rational design of fluorophores with the desired sensitivity to halides. For instance, substitutions on the quinolinium ring that decrease the affinity for electrons are likely to decrease the quenching efficiency.

8.14.2. Intracellular Chloride Imaging

Chloride-sensitive fluorophores have found use for measurements of intracellular chloride and for imaging the local chloride concentrations.[125–126] When using fluorescence microscopy for imaging it is difficult to use the local intensity values because of photobleaching and the unknown probe concentrations at each position in the cells. In contrast to probes for pH, calcium, and other cations (Chapter 14), collisionally quenched probes do not show spectral shifts. Direct wavelength-ratiometric probes for chloride are not available.

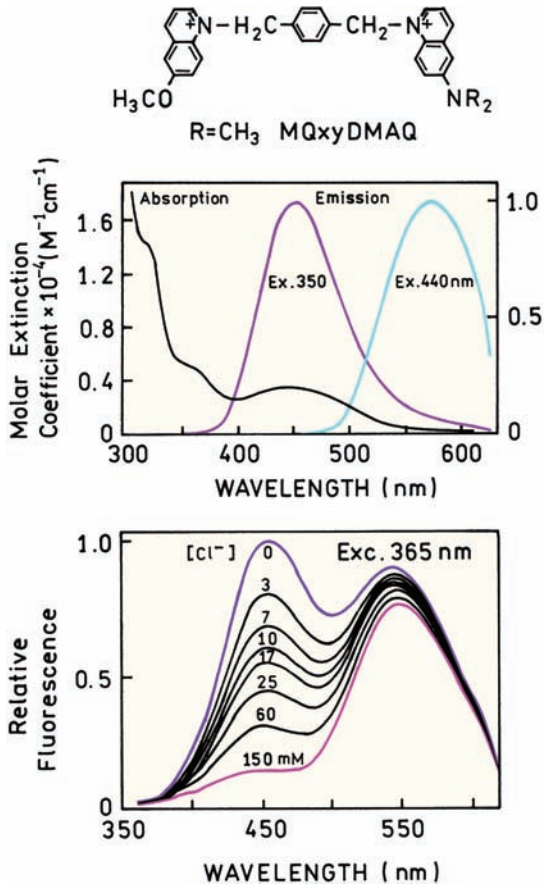

Figure 8.49. Structure and spectra of a wavelength-ratiometric chloride probe. Revised from [129].

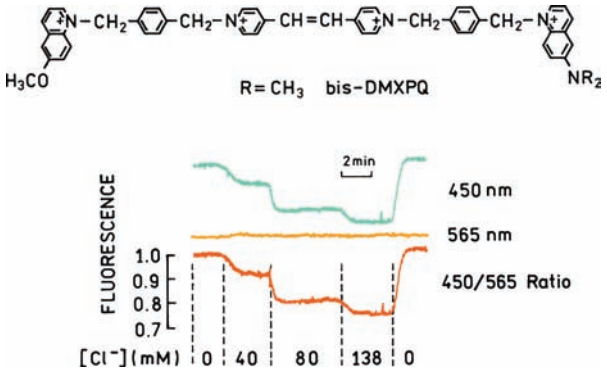

Figure 8.50. Structure and intracellular calibration of the chloride probe bis-DMXPQ. Revised from [129].

Knowledge of the mechanism of chloride quenching has allowed the design of wavelength-ratiometric chloride probes.[127–129] This was accomplished by linking two fluorophores, one which is quenched by chloride and one which is not sensitive to chloride (Figure 8.49). This probe contains two quinoline rings. The methoxy-substituted ring on the left readily accepts electrons and is quenched by chloride. The ring on the right, with the amino group, does not accept electrons from chloride and is not quenched. The lower panel shows the emission spectra of MQxyDMAQ in the presence of increasing chloride concentrations. The shorter-wavelength emission is quenched, but the longer-wavelength emission is not sensitive to chloride. Examination of the spectra in Figure 8.49 suggests that there will be RET from the MQ to the DMAQ ring. In this probe some energy transfer occurs, which reduces the lifetime of the MQ ring and makes it less sensitive to quenching by chloride. However, the RET efficiency is modest, so that the MQ ring remains sensitive to chloride.

When used in an intracellular environment, the sensitivity of a probe can change from its sensitivity in a pure solution. For this reason the chloride-sensitive probes were calibrated in cells by changing the intracellular chloride concentration. This is accomplished by exposing the membrane permeability of the 3T3 fibroblast cells using valinomycin and other similar compounds, followed by exposing the cells to different chloride concentrations (Figure 8.50). The intensity of the short-wavelength MQ emission at 450 nm is decreased as the chloride concentration increases. The intensity of the long-wavelength emission at 565 nm is not affected.

The wavelength-ratiometric chloride probes were used to measure local chloride concentrations in CHO cells (Figure 8.51). This was accomplished by collecting the intensity images at 450 and 565 nm. The intensity at 450 nm will be sensitive to the local chloride concentration.[129] However, the image at 450 nm alone does not allow the chloride concentrations to be determined because the concentration of the probe can be different in each region of the cell. The concentration of chloride can be determined from the ratio of the emission intensities. These images show that the chloride concentrations in these cells is rather uniform, with a somewhat lower chloride concentration in the nuclei.

8.14.3. Chloride-Sensitive GFP

Green fluorescent protein (GFP) and its mutants are widely used to study gene expression and as sensors.[130–131] A yellow variant of GFP (YFP) is known to be sensitive to chloride.[132–133] The intensity of YFP-H148Q decreases progressively in response to added chloride in a manner and concentration range that suggests collisional quenching (Figure

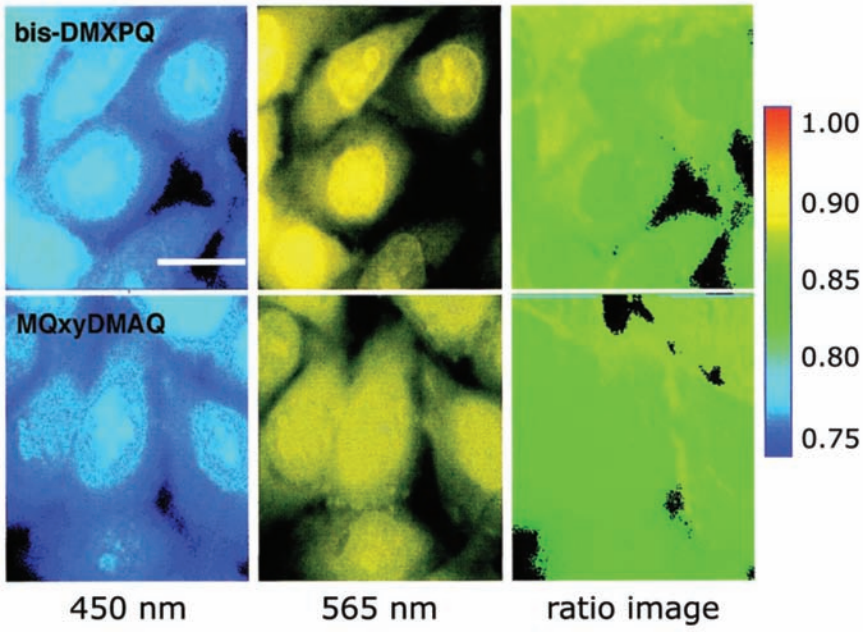

Figure 8.51. Fluorescence microscopy images of CHO cells labeled with the chloride probes. The intensities of 450 and 565 nm were color coded for clarity. The images on the right are the chloride concentrations calculated from the intensity ratios. Reprinted with permission from [129].

8.52). The extent of quenching depends on pH, which is not expected for collisional quenching. Additionally, the chromophore in GFP is known to be buried in a β-barrel structure (Figure 8.53) and not expected to be accessible to freely diffusing chloride. These considerations suggest that the chloride sensitivity of this YFP is not due to collisional quenching.

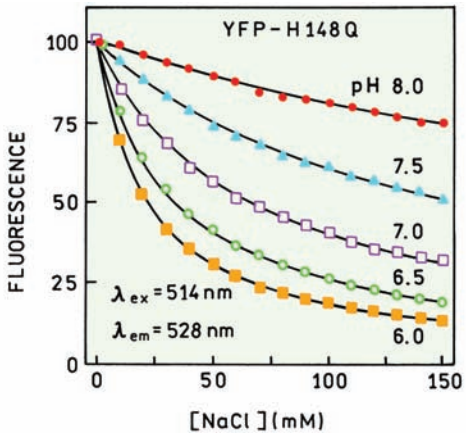

Figure 8.52. Fluorescence intensity of YFP-H148Q in the presence of NaCl. Revised from [132].

Figure 8.54 shows the absorption spectra of YFP-H148Q in the presence of chloride. As [Cl^-] increases the absorption at the excitation wavelength 514 nm decreases, and the short-wavelength absorption increases. There appears to be an isoelectric point near 430 nm, which indicates the presence of two species. It appears that chloride changes the structures or conformation of the protein or chromophore, decreasing the absorbance and giving the appearance of quenching. The x-ray structure has been solved with bound iodide ions (Figure 8.53), one of which is next to the chromophore. An iodide or chloride next to the chromophore might result in static quenching. However, static quenching by chloride is not the reason for the chloride sensitivity of YFP. For YFP the apparent quenching by chloride is due to a change in the structure of the chromophore. It is now thought that chloride binds near the chromophore in contact with the imidizolinone oxygen atom. This binding probably forces the equilibrium to the left side in Figure 8.54. The larger amount of chloride quenching at lower pH (Figure 8.52) is consistent with protonation of the phenolic oxygen upon binding of chloride. Hence the apparent quenching of YFP by chloride in Figure 8.52 is not due to collisional or static quenching, but instead due to a specific binding interaction which changes the structure of the chromophore.

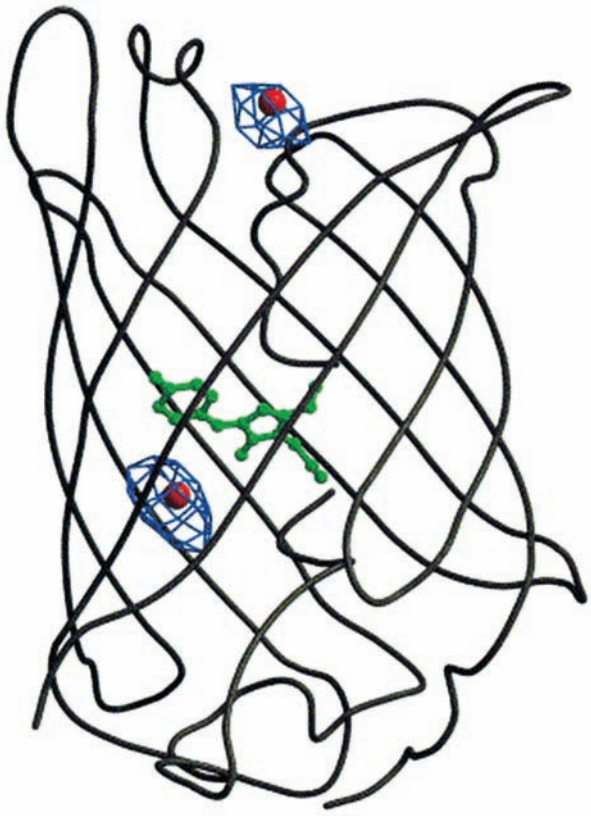

Figure 8.53. Three-dimensional structure of yellow fluorescent protein YFP-H48Q. The solid line is the peptide backbone, and the green structure is the native chromophore. The red and blue surfaces show the location of bound iodide ions. Reprinted with permission from [132].

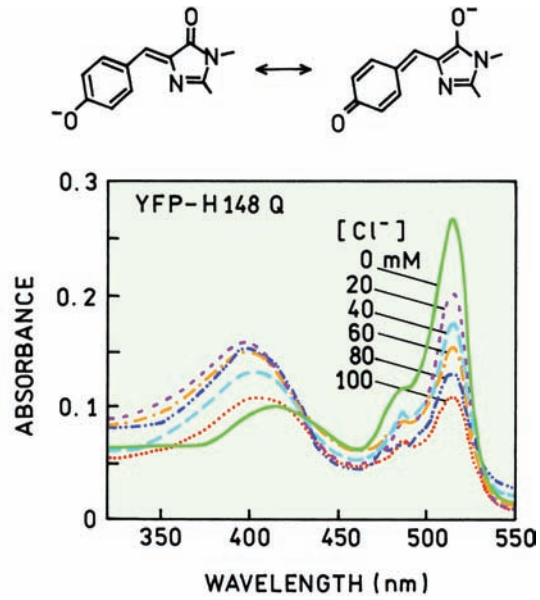

Figure 8.54. Absorption spectra of YFP-H148Q in the presence of NaCl, pH 6.4. Binding of chloride is thought to stabilize the right side structure in the upper panel. Revised from [133].

As discussed in Chapter 19, a wide variety of fluorophores are available that can be used for intracellular sensing. It is difficult to use these probes in an intracellular environment because they are likely to bind to macromolecules that can shift the analyte calibration curves. GFP and its variants are promising intracellular sensors because the chromophore is buried in the β-barrel and unable to interact directly with biomolecules. With this consideration in mind, YFP-H148Q was used to measure the intracellular pH of Swiss 3T3 fibroblasts.[133] An advantage of GFP is that the probe is synthesized by the cell itself, and not added to the cells. The fibroblast were transfected with the gene for YFP-H148Q, which appeared as a bright green fluorescence in the epifluorescence microscope (Figure 8.55). The response of the protein to pH and chloride was tested using ionophores to modify the internal ion concentrations.[133] When excited at 480 nm the emission intensity decreased with increasing pH and decreased with increasing chloride concentrations. These remarkable results show that it is now possible to insert genes that cause the cells to synthesize their own fluorophores, and the genetically engineered protein-fluorophore can be designed to have sensitivity to a desired analyte.

8.14.4. Amplified Quenching

Collisional quenching was useful for sensing and imaging of chloride because of its high physiological concentration. However, quenching does not usually provide high sensitivity detection.[134] However, it is now possible to amplify quenching to obtain higher sensitivity detection.[135] Amplification is accomplished in two ways. The fluorophore is bound to a fluorescent conjugated polymer (Figure 8.56). In this case the polymer contained conjugated stilbene residues. This polymer was found to be highly sensitive to quenching by the PET acceptor methylviologen (MV^{2+}). The Stern-Volmer quenching constant is near 10^7 M^{-1}, which is clearly too large for collisional quenching.

There are two reasons for the large quenching constant. The positively charged MV^{2+} binds electrostatically to the polymer. Secondly, the excited state migrates rapidly between the stilbene residues. If any one residue is excited this energy migrates until it encounters the bound MV^{2+}. One MV^{2+} quenches the emission from about 1000 stil-

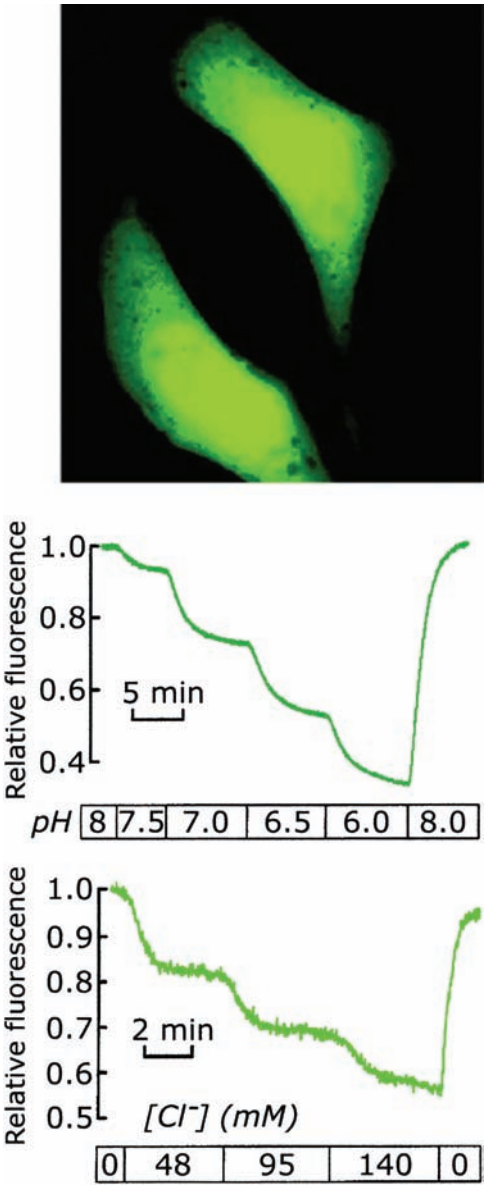

Figure 8.55. pH and chloride sensing using YFP-H148Q in Swiss 3T3 fibroblasts. Reprinted with permission from [133].

benes, resulting in nearly complete quenching at low MV^{2+} concentrations.

Amplified quenching can be applied to sensing by the addition of specific binding partners. This was accomplished by covalent linkage of MV^{2+} to biotin (B–MV^{2+}). Protein-bound MV^{2+} also quenched the polymer with high sensitivity (Figure 8.57). The polymer fluorescence returned when B-MV^{2+} was removed from the polymer by avidin. One can imagine this approach being used in protein or nucleic acid binding assays.

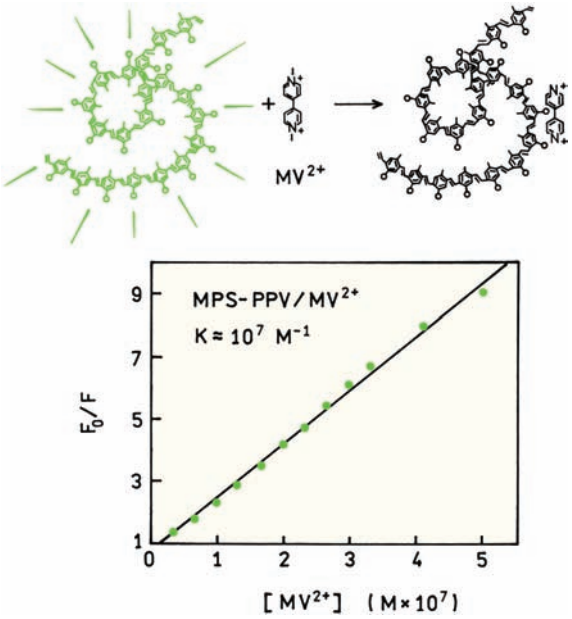

Figure 8.56. Quenching of a conjugated stilbene polymer by methylviologen. Revised from [135].

8.15. APPLICATIONS OF QUENCHING TO MOLECULAR BIOLOGY

During the past decade there have been many advances in the use of sensing for DNA analysis (Chapter 21). Many of these applications depend on RET, but some make use of quenching. A typical situation is the need to detect a target oligomer of known sequence in a sample containing many sequences. Detection of the target oligomer is usually accomplished by synthesis of a probe oligomer with the complementary sequence. The probe oligomer also contains bound fluorophores that display spectral changes upon hybridization with the target oligomers. The spectral changes can be due to RET, intercalation or quenching.

8.15.1. Release of Quenching Upon Hybridization

One approach to target detection is to change the extent of quenching upon hybridization. One example is shown in Figure 8.58.[136] In this case the fluorescein label is quenched by a nearby pyrene residue. In the absence of target DNA the fluorescence is quenched by the pyrene. Upon binding to the target sequence the pyrene intercalates into the double helical DNA, resulting in a several-fold increase in the fluorescein emission. This approach is general and could be used with a variety of fluorophore-quencher pairs.

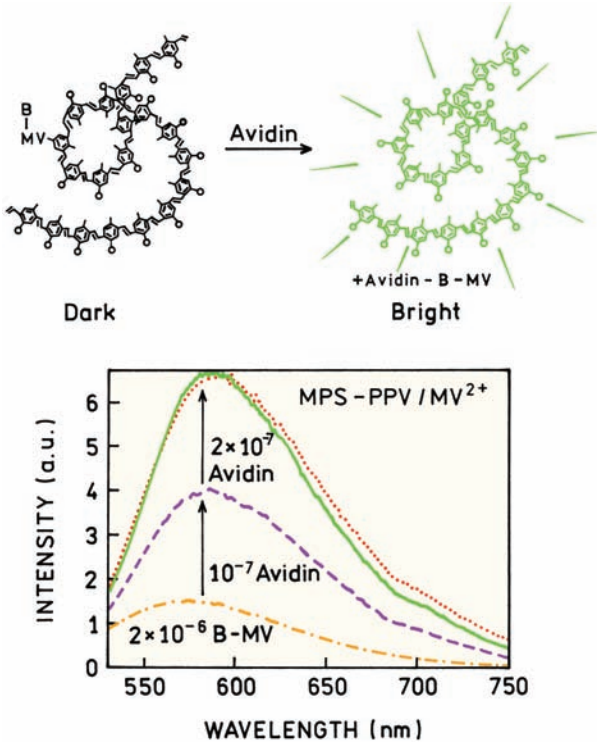

Figure 8.57. Reversal of biotin–methylviologen quenching by avidin. Revised from [135].

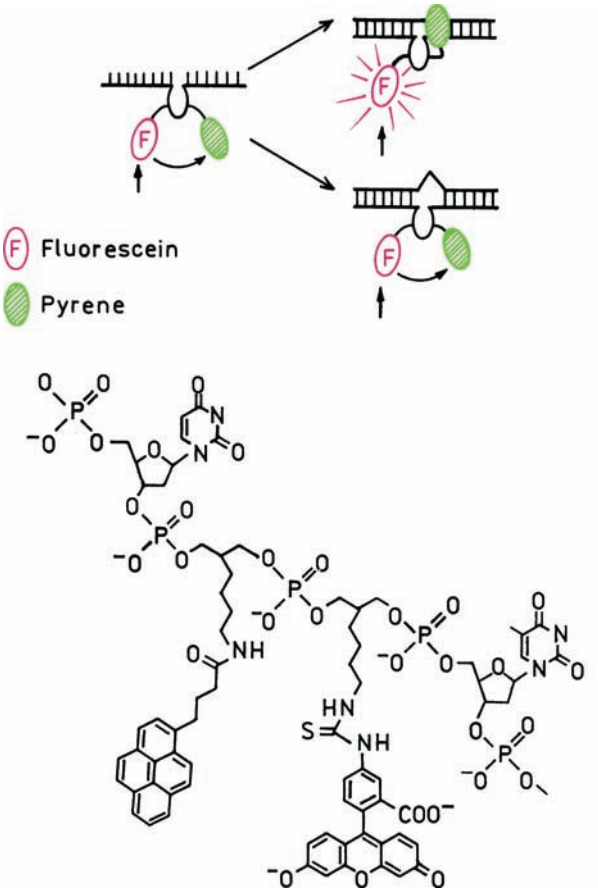

Figure 8.58. Molecular beacon based on release of quenching upon hybridization. Revised from [136].

8.15.2. Molecular Beacons in Quenching by Guanine

Among the nucleic acid bases guanine shows efficient quenching of many fluorophores. This quenching is probably due to photoinduced electron transfer.[137–139] The other bases can also act as quenchers, but are usually much less efficient. Figure 8.59 shows Stern-Volmer plots for four fluorophores with dGMP as the quencher. This result shows that quenching by guanine is not limited to a single fluorophore but can occur with many fluorophores. Among these four probes MR121 is the most sensitive to quenching by dGMP. Among the four nucleotide manophosphates, dGMP is the most efficient quencher, with the others having no quenching effect on MR121.

Quenching by guanine was used to design a molecular beacon.[140] The fluorophore JA242 was positioned at one end of the beacon, and the other end was terminated with several guanine residues. The residues quench the fluorophore when in the folded state (Figure 8.60). The emission intensity increases about fivefold when the beacon is unfolded and hybridized with the target sequence.

8.15.3. Binding of Substrates to Ribozymes

Quenching by guanine has also been applied to structural studies of RNA. In contrast to DNA, RNA is rather flexible and frequently forms base-paired regions within a single strand of RNA. Single strands of RNA can adopt well-defined three-dimensional structures in solution, similar to the folding behavior of peptide chains. One type of structural RNAs are the ribozymes, which display catalytic enzyme-like behavior.

The catalytic properties of these highly structured RNAs was first reported in 1982, showing that certain RNAs displayed autocatalytic activity. Since that time there have been numerous studies of ribozymes and their catalytic behavior. One example is the hairpin ribozyme that cleaves single-stranded RNA (Figure 8.61). The observations of quenching by quanosine nucleotides[17–18] (Section 8.5) suggested the use of guanine quenching to study substrate binding to ribozymes. The substrate contained a fluo-

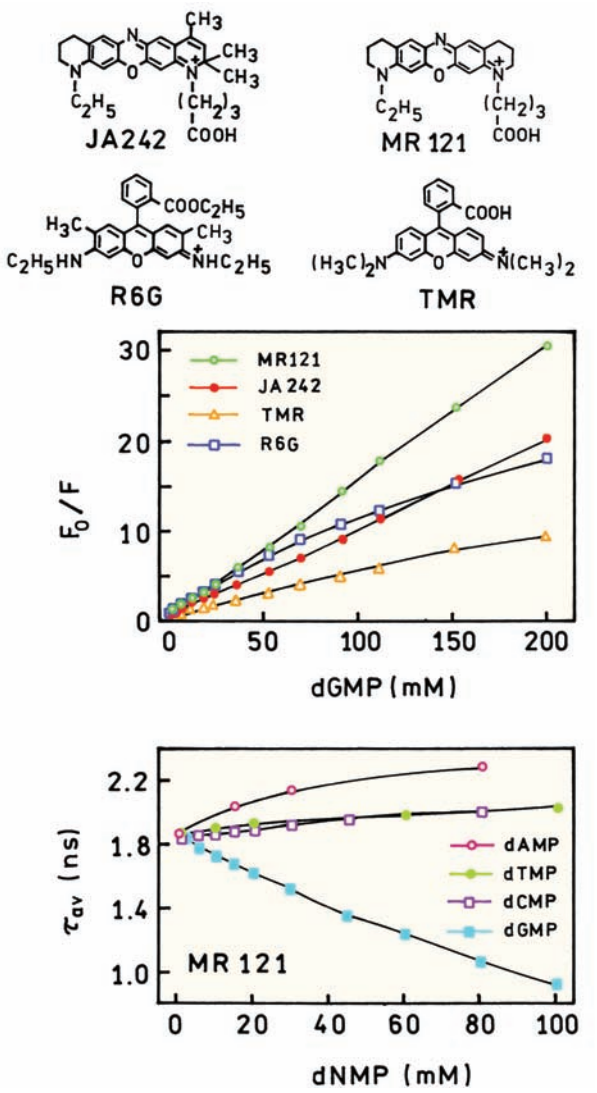

Figure 8.59. Quenching of four fluorophores by dGMP (top). Quenching of MR121 by four nucleotide monophosphates (bottom). Revised from [139].

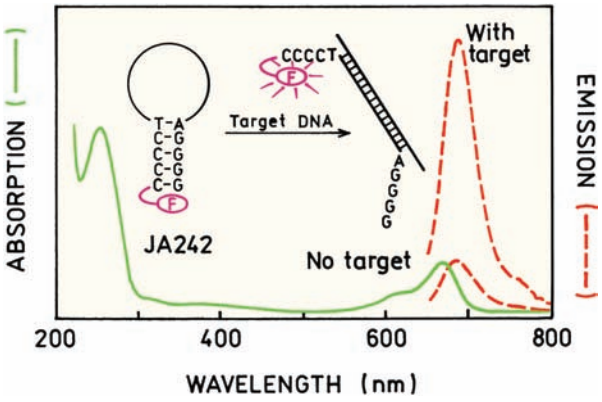

Figure 8.60. Absorption and emission spectra of a molecular beacon based on guanine quenching of JA242. Revised and reprinted with permission from [140]. Copyright © 2000, American Chemical Society.

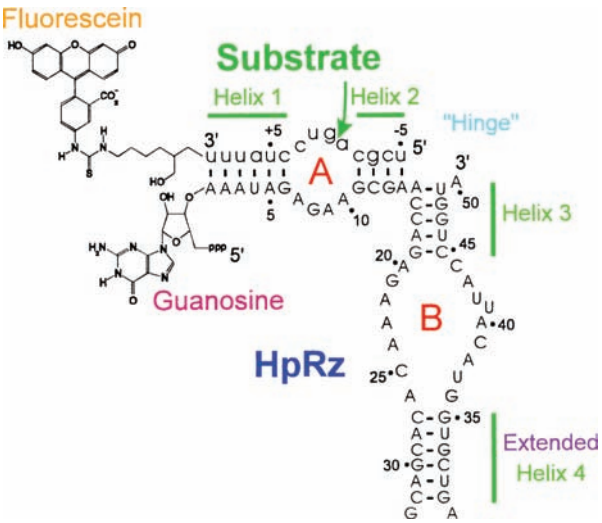

Figure 8.61. Structure of the hairpin ribozyme (HpRz) and the fluorescein-labeled substrate. The substrate-binding strand is the region adjacent to the substrate. Reprinted with permission from [141]. Copyright © 1997, Cambridge University Press.

rescein residue covalently linked at the 3' end (Figure 8.61). The hairpin ribozyme contains a guanosine residue at the 5N end. Upon binding of substrate nucleotide to the ribozyme, the fluorescein emission is quenched (Figure 8.62). Quenching also occurs when the fluorescein-labeled substrate binds to the substrate-binding strand (SBS) that contains a 5N-guanosine residue (G-SBS). The guanosine residue is needed for quenching, and the emission of fluorescein is unchanged in the presence of the substrate-binding strand without a 5' terminal guanosine residue (not shown). The example shows how fundamental studies of nucleotide quenching have found useful applications in modern biochemistry.

8.15.4. Association Reactions and Accessibility to Quenchers

In the previous examples the association reactions were detected by the spectral changes which occurred upon binding. However, a useful spectral change may not occur for

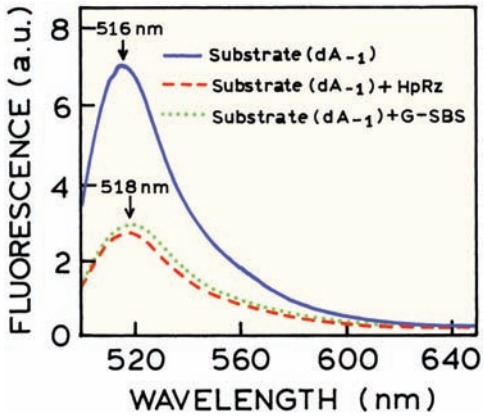

Figure 8.62. Emission spectra of the fluorescein-labeled substrate analogue (dA_{-1}) in solution, and when bound to the hairpin ribozyme (HpRz) or the guanine-containing substrate binding strand. From [141].

the reaction of interest. One example is the binding of ε-ADP to the DNA β helicase hexamer. The fluorescence of ε-ADP displayed only a small increase upon binding to the protein. The change in intensity was too small to be used to measure binding. Collisional quenching was used to induce a larger change in fluorescence on binding.[142] Acrylamide is an efficient quencher of ε-ADP, which should be quenched more strongly in solution than when bound to the helicase. Hence, if the binding is studied in a solution which contains a high concentration of acrylamide, there should be an increase in ε-ADP fluorescence on binding to the helicase.

Solutions of ε-ADP were titrated with the helicase (Figure 8.63). In the absence of acrylamide there was little change in the ε-ADP fluorescence. The titrations were performed again, in solutions with increasing amounts of acrylamide. Under these conditions ε-ADP showed an increase in fluorescence upon binding. This increase occurred because the ε-ADP became shielded from acrylamide upon binding to helicase. The authors also showed that acrylamide had no effect in the affinity of ε-ADP for helicase.[142] In this system the use of a quencher allowed measurement of a binding reaction when there was no change in intensity due to the binding reaction alone.

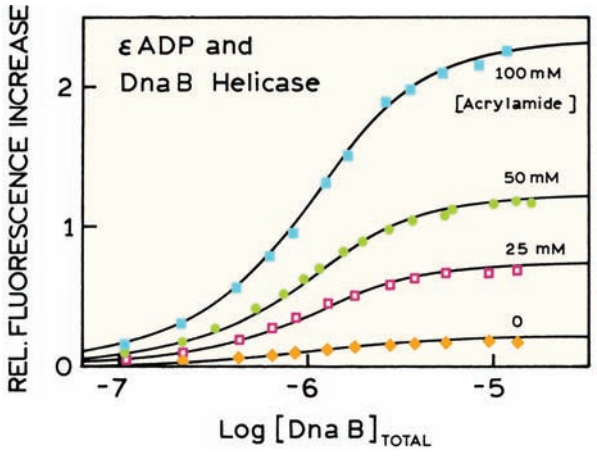

Figure 8.63. Fluorescence titration of ε-ADP, at the same concentration of nucleotide, with the DNA β helicase in buffer containing different concentrations of acrylamide. Revised and reprinted from [142]. Copyright © 1997, with permission from Elsevier Science.

8.16. QUENCHING ON GOLD SURFACES

During the past several years there has been increased interest in the interactions of fluorophores with metallic surfaces or particles.[143–145] Gold and silver colloids display intense colors due to their strong interactions with light.[143–145] The intensity of fluorophores near silver particles is usually increased,[146] and fluorophores near gold particles are usually quenched. The interactions of fluorophores with metallic surfaces is described in Chapter 25. We now describe DNA molecular beacons that are based on the strong quenching by gold colloids and surfaces.

8.16.1. Molecular Beacon Based on Quenching by Gold Colloids

During the past several years there have been developments in the use of gold colloids and surfaces for DNA analysis. Many of these reports make use of the high extinction coefficients and light scattering cross-sections of gold particles.[147–151] It is also possible to create molecular beacons based on the strong quenching of fluorophores near gold surfaces.[152–153] One example is shown in Figure 8.64. In this case the DNA oligomer contained a tetramethylrhodamine (TMR) on the 5' end. The 3' end contained a thiol group that spontaneously binds to gold surfaces. The beacon was made by incubating the thiolated oligomers with gold colloids. When bound to the colloids the TMR adsorbed to the gold surface and was completely quenched. The mechanism of quenching by gold is probably RET to the absorption bands of gold. Addition of a complementary oligomer results in a dramatic increase in intensity. Apparently, the stiffness of double-stranded DNA overcomes the attraction between the gold surface and the TMR. If the added oligomer has a single-base mismatch then the increase in fluorescence is less dramatic. This is probably due to the less-rigid or bent structures of the hybridized DNA with the single-base mis-

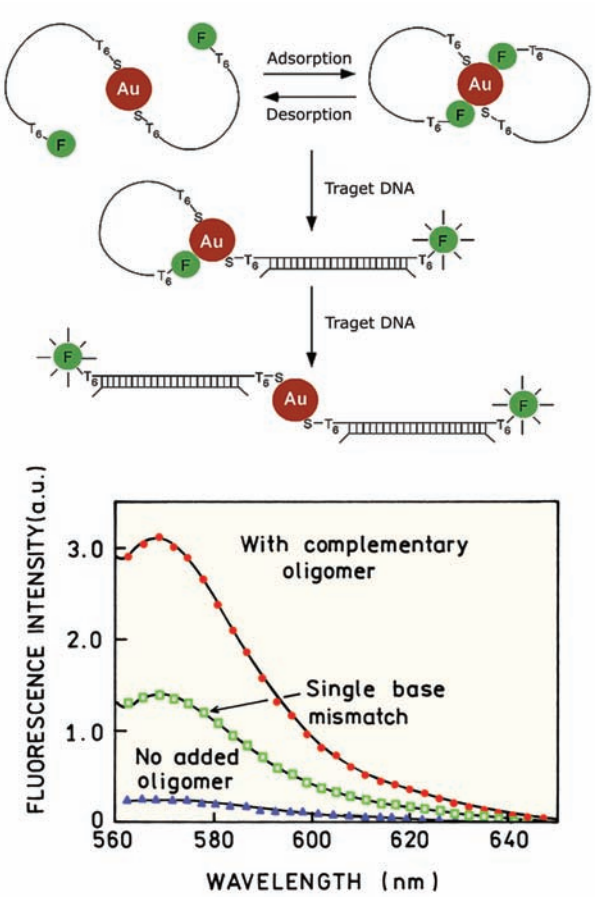

Figure 8.64. Schematic and emission spectra for a TMR-labeled oligo bound to gold colloids. Revised and reprinted with permission from [152]. Copyright © 2002, American Chemical Society.

match. Molecular beacons are most useful if they display a high contrast ratio, that is, a large difference in intensity between the unhybridized and hybridized states. The strong quenching by gold resulted in a high contrast ratio for this gold colloid-based beacon.

8.16.2. Molecular Beacons Based on Quenching by a Gold Surface

Another approach to a molecular beacon is shown in Figure 8.65.[153] In this case the rhodamine-labeled and thiolated beacon was bound to a continuous gold surface. In the absence of a complementary oligomer the fluorophore was held close to the gold surface by the folded beacon and was quenched. Addition of the complementary oligomer was expected to move the rhodamine away from the gold surface and to decrease the extent of quenching. Figure 8.65 shows real color photographs of this beacon on the gold surface. In the absence of complementary oligomers no emission is seen (top). The rhodamine emission is easily seen when the beacon is hybridized with the target sequences (middle). A lower intensity is seen with an excess of nonspecific DNA (bottom). An advantage of this approach is that only a single fluorophore is needed. One can readily imagine the use of gold surfaces with the DNA arrays used to monitor gene expression (Chapter 21).

8.17. INTRAMOLECULAR QUENCHING

In the previous sections the fluorophores and quenchers were not covalently linked. Quenching can also occur between covalently linked fluorophore–quencher pairs.[154–155] One common example is the formation of exciplexes by covalently linked aromatic hydrocarbon and amines. Another example are covalent adducts of indole and acrylamide (Figure 8.66). The lifetime of N-acetyl tryptamine is near 5.1 ns. When the acetyl group is replaced by an acrylolyl group the lifetime is reduced to 31 ps. Similarly, covalent attachment of spin labels to a naphthalene derivative reduced its lifetime from 33.7 to 1.1 ns.

8.17.1. DNA Dynamics by Intramolecular Quenching

Intramolecular quenching has recently been used to measure end-to-end motions of single-stranded DNA.[156] Most fluorophores have nanosecond lifetimes, which are too short for significant end-to-end motions of most biopolymers. A novel fluorophore with a long lifetime was used to allow time for end-to-end collisions. This diazo compound DBO (Figure 8.67) displays an unquenched lifetime near 215 ns when not quenched by a DNA base. DBO was quenched strongly by guanine (G), and less strongly by the other DNA bases. The data analysis is complicated by the presence of some quenching by the bases aside from guanine, but the presence of a guanine residue on the end opposite from DBO clearly reduces the lifetime (Figure 8.67). The rate of quenching can be calculated from a modified form of the Stern-Volmer equation. For a covalently attached quencher the Stern-Volmer equation becomes

$$\frac{\tau_0}{\tau} = 1 + k_q\tau_0 \qquad (8.49)$$

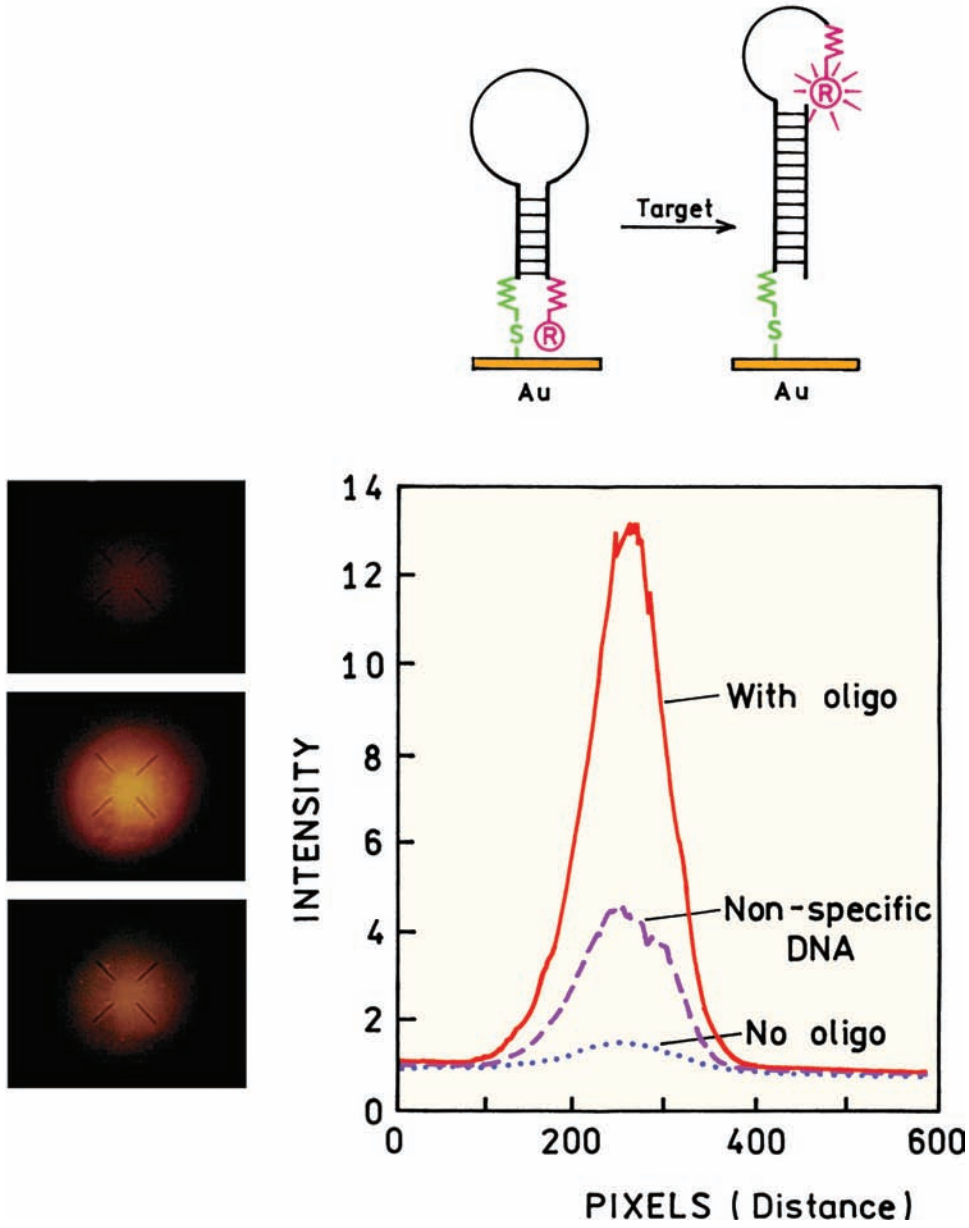

Figure 8.65. Rhodamine-labeled molecular beacon on a gold surface. Photos on the left show the beam without complementary oligo (top), with the complementary oligo (middle), and with an excess of nonspecific salmon sperm DNA. Also shown are the spatial intensity profiles from the CCD camera. Revised and reprinted with permission from [153]. Copyright © 2003, American Chemical Society.

where k_q is the unimolecular rate constant for quenching. Rearrangement of eq. 8.49 yields

$$k_q = \frac{1}{\tau} - \frac{1}{\tau_0} \tag{8.50}$$

The lifetime of the oligonucleotides containing two uridine residues in Figure 8.67 are $\tau_0 = 120$ ns without guanine and $\tau = 58$ ns with a terminal guanine residues. Hence the collision rate is 9×10^6 s^{-1}.

8.17.2. Electron-Transfer Quenching in a Flavoprotein

In solution flavins are highly fluorescent. However, the flavin emission from flavoproteins is usually highly

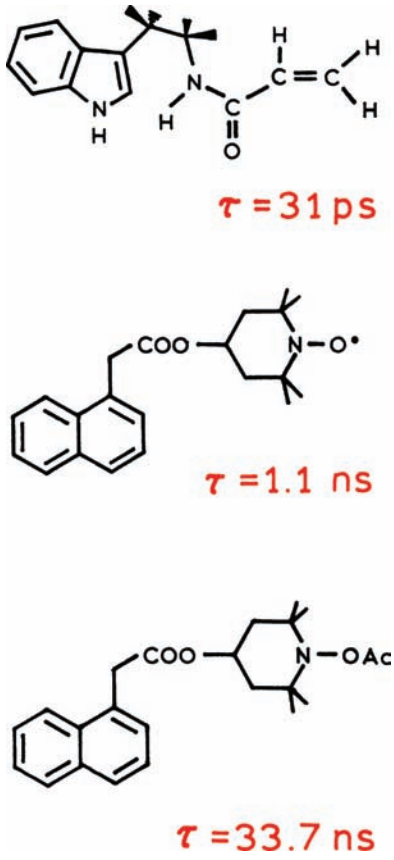

Figure 8.66. Fluorophore-quencher conjugates that display intramolecular quenching. Revised and reprinted with permission from [154–155]. Copyright © 1990, American Chemical Society.

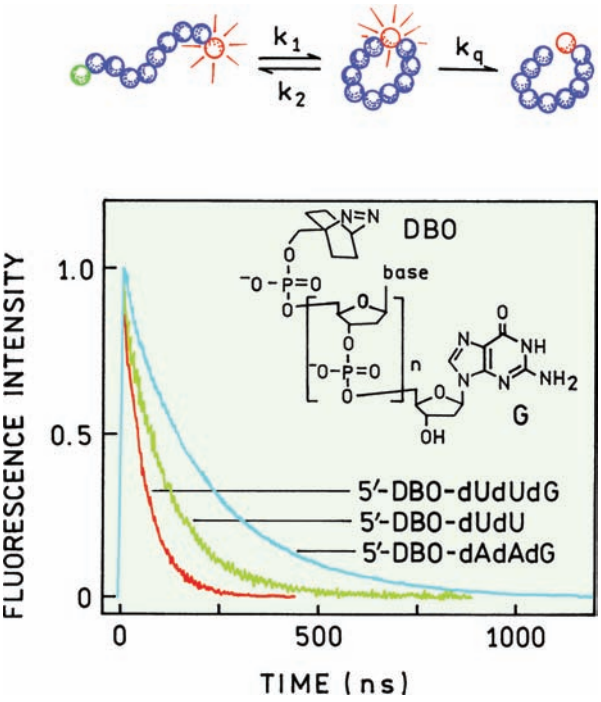

Figure 8.67. Intramolecular quenching of a DBO-labeled oligomer by a terminal guanine residue. Revised and reprinted with permission from [156]. Copyright © 2004, American Chemical Society.

quenched. It is now known that this quenching is due to electron transfer.[157–158] The amino-acid residues responsible for flavin quenching were identified using site-directed mutagenesis. Figure 8.68 shows the intensity decays of FMN free in solution and when bound to flavin reductase from *Escherichia coli*. The lifetime of FMN bound to the wild-type (WT) protein is much shorter than for FMN in solution. This flavin reductase contains three tyrosine (Y) residues at position 35, 72, and 116. Mutant proteins were prepared that contained only two of these residues. The flavin lifetime was still short for the mutants without tyr 72 or tyr 116, indicating that these tyrosines were not responsible for quenching. The lifetime of FMN increased dramatically when tyr 35 was removed, demonstrating that this residue is responsible for quenching. The quenching mechanism is electron transfer from try 35 to FMN. Tyr 35 is 4.5D away from FMN (upper panel). The other two residues are further away from the flavin: 9.6D and 7.0D for tyr 72 and tyr 116, respectively. Electron-transfer reactions only occur over short distances, which explains the lack of quenching by tyr 72 and tyr 116.

8.17.3. Sensors Based on Intramolecular PET Quenching

Intramolecular photoinduced electron transfer (PET) often results in quenching. The phenomenon of PET has been widely used to develop fluorescent sensors.[159–163] In a typical PET sensor an aromatic fluorophore such as anthracene is covalently linked to an aliphatic amine, typically by a short methylene chain. If the amine is not protonated it quenches the fluorophore. Protonation of the amine decreases its ability to donate an electron, so the fluorescence intensity increases.

Figure 8.69 shows the structure of a typical PET sensor.[163] The anthracene group is quenched by the amino groups. Addition of pyrophosphate (PPi) resulted in an increase in fluorescence because of protonation of some of the linked amino groups. The increased fluorescence may have also been due in part to less motion of the side chain during the excited-state lifetime, and thus less quenching.

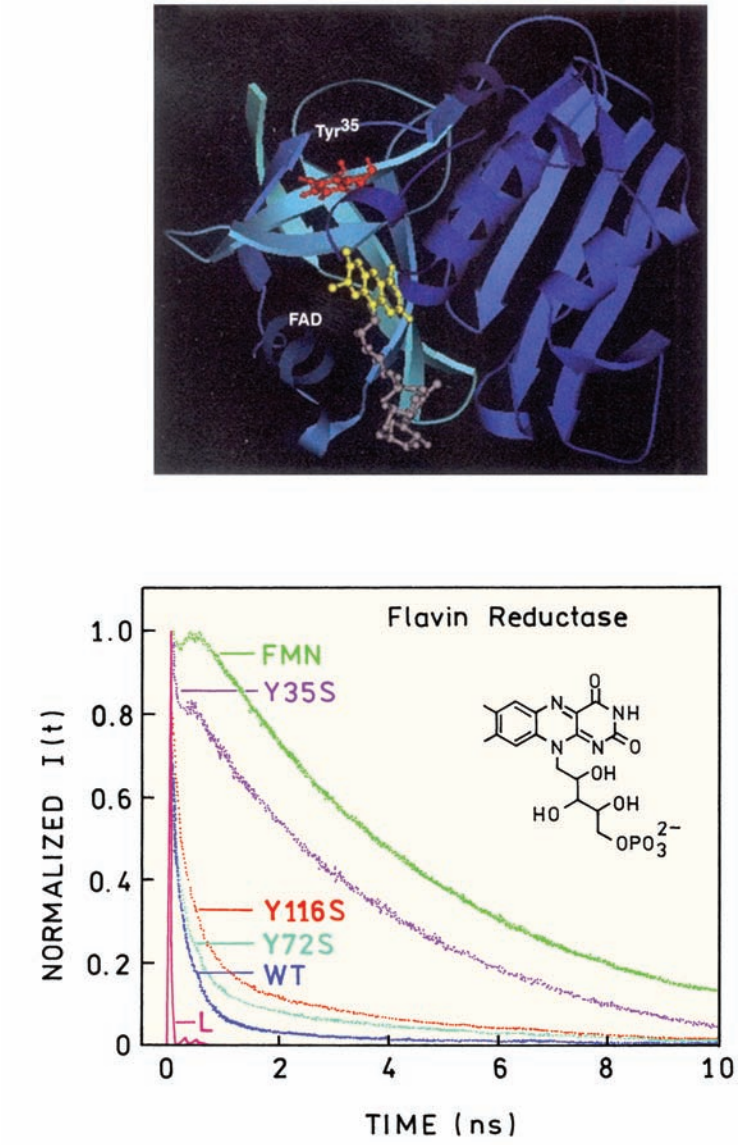

Figure 8.68. Intensity decays of FMN bound to flavin reductase. Intensity decays are shown for free FMN, and for FMN bound to the mutants and wild type protein. L is the lamp profile. The upper panel shows the crystal structure of flavin reductase with bound FMN. Reprinted from [158].

8.18. QUENCHING OF PHOSPHORESCENCE

Phosphorescence is not usually observed in fluid solutions near room temperature. One reason for the absence of phosphorescence is the long phosphorescence lifetimes and the presence of dissolved oxygen and other quenchers. For instance, the phosphorescent lifetime of tryptophan in water has been reported to be 1.2 ms in the absence of oxygen.[164] Suppose the oxygen bimolecular quenching constant is 1 x 10^{10} M^{-1} s^{-1}, and that the aqueous sample is in equilibrium with dissolved oxygen from the air (0.255 mM O_2). Using eq. 8.1 the intensity is expected to be quenched 3000-fold. For this reason, methods have been developed to remove dissolved oxygen from samples used to study phosphorescence.[165–166] In practice, other dissolved quenchers and nonradiative decay rates result in vanishingly small phosphorescence quantum yields in room-temperature solutions. Some exceptions are known, such as when fluorophores are located in highly protected environments within proteins.[167–170] Phosphorescence has also been observed at room temperature for probes bound to cyclodextrins, even in the presence of oxygen.[171] Other small molecules such as

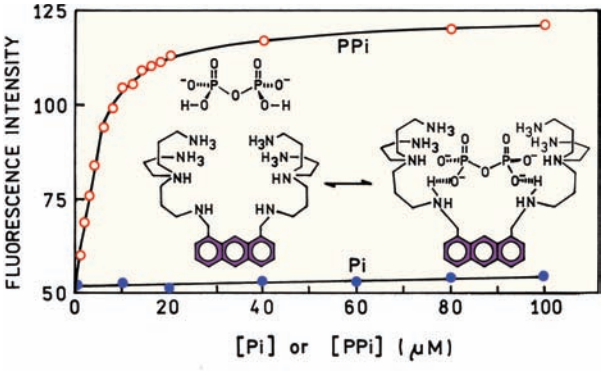

Figure 8.69. Fluorescence sensor for pyrophosphate based on intramolecular PET. The nitrogens are positively charged, which is not shown for clarity. Revised from [163].

amino acids, H_2O, and CS_2 can also quench protein phosphorescence.[172–173] For these reasons, phosphorescence is not commonly observed near room temperature.

Protein phosphorescence can be quenched by oxygen. An example of the dramatic quenching of phosphorescence by even low concentration of oxygen is shown for alkaline phosphatase[174] (Figure 8.70). It is now known that the phosphorescence from alkaline phosphatase results from one of its three nonidentical tryptophan residues: trp-109. This residue is located in a highly shielded environment near the dimer interface. In the presence of 7.8 μM oxygen the phosphorescence lifetime is reduced from 1.57 s to 0.1 ns. Note that an oxygen concentration of 7.8 μM would have an insignificant effect on ns fluorescence. It is also important to notice that trp-109 in alkaline phosphatase is one of the most shielded residues identified to date in a protein. The lifetimes in the absence and presence of 7.8 μM oxygen can be used to calculate the bimolecular quenching constant k_q = 1.2 x 10^6 M^{-1} s^{-1}. If the residue were more typical, with a k_q value of 0.1 x 10^9 M^{-1} s^{-1}, one could calculate that the decay time in 7.8 μM oxygen would have been reduced to 1.28 ms, and thus quenched by over 1000-fold for a micromolar quencher concentration.

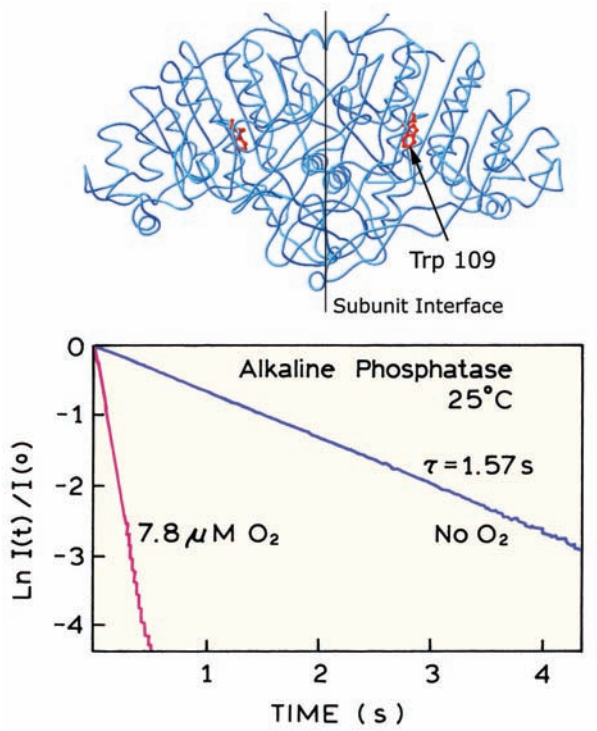

Figure 8.70. Phosphorescence decay of alkaline phosphatase, 25°C, in the absence of oxygen and in the presence of 7.8 μM oxygen. Revised and reprinted with permission from [174]. Copyright © 1987, Biophysical Society.

REFERENCES

1. Kautsky H, 1939. Quenching of luminescence by oxygen. *Trans Faraday Soc* **35**:216–219.
2. Knibbe H, Rehm D, Weller A. 1968. Intermediates and kinetics of fluorescence quenching by electron transfer. *Ber Bunsenges Phys Chem* **72**:257–263.
3. Kasha M. 1952. Collisional perturbation of spin-orbital coupling and the mechanism of fluorescence quenching: a visual demonstration of the perturbation. *J Chem Phys* **20**:71–74.
4. Steiner RF, Kirby EP. 1969. The interaction of the ground and excited states of indole derivatives with electron scavengers. *J Phys Chem* **73**:4130–4135.
5. Eftink MR, Ghiron C. 1981. Fluorescence quenching studies with proteins. *Anal Biochem* **114**:199–227.
6. Eftink MR. 1991. Fluorescence quenching reactions: probing biological macromolecular structures. In *Biophysical and biochemical aspects of fluorescence spectroscopy*, pp. 1–41. Ed TG Dewey. Plenum Press, New York.
7. Eftink MR. 1991. Fluorescence quenching: theory and applications. In *Topics in fluorescence spectroscopy*, Vol. 2: *Principles*, pp. 53–126. Ed JR Lakowicz. Plenum Press, New York.
8. Davis GA. 1973. Quenching of aromatic hydrocarbons by alkylpyridinium halides. *JCS Chem Comm*, 728–729.
9. Shinitzky M, Rivnay B. 1977. Degree of exposure of membrane proteins determined by fluorescence quenching. *Biochemistry* **16**:982–986.
10. Spencer RD, Weber G. 1972. Thermodynamics and kinetics of the intramolecular complex in flavin-adenine dinucleotide. In *Structure and function of oxidation reduction enzymes*, pp. 393–399. Ed A Akeson, A Ehrenberg. Pergamon Press, New York.
11. Scott TG, Spencer RD, Leonard NJ, Weber G. 1970. Emission properties of NADH: studies of fluorescence lifetimes and quantum efficiencies of NADH, AcPyADH, and simplified synthetic models. *J Am Chem Soc* **92**:687–695.

12. Ware WR. 1962. Oxygen quenching of fluorescence in solution: An experimental study of the diffusion process. *J Phys Chem* **66**:455–458.
13. Othmer DF, Thakar MS. 1953. Correlating diffusion coefficients in liquids. *Ind Eng Chem Res* **45**:589–593.
14. Lakowicz JR, Weber G. 1973. Quenching of fluorescence by oxygen: a probe for structural fluctuation in macromolecule. *Biochemistry* **12**:4161–4170.
15. Eftink MR, Ghiron CA. 1977. Exposure of tryptophanyl residues and protein dynamics. *Biochemistry* **16**:5546–5551.
16. Johnson DA, Yguerabide J. 1985. Solute accessibility to N'-fluorescein isothiocyanate-lysine-23: cobra α-toxin bound to the acetylcholine receptor. *Biophys J* **48**:949–955.
17. Kubota Y, Nakamura H, Morishita M, Fujisaki Y. 1978. Interaction of 9-aminoacridine with 7-methylguanosine and 1,N^6-ethenoadenosine monophosphate. *Photochem Photobiol* **27**:479–481.
18. Kubota Y, Motoda Y, Shigemune Y, Fujisaki Y. 1979. Fluorescence quenching of 10-methylacridinium chloride by nucleotides. *Photochem Photobiol* **29**:1099–1106.
19. Seidel CAM, Schulz A, Sauer MHM. 1996. Nucleobase-specific quenching of fluorescent dyes, 1: nucleobase one-electron redox potentials and their correlation with static and dynamic quenching efficiencies. *J Phys Chem* **100**:5541–5553.
20. Eftink MR, Ghiron CA. 1976. Fluorescence quenching of indole and model micelle systems. *J Phys Chem* **80**:486–493.
21. Casali E, Petra PH, Ross JBA. 1990. Fluorescence investigation of the sex steroid binding protein of rabbit serum: steroid binding and subunit dissociation. *Biochemistry* **29**:9334–9343.
22. Frank IM, Vavilov SI. 1931. Über die wirkungssphäre der auslöschuns-vargänge in den flureszierenden flussig-keiten. *Z Phys* **69**:100–110.
23. Maniara G, Vanderkooi JM, Bloomgarden DC, Koloczek H. 1988. Phosphorescence from 2-(p-toluidinyl)naphthalene-6-sulfonate and 1-anilinonaphthalene-8-sulfonate, commonly used fluorescence probes of biological structures. *Photochem Photobiol* **47**(2): 207–208.
24. Kim H, Crouch SR, Zabik MJ. 1989. Room-temperature phosphorescence of compounds in mixed organized media: synthetic enzyme model-surfactant system. *Anal Chem* **61**:2475–2478.
25. Encinas MV, Lissi EA, Rufs AM. 1993. Inclusion and fluorescence quenching of 2,3-dimethylnaphthalene in β-cyclodextrin cavities. *Photochem Photobiol* **57**(4):603–608.
26. Turro NJ, Bolt JD, Kuroda Y, Tabushi I. 1982. A study of the kinetics of inclusion of halonaphthalenes with β-cyclodextrin via time correlated phosphorescence. *Photochem Photobiol* **35**:69–72.
27. Waka Y, Hamamoto K, Mataga N. 1980. Heteroexcimer systems in aqueous micellar solutions. *Photochem Photobiol* **32**:27–35.
28. Atherton SJ, Beaumont PC. 1986. Quenching of the fluorescence of DNA-intercalated ethidium bromide by some transition metal ions. *J Phys Chem* **90**:2252–2259.
29. Pasternack RF, Caccam M, Keogh B, Stephenson TA, Williams AP, Gibbs EJ. 1991. Long-range fluorescence quenching of ethidium ion by cationic porphyrins in the presence of DNA. *J Am Chem Soc* **113**: 6835–6840.
30. Poulos AT, Kuzmin V, Geacintov NE. 1982. Probing the microenvironment of benzo[a]pyrene diol epoxide-DNA adducts by triplet excited state quenching methods. *J Biochem Biophys Methods* **6**:269–281.
31. Zinger D, Geacintov NF. 1988. Acrylamide and molecular oxygen fluorescence quenching as a probe of solvent-accessibility of aromatic fluorophores complexed with DNA in relation to their conformations: coronene-DNA and other complexes. *Photochem Photobiol* **47**:181–188.
32. Suh D, Chaires JB. 1995. Criteria for the mode of binding of DNA binding agents. *Bioorgan Med Chem* **3**(6):723–728.
33. Ando T, Asai H. 1980. Charge effects on the dynamic quenching of fluorescence of fluorescence of 1,N^6-ethenoadenosine oligophosphates by iodide, thallium (I) and acrylamide. *J Biochem* **88**: 255–264.
34. Ando T, Fujisaki H, Asai H. 1980. Electric potential at regions near the two specific thiols of heavy meromyosin determined by the fluorescence quenching technique. *J Biochem* **88**:265–276.
35. Miyata H, Asai H. 1981. Amphoteric charge distribution at the enzymatic site of 1,N^6-ethenoadenosine triphosphate-binding heavy meromyosin determined by dynamic fluorescence quenching. *J Biochem* **90**:133–139.
36. Midoux P, Wahl P, Auchet J-C, Monsigny M. 1984. Fluorescence quenching of tryptophan by trifluoroacetamide. *Biochim Biophys Acta* **801**:16–25.
37. Lehrer SS. 1971. Solute perturbation of protein fluorescence: the quenching of the tryptophan fluorescence of model compounds and of lysozyme by iodide ion. *Biochemistry* **10**:3254–3263.
38. Kao S, Asanov AN, Oldham PB. 1998. A comparison of fluorescence inner-filter effects for different cell configurations. *Instrum Sci Technol* **26**(4):375–387.
39. Fanget B, Devos O. 2003. Correction of inner filter effect in mirror coating cells for trace level fluorescence measurements. *Anal Chem* **75**:2790–2795.
40. Eftink MR, Selvidge LA. 1982. Fluorescence quenching of liver alcohol dehydrogenase by acrylamide. *Biochemistry* **21**:117–125.
41. Eftink M, Hagaman KA. 1986. Fluorescence lifetime and anisotropy studies with liver alcohol dehydrogenase and its complexes. *Biochemistry* **25**:6631–6637.
42. Xing D, Dorr R, Cunningham RP, Scholes CP. 1995. Endonuclease III interactions with DNA substrates, 2: the DNA repair enzyme endonuclease III binds differently to intact DNA and to apyrimidinic/apurinic DNA substrates as shown by tryptophan fluorescence quenching. *Biochemistry* **34**:2537–2544.
43. Sontag B, Reboud A-M, Divita G, Di Pietro A, Guillot D, Reboud JP. 1993. Intrinsic tryptophan fluorescence of rat liver elongation factor eEF-2 to monitor the interaction with guanylic and adenylic nucleotides and related conformational changes. *Biochemistry* **32**: 1976–1980.
44. Wasylewski M, Malecki J, Wasylewski Z. 1995. Fluorescence study of Escherichia coli cyclic AMP receptor protein. *J Protein Chem* **14**(5):299–308.
45. Hannemann F, Bera AK, Fischer B, Lisurek M, Teuchner K, Bernhardt R. 2002. Unfolding and conformational studies on bovine adrenodoxin probed by engineered intrinsic tryptophan fluorescence. *Biochemistry* **41**:11008–11016.
46. Soulages JL, Arrese EL. 2000. Fluorescence spectroscopy of single tryptophan mutants of apolipophorin-III in discoidal lipoproteins of dimyristoylphosphatidylcholine. *Biochemistry* **39**:10574–10580.

47. Raja SM, Rawat SS, Chattopadhyay A, Lala AK. 1999. Localization and environment of tryptophans in soluble and membrane-bound states of a pore-forming toxin from *Staphylococcus aureus*. *Biophys J* **76**:1469–1479.
48. Weber J, Senior AE. 2000. Features of F_1-ATPase catalytic and noncatalytic sites revealed by fluorescence lifetimes and acrylamide quenching of specifically inserted tryptophan residues. *Biochemistry* **39**:5287–5294.
49. Wells TA, Nakazawa M, Manabe K, Song P-S. 1994. A conformational change associated with the phototransformation of *Pisum* phytochrome A as probed by fluorescence quenching. *Biochemistry* **33**:708–712.
50. Eftink MR, Zajicek JL, Ghiron CA. 1977. A hydrophobic quencher of protein fluorescence: 2,2,2-trichloroethanol. *Biochim Biophys Acta* **491**:473–481.
51. Blatt E, Husain A, Sawyer WH. 1986. The association of acrylamide with proteins: the interpretation of fluorescence quenching experiments. *Biochim Biophys Acta* **871**:6–13.
52. Eftink MR, Ghiron CA. 1987. Does the fluorescence quencher acrylamide bind to proteins? *Biochim Biophys Acta* **916**:343–349.
53. Punyiczki M, Norman JA, Rosenberg A. 1993. Interaction of acrylamide with proteins in the concentration range used for fluorescence quenching studies. *Biophys Chem* **47**:9–19.
54. Bastyns K, Engelborghs Y. 1992. Acrylamide quenching of the fluorescence of glyceraldehyde-3-phosphate dehydrogenase: reversible and irreversible effects. *Photochem Photobiol* **55**:9–16.
55. Merrill AR, Palmer LR, Szabo AG. 1993. Acrylamide quenching of the intrinsic fluorescence of tryptophan residues genetically engineered into the soluble colicin E1 channel peptide: structural characterization of the insertion-competent state. *Biochemistry* **32**:6974–6981.
56. Lakowicz JR. 1980. Fluorescence spectroscopic investigations of the dynamic properties of proteins, membranes, and nucleic acids. *J Biochem Biophys Methods* **2**:90–119.
57. Subczynski WK, Hyde JS, Kusumi A. 1989. Oxygen permeability of phosphatidylcholine-cholesterol membranes. *Proc Natl Acad Sci USA* **86**:4474–4478.
58. Fischkoff S, Vanderkooi JM. 1975. Oxygen diffusion in biological and artificial membranes determined by the fluorochrome pyrene. *J Gen Physiol* **65**:663–676.
59. Dumas D, Muller S, Gouin F, Baros F, Viriot M-L, Stoltz J-F. 1997. Membrane fluidity and oxygen diffusion in cholesterol-enriched erythrocyte membrane. *Arch Biochem Biophys* **341**(1):34–39.
60. Subczynski WK, Hyde JS, Kusumi A. 1991. Effect of alkyl chain unsaturation and cholesterol intercalation on oxygen transport in membranes: a pulse ESR spin labeling study. *Biochemistry* **30**:8578–8590.
61. Caputo GA, London E. 2003. Using a novel dual fluorescence quenching assay for measurement of tryptophan depth within lipid bilayers to determine hydrophobic α-helix locations within membranes. *Biochemistry* **42**:3265–3274.
62. Lala AK, Koppaka V. 1992. Fluorenyl fatty acids as fluorescent probes for depth-dependent analysis of artificial and natural membranes. *Biochemistry* **31**:5586–5593.
63. Sassaroli M, Ruonala M, Virtanen J, Vauhkonen M, Somerharju P. 1995. Transversal distribution of acyl-linked pyrene moieties in liquid-crystalline phosphatidylcholine bilayers. A fluorescence quenching study. *Biochemistry* **34**:8843–8851.
64. Ladokhin A, Wang L, Steggles AW, Holloway PW. 1991. Fluorescence study of a mutant cytochrome b_5 with a single tryptophan in the membrane-binding domain. *Biochemistry* **30**:10200–10206.
65. Everett J, Zlotnick A, Tennyson J, Holloway PW. 1986. Fluorescence quenching of cytochrome b_5 in vesicles with an asymmetric transbilayer distribution of brominated phosphatidylcholine. *J Biol Chem* **261**(15):6725–6729.
66. Gonzalez-Manas JM, Lakey JH, Pattus F. 1992. Brominated phospholipids as a tool for monitoring the membrane insertion of colicin A. *Biochemistry* **31**:7294–7300.
67. Silvius JR. 1990. Calcium-induced lipid phase separations and interactions of phosphatidylcholine/anionic phospholipid vesicles: fluorescence studies using carbazole-labeled and brominated phospholipids. *Biochemistry* **29**:2930–2938.
68. Silvius JR. 1992. Cholesterol modulation of lipid intermixing in phospholipid and glycosphingolipid mixtures: evaluation using fluorescent lipid probes and brominated lipid quenchers. *Biochemistry* **31**:3398–3403.
69. Chattopadhyay A, London E. 1987. Parallax method for direct measurement of membrane penetration depth utilizing fluorescence quenching by spin-labeled phospholipids. *Biochemistry* **26**:39–45.
70. Abrams FS, London E. 1992. Calibration of the parallax fluorescence quenching method for determination of membrane penetration depth: refinement and comparison of quenching by spin-labeled and brominated lipids. *Biochemistry* **31**:5312–5322.
71. Abrams FS, Chattopadhyay A, London E. 1992. Determination of the location of fluorescent probes attached to fatty acids using parallax analysis of fluorescence quenching: effect of carboxyl ionization state and environment on depth. *Biochemistry* **31**:5322–5327.
72. Abrams FS, London E. 1993. Extension of the parallax analysis of membrane penetration depth to the polar region of model membranes: use of fluorescence quenching by a spin-label attached to the phospholipid polar headgroup. *Biochemistry* **32**:10826–10831.
73. Asuncion-Punzalan E, London E. 1995. Control of the depth of molecules within membranes by polar groups: determination of the location of anthracene-labeled probes in model membranes by parallax analysis of nitroxide-labeled phospholipid induced fluorescence quenching. *Biochemistry* **34**:11460–11466.
74. Kachel K, Asuncion-Punzalan E, London E. 1995. Anchoring of tryptophan and tyrosine analogs at the hydrocarbon-polar boundary in model membrane vesicles: parallax analysis of fluorescence quenching induced by nitroxide-labeled phospholipids. *Biochemistry* **34**:15475–15479.
75. Ren J, Lew S, Wang Z, London E. 1997. Transmembrane orientation of hydrophobic α-helices is regulated both by the relationship of helix length to bilayer thickness and by the cholesterol concentration. *Biochemistry* **36**:10213–10220.
76. Ladokhin AS. 1999. Analysis of protein and peptide penetration into membranes by depth-dependent fluorescence quenching: theoretical considerations. *Biophys J* **76**:946–955.
77. Ladokhin AS. 1999. Evaluation of lipid exposure of tryptophan residues in membrane peptides and proteins. *Anal Biochem* **276**: 65–71.

78. Ladokhin AS. 1997. Distribution analysis of depth-dependent fluorescence quenching in membranes: a practical guide. *Methods Enzymol* **278**:462–473.
79. London E, Ladokhin AS. 2002. Measuring the depth of amino acid residues in membrane-inserted peptides by fluorescence quenching. *Current Top Membr* **52**:89–111.
80. London E, Feigenson GW. 1981. Fluorescence quenching in model membranes, 1: characterization of quenching caused by a spin-labeled phospholipid. *Biochemistry* **20**:1932–1938.
81. London E, Feigenson GW. 1981. Fluorescence quenching in model membranes, 2: determination of the local lipid environment of the calcium adenosinetriphosphatase from sarcoplasmic reticulum. *Biochemistry* **20**:1939–1948.
82. East JM, Lee AG. 1982. Lipid selectivity of the calcium and magnesium ion dependent adenosinetriphosphatase, studied with fluorescence quenching by a brominated phospholipid. *Biochemistry* **21**:4144–4151.
83. Caffrey M, Feigenson GW. 1981. Fluorescence quenching in model membranes, 3: relationship between calcium adenosinetriphosphatase enzyme activity and the affinity of the protein for phosphatidylcholines with different acyl chain characteristics. *Biochemistry* **20**:1949–1961.
84. Markello T, Zlotnick A, Everett J, Tennyson J, Holloway PW. 1985. Determination of the topography of cytochrome b_5 in lipid vesicles by fluorescence quenching. *Biochemistry* **24**:2895–2901.
85. Froud RJ, East JM, Rooney EK, Lee AG. 1986. Binding of long-chain alkyl derivatives to lipid bilayers and to (Ca^{2+}–Mg^{2+})-ATPase. *Biochemistry* **25**:7535–7544.
86. Yeager MD, Feigenson GW. 1990. Fluorescence quenching in model membranes: phospholipid acyl chain distributions around small fluorophores. *Biochemistry* **29**:4380–4392.
87. Lakowicz JR, Hogen D, Omann G. 1977. Diffusion and partitioning of a pesticide, lindane, into phosphatidylcholine bilayers: a new fluorescence quenching method to study chlorinated hydrocarbon-membrane interactions. *Biochim Biophys Acta* **471**:401–411.
88. Omann GM, Glaser M. 1985. Dynamic quenchers in fluorescently labeled membranes. *Biophys J* **47**:623–627.
89. Fato R, Battino M, Esposti MD, Castelli GP, Lenaz G. 1986. Determination of partition of lateral diffusion coefficients of ubiquinones by fluorescence quenching of n-(9-anthroyloxy)stearic acids in phospholipid vesicles and mitochondrial membranes. *Biochemistry* **25**:3378–3390.
90. Vermeir M, Boens N. 1992. Partitioning of (±)-5,6-dihydro-6-phenyl-2-n-alkyl-imidazo-[2,1-b]thiazoles into large unilamellar liposomes: a steady-state fluorescence quenching study. *Biochim Biophys Acta* **1104**:63–72.
91. Lakos Z, Szarka A, Somogyi B. 1995. Fluorescence quenching in membrane phase. *Biochem Biophys Res Commun* **208**(1):111–117.
92. Prieto MJE, Castanho M, Coutinho A, Ortiz A, Aranda FJ, Gomez-Fernandez JC. 1994. Fluorescence study of a derivatized diacylglycerol incorporated in model membranes. *Chem Phys Lipids* **69**:75–85.
93. Ranganathan R, Vautier-Giongo C, Bales BL. 2003. Toward a hydrodynamic description of biomolecular collisions in micelles: an experimental test of the effect of the nature of the quencher on the fluorescence quenching of pyrene in SDS micelles and in bulk liquids. *J Phys Chem B* **107**:10312–10318.
94. Infelta PP. 1979. Fluorescence quenching in micellar solutions and its application to the determination of aggregation numbers. *Chem Phys Lett* **61**(1):88–91.
95. Waka Y, Hamamoto K, Mataga N. 1980. Heteroexcimer systems in aqueous micellar solutions. *Photochem Photobiol* **32**:27–35.
96. Tachiya M. 1982. Kinetics of quenching of luminescent probes in micellar systems, II. *J Chem Phys* **76**(1):343–348.
97. Naqvi KR. 1974. Diffusion-controlled reactions in two-dimensional fluids: discussion of measurements of lateral diffusion of lipids in biological membranes. *Chem Phys Lett* **28**(2):280–284.
98. Owen CS. 1975. Two-dimensional diffusion theory: cylindrical diffusion model applied to fluorescence quenching. *J Chem Phys* **62**(8):3204–3207.
99. Medhage B, Almgren M. 1992. Diffusion-influenced fluorescence quenching: dynamics in one to three dimensions. *J Fluoresc* **2**(1): 7–21.
100. Caruso F, Grieser F, Thistlethwaite PJ. 1993. Lateral diffusion of amphiphiles in fatty acid monolayers at the air–water interface: a steady-state and time-resolved fluorescence quenching study. *Langmuir* **9**:3142–3148.
101. Blackwell MF, Gounaris K, Zara SJ, Barber J. 1987. A method for estimating lateral diffusion coefficients in membranes from steady-state fluorescence quenching studies. *Biophys J* **51**:735–744.
102. Caruso F, Grieser F, Thistlethwaite PJ, Almgren M. 1993. Two-dimensional diffusion of amphiphiles in phospholipid monolayers at the air–water interface. *Biophys J* **65**:2493–2503.
103. Wasylewski Z, Kaszycki P, Guz A, Stryjewski W. 1988. Fluorescence quenching resolved spectra of fluorophores in mixtures and micellar solutions. *Eur J Biochem* **178**:471–476.
104. Wasylewski Z, Koloczek H, Wasniowska A. 1988. Fluorescence quenching resolved spectroscopy of proteins. *Eur J Biochem* **172**:719–724.
105. Laws WR, Shore JD. 1978. The mechanism of quenching of liver alcohol dehydrogenase fluorescence due to ternary complex formation. *J Biol Chem* **23**:8593–8597.
106. Stryjewski W, Wasylewski Z. 1986. The resolution of heterogeneous fluorescence of multitryptophan-containing proteins studied by a fluorescence quenching method. *Eur J Biochem* **158**:547–553.
107. Blicharska Z, Wasylewski Z. 1995. Fluorescence quenching studies of Trp repressor using single-tryptophan mutants. *J Protein Chem* **14**(8):739–746.
108. Wasylewski Z, Kaszycki P, Drwiega M. 1996. A fluorescence study of Tn10-encoded tet repressor. *J Protein Chem* **15**(1):45–52.
109. Hansen D, Altschmied L, Hillen W. 1987. Engineered tet repressor mutants with single tryptophan residues as fluorescent probes. *J Biol Chem* **29**:14030–14035.
110. Lange R, Anzenbacher P, Müller S, Maurin L, Balny C. 1994. Interaction of tryptophan residues of cytochrome P45scc with a highly specific fluorescence quencher, a substrate analogue, compared to acrylamide and iodide. *Eur J Biochem* **226**:963–970.
111. Johansson JS, Eckenhoff RG, Dutton L. 1995. Binding of halothane to serum albumin demonstrated using tryptophan fluorescence. *Anesthesiology* **83**:316–324.
112. Johansson JS. 1997. Binding of the volatile anesthetic chloroform to albumin demonstrated using tryptophan fluorescence quenching. *J Biol Chem* **272**:17961–17965.

113. Gonzalez-Jimenez J, Frutos G, Cayre I. 1992. Fluorescence quenching of human serum albumin by xanthines. *Biochem Pharmacol* **44**(4):824–826.
114. Johansson JS, Scharf D, Davies LA, Reddy KS, Eckenhoff RG. 2000. A designed four-α-helix bundle that binds the volatile general anesthetic halothane with high affinity. *Biophys J* **78**:982–993.
115. Johansson JS, Solt K, Reddy KS. 2003. Binding of the general anesthetics chloroform and 2,2,2-trichloroethanol to the hydrophobic core of a four-α-helix bundle protein. *Photochem Photobiol* **77**(1):89–95.
116. Geddes CG. 2001. Optical halide sensing using fluorescence quenching: theory, simulations and applications—a review. *Meas Sci Technol* **12**:R53–R88.
117. Geddes CG. 2000. Optical thin film polymeric sensors for the determination of aqueous chloride, bromide and iodide ions at high pH, based on the quenching of fluorescence of two acridinium dyes. *Dyes Pigm* **45**:243–251.
118. Geddes CG, Apperson K, Birch DJS. 2000. New fluorescent quinolinium dyes—applications in nanometre particle sizing. *Dyes Pigm* **44**:69–74.
119. Huber C, Werner T, Krause C, Wolfbeis OS. 1999. Novel chloride-selective optode based on polymer-stabilised emulsions doped with a lipophilic fluorescent polarity-sensitive dye. *Analyst* **124**:1617–1622.
120. Huber C, Fähnrich K, Krause C, Werner T. 1999. Synthesis and characterization of new chloride-sensitive indicator dyes based on dynamic fluorescence quenching. *J Photochem Photobiol A: Chem* **128**:111–120.
121. Geddes CG, Apperson K, Karolin J, Birch JDS. 2001. Chloride-sensitive fluorescent indicators. *Anal Biochem* **293**:60–66.
122. Geddes CG. 2001. Halide sensing using the SPQ molecule. *Sens Actuators B* **72**:188–195.
123. Jayaraman S, Verkman AS. 2000. Quenching mechanism of quinolinium-type chloride-sensitive fluorescent indicators. *Biophys Chem* **85**:45–57.
124. Rehm D, Weller A. 1970. Kinetics of fluorescence quenching by electron and H-atom transfer. *Isr J Chem* **8**:259–271.
125. Jayaraman S, Song Y, Vetrivel L, Shankar L, Verkman AS. 2001. Noninvasive in vivo fluorescence measurement of airway-surface liquid depth, salt concentration, and pH. *J Clin Invest* **107**(3):317–324.
126. Inglefield JR, Schwartz-Bloom RD. 1999. Fluorescence imaging of changes in intracellular chloride in living brain slices. *Methods: A Companion to Methods in Enzymology* **18**:197–203.
127. Sonawane ND, Thiagarajah JR, Verkman AS. 2002. Chloride concentration in endosomes measured using a ratioable fluorescent Cl^- indicator. *J Biol Chem* **277**(7):5506–5513.
128. Jayaraman S, Teitler L, Skalski B, Verkman AS. 1999. Long-wavelength iodide-sensitive fluorescent indicators for measurement of functional CFTR expression in cells. *Am J Physiol* **277**:C1008–C1018.
129. Jayaraman S, Biwersi J, Verkman AS. 1999. Synthesis and characterization of dual-wavelength Cl^- sensitive fluorescent indicators for ratio imaging. *Am J Physiol* **276**:C747–C757.
130. Zhang J, Campbell RE, Ting AY, Tsien R. 2002. Creating new fluorescent probes for cell biology. *Nature Rev Mol Cell Biol* **3**(12):906–918.
131. Zimmer M. 2002. Green fluorescent protein (GFP): applications, structure, and related photophysical behavior. *Chem Rev* **102**:759–781.
132. Wachter RM, Yarbrough D, Kallio K, Remington SJ. 2000. Crystallographic and energetic analysis of binding of selected anions to the yellow variants of green fluorescent protein. *J Mol Biol* **301**:157–171.
133. Jayaraman S, Haggie P, Wachter RM, Remington SJ, Verkman AS. 2000. Mechanism and cellular applications of a green fluorescent protein-based halide sensor. *J Biol Chem* **275**(9):6047–6050.
134. Rakicioglu Y, Young MM, Schulman SG. 1998. Limitations of quenching as a method of fluorometric analysis of non-fluorescent analytes. *Anal Chim Acta* **359**:269–273.
135. Chen L, McBranch DW, Wang H-L, Helgeson R, Wudi F, Whitten DG. 1999. Highly sensitive biological and chemical sensors based on reversible fluorescence quenching in a conjugated polymer. *Proc Natl Acad Sci USA* **96**(22):12287–12292.
136. Yamane A. 2002. MagiProbe: a novel fluorescence quenching-based oligonucleotide probe carrying a fluorophore and an intercalator. *Nucleic Acids Res* **30**(19):e97.
137. Sauer M, Drexhage KH, Lieberwirth U, Müller R, Nord S, Zander C. 1998. Dynamics of the electron transfer reaction between an oxazine dye and DNA oligonucleotides monitored on the single-molecule level. *Chem Phys Lett* **284**:153–163.
138. Torimura M, Kurata S, Yamada K, Yokomaku T, Kamagata Y, Kanagawa T, Kurane R. 2001. Fluorescence-quenching phenomenon by photoinduced electron transfer between a fluorescent dye and a nucleotide base. *Anal Sci* **17**:155–160.
139. Heinlein T, Knemeyer J-P, Piestert O, Sauer M. 2003. Photoinduced electron transfer between fluorescent dyes and guanosine residues in DNA-hairpins. *J Phys Chem* **107**:7957–7964.
140. Knemeyer J-P, Marmé N, Sauer M. 2000. Probes for detection of specific DNA sequences at the single-molecule level. *Anal Chem* **72**:3717–3724.
141. Walter NG, Burke JM. 1997. Real-time monitoring of hairpin ribozyme kinetics through base-specific quenching of fluorescein-labeled substrates. *RNA* **3**:392–404.
142. Jezewska MJ, Bujalowski W. 1997. Quantitative analysis of ligand-macromolecule interactions using differential dynamic quenching of the ligand fluorescence to monitor the binding. *Biophys Chem* **64**:253–269.
143. Thomas KG, Kamat PV. 2003. Chromophore-functionalized gold nanoparticles. *Acc Chem Res* **36**(12):888–898.
144. Kerker M. 1985. The optics of colloidal silver: something old and something new. *J Colloid Interface Sci* **105**(2):297–314.
145. Link S, El-Sayed M. 1999. Spectral properties and relaxation dynamics of surface plasmon electronic oscillations in gold and silver nanodots and nanorods. *J Phys Chem B* **103**:8410–8426.
146. Lakowicz JR. 2001. Radiative decay engineering: Biophysical and biomedical applications. *Anal Biochem* **298**:1–24.
147. Storhoff JJ, Lucas AD, Garimella V, Bao YP, Müller UR. 2004. Homogeneous detection of unamplified genomic DNA sequences based on colorimetric scatter of gold nanoparticles probes. *Nature Biotechnol* **22**:883–887.
148. Storhoff JJ, Elghanian R, Mucic RC, Mirkin CA, Letsinger RL. 1998. One-pot colorimetric differentiation of polynucleotides with

single base imperfections using gold nanoparticle probes. *J Am Chem Soc* **120**:1959–1964.
149. He L, Musick MD, Nicewarner SR, Salinas FG, Benkovic SJ, Natan MJ, Keating CD. 2000. Colloidal Au-enhanced surface plasmon resonance for ultrasensitive detection of DNA hybridization. *J Am Chem Soc* **122**:9071–9077.
150. Taton TA, Mirkin CA, Letsinger RL. 2000. Scanometric DNA array detection with nanoparticle probes. *Science* **289**:1757–1760.
151. Dubertret B, Calame M, Libchaber AJ. 2001. Single-mismatch detection using gold-quenched fluorescent oligonucleotides. *Nature Biotechnol* **19**:365–370.
152. Maxwell DJ, Taylor JR, Nie S. 2002. Self-assembled nanoparticle probes for recognition and detection of biomolecules. *J Am Chem Soc* **124**:9606–9612.
153. Du H, Disney MD, Miller BL, Krauss TD. 2003. Hybridization-based unquenching of DNA hairpins on Au surfaces: prototypical "molecular beacon" biosensors. *J Am Chem Soc* **125**:4012–4013.
154. Eftink MR, Jia Y-W, Graves DE, Wiczk W, Gryczynski I, Lakowicz JR. 1989. Intramolecular fluorescence quenching in covalent acrylamide-indole adducts. *Photochem Photobiol* **49**(6):725–729.
155. Green SA, Simpson DJ, Zhou G, Ho PS, Blough NV. 1990. Intramolecular quenching of excited singlet states by stable nitroxyl radicals. *J Am Chem Soc* **112**:7337–7346.
156. Wang X, Nau WM. 2004. Kinetics of end-to-end collision in short single-stranded nucleic acids. *J Am Chem Soc* **126**:808–813.
157. van den Berg PAW, van Hoek A, Walentas CD, Perham RN, Visser AJWG. 1998. Flavin fluorescence dynamics and photoinduced electron transfer in *Escherichia coli* glutathione reductase. *Biophys J* **74**:2046–2058.
158. Yang H, Luo G, Karnchanaphanurach P, Louie T-M, Rech I, Cova S, Xun L, Xie XS. 2003. Protein conformational dynamics probed by single-molecule electron transfer. *Science* **302**:262–266.
159. Kavarnos GJ. 1993. *Fundamentals of photoinduced electron transfer*. VCH Publishers, New York.
160. Pina F, Bernando MA, García-España E. 2000. Fluorescent chemosensors containing polyamine receptors. *Eur J Inorg Chem* 2143–2157.
161. de Silva AP, Fox DB, Moody TS, Weir SM. 2001. The development of molecular fluorescent switches. *Trends Biotechnol* **19**(1):29–34.
162. de Silva AP, Gunaratne HQN, Gunnlaugsson T, Huxley AJM, McCoy CP, Rademacher JT, Rice TE. 1997. Signaling recognition events with fluorescent sensors and switches. *Chem Rev* **97**:1515–1566.
163. Czarnik AW. 1994. Fluorescent chemosensors of ion and molecule recognition. *Interfacial Des Chem Sens* **561**:314–323.
164. Strambini GB, Gonnelli M. 1995. Tryptophan phosphorescence in fluid solution. *J Am Chem Soc* **117**:7646–7651.
165. Englander SW, Calhoun DB, Englander JJ. 1987. Biochemistry without oxygen. *Anal Biochem* **161**:300–306.
166. Zhang HR, Zhang J, Wei YS, Jin EJ, Liu CS. 1997. Study of new facile deoxygenation methods in cyclodextrin induced room temperature phosphorescence. *Anal Chim Acta* **357**:119–125.
167. Cioni P, Puntoni A, Strambini GB. 1993. Tryptophan phosphorescence as a monitor of the solution structure of phosphoglycerate kinase from yeast. *Biophys Chem* **46**:47–55.
168. Gonnelli M, Strambini GB. 1993. Glycerol effects on protein flexibility: a tryptophan phosphorescence study. *Biophys J* **65**:131–137.
169. Strambini GB, Gabellieri E. 1996. Proteins in frozen solutions: evidence of ice-induced partial unfolding. *Biophys J* **70**:971–976.
170. Vanderkooi JM, Calhoun DB, Englander SW. 1987. On the prevalence of room-temperature protein phosphorescence. *Science* **236**:568–569.
171. Turro NJ, Cox GS, Li X. 1983. Remarkable inhibition of oxygen quenching of phosphorescence by complexation with cyclodextrins. *Photochem Photobiol* **37**(2):149–153.
172. Gonnelli M, Strambini GB. 1995. Phosphorescence lifetime of tryptophan in proteins. *Biochemistry* **34**:13847–13857.
173. Wright WW, Owen CS, Vanderkooi JM. 1992. Penetration of analogues of H_2O and CO_2 in proteins studied by room temperature phosphorescence of tryptophan. *Biochemistry* **31**:6538–6544.
174. Strambini GB. 1987. Quenching of alkaline phosphatase phosphorescence by O_2 and NO. *Biophys J* **52**:23–28.
175. Courtesy of Dr. Ari Gafni, University of Michigan.
176. Boaz H, Rollefson GK. 1950. The quenching of fluorescence: deviations from the Stern-Volmer law. *J Am Chem Soc* **72**:3425–3443.
177. Harrison M, Powell B, Finbow ME, Findlay JBC. 2000. Identification of lipid-accessible sites on the *Nephrops* 16-kDa proteolipid incorporated into a hybrid vacuolar H^+-ATPase: site-directed labeling with N-(1-pyrenyl)cyclohexylcarbodiimide and fluorescence quenching analysis. *Biochemistry* **39**:7531–7537.
178. Moro A, Gatti C, Delorenzi N. 2001. Hydrophobicity of whey protein concentrates measured by fluorescence quenching and its relation with surface functional properties. *J Agric Food Chem* **49**:4784-4789.
179. Galletto R, Bujalowski W. 2002. Kinetics of the *E. coli* replication factor DnaC protein–nucleotide interactions, II: fluorescence anisotropy and transient, dynamic quenching stopped-flow studies of the reaction intermediates. *Biochemistry* **41**:8921–8934.
180. Eftink MR, Ghiron CA. 1976. Exposure of tryptophanyl residues in proteins: quantitative determination by fluorescence quenching studies. *Biochemistry* **15**(3):672–680.
181. Saik VO, Goun AA, Fayer MD. 2004. Photoinduced electron transfer and geminate recombination for photoexcited acceptors in a pure donor solvent. *J Chem Phys* **120**(20):9601–9611.
182. Schneider S, Stammler W, Bierl R, Jager W. 1994. Ultrafast photoinduced charge separation and recombination in weakly bound complexes between oxazine dyes and N,N-dimethylaniline. *Chem Phys Lett* **219**:433–439.
183. Yoshihara K, Yartsev A, Nagasawa Y, Kandori H, Douhal A, Kemnitz K. 1993. Femtosecond intermolecular electron transfer between dyes and electron-donating solvents. *Pure Appl Chem* **65**(8):1671–1675.
184. Pischel U Abad S, Miranda MA. 2003. Stereoselectove fluorescence quenching by photoinduced electron transfer in naphthalene-amine dyads. *Chem Commun* **9**:1088–1089.
185. Morandeira A, Fürstenberg A, Gumy JC, Vauthey E. 2003. Fluorescence quenching in electron-donating solvents, 1: influence of the solute-solvent interactions on the dynamics. *J Phys Chem* **107**:5375–5383.
186. Goodpaster JV, McGuffin VL. 2000. Selective fluorescence quenching of polycyclic aromatic hydrocarbons by aliphatic amines. *Anal Chem* **72**:1072–1077.
187. Bisht PB, Tripathi HB. 1993. Fluorescence quenching of carbazole by triethylamine: exciplex formation in polar and nonpolar solvents. *J Luminesc* **55**:153–158.

188. Sikaris KA, Sawyer WH. 1982. The interaction of local anaesthetics with synthetic phospholipid bilayers. *Biochem Pharmacol* **31**(16): 2625–2631.
189. Fernandez MS, Calderon E. 1990. The local anaesthetic tetracaine as a quencher of perylene fluorescence in micelles. *J Photochem Photobiol B: Biol* **7**:75–86.
190. Hutterer R, Krämer K, Schneider FW, Hof M. 1997. The localization of the local anesthetic tetracaine in phospholipid vesicles: a fluorescence quenching and resonance energy transfer study. *Chem Phys Lipids* **90**:11–23.
191. Winkler MH. 1969. A fluorescence quenching technique for the investigation of the configurations of binding sites for small molecules. *Biochemistry* **8**:2586–2590.
192. Berlman IB. 1973. Empirical study of heavy-atom collisional quenching of the fluorescence state of aromatic compounds in solution. *J Phys Chem* **77**(4):562–567.
193. Groenzin H, Mullins OC, Mullins WW. 1999. Resonant fluorescence quenching of aromatic hydrocarbons by carbon disulfide. *J Phys Chem A* **103**:1504–1508.
194. James DR, Ware WR. 1985. Multiexponential fluorescence decay of indole-3-alkanoic acids. *J Phys Chem* **89**:5450–5458.
195. Fonseca MM, Scofano HM, Carvalho-Alves PC, Barrabin H, Mignaco JA. 2002. Conformational changes of the nucleotide site of the plasma membrane Ca^{2+}-ATPase probed by fluorescence quenching. *Biochemistry* **41**:7483–7489.
196. Daems D, Boens N, Schryver FC. 1989. Fluorescence quenching with lindane in small unilamellar L,α-dimyristoylphosphatidylcholine vesicles. *Eur Biophys J* **17**:25–36.
197. Namiki A, Nakashima N, Yoshihara K. 1979. Fluorescence quenching due to the electron transfer: indole-chloromethanes in rigid ethanol glass. *J Chem Phys* **71**(2):925–930.
198. Johnson GE, 1980. Fluorescence quenching of carbazoles. *J Phys Chem* **84**:2940–2946.
199. Jones OT, Lee AG. 1985. Interactions of hexachlorocyclohexanes with lipid bilayers. *Biochim Biophys Acta* **812**:731–739.
200. Chao AC, Dix JA, Sellers MC, Verkman AS. 1989. Fluorescence measurement of chloride transport in monolayer cultured cells. *Biophys J* **56**:1071–1081.
201. Verkman AS. 1990. Development and biological applications of chloride-sensitive fluorescent indicators. *Am J Phys* **253**:C375–C388.
202. Martin A, Narayanaswamy R. 1997. Studies on quenching of fluorescence of reagents in aqueous solution leading to an optical chloride-ion sensor. *Sens Actuators B* **38–39**:330–333.
203. Bigger SW, Watkins PI, Verity B. 2000. Quinine fluorescence quenching at low ionic strength. *Int J Chem Kinet* **32**(8):473–477.
204. Hariharan C, Vijaysree V, Mishra AK. 1997. Quenching of 2,5-diphenyloxazole (PPO) fluorescence by metal ions. *J Luminesc* **75**: 205–211.
205. Morris SJ, Bradley D, Blumenthal R. 1985. The use of cobalt ions as a collisional quencher to probe surface charge and stability of fluorescently labeled bilayer vesicles. *Biochem Biophys Acta* **818**: 365–372.
206. Homan R, Eisenberg M. 1985. A fluorescence quenching technique for the measurement of paramagnetic ion concentrations at the membrane/water interface: intrinsic and X537A-mediated cobalt fluxes across lipid bilayer membranes. *Biochim Biophys Acta* **812**:485–492.
207. Salthammer T, Dreeskamp H, Birch DJS, Imhof RE. 1990. Fluorescence quenching of perylene by Co^{2+} ions via energy transfer in viscous and non-viscous media. *J Photochem Photobiol A: Chem.* **55**:53–62.
208. Holmes AS, Birch DJS, Suhling K, Imhof RE, Salthammer T, Dreeskamp H. 1991. Evidence for donor–donor energy transfer in lipid bilayers: perylene fluorescence quenching by Co^{2+} ions. *Chem Phys Lett* **186**(2,3):189–194.
209. Birch DJS, Suhling K, Holmes AS, Salthammer T, Imhof RE. 1992. Fluorescence energy transfer to metal ions in lipid bilayers. *SPIE* **1640**:707–718.
210. Perochon E, Tocanne J-F. 1991. Synthesis and phase properties of phosphatidylcholine labeled with 8-(2-anthroyl)octanoic acid, a solvatochromic fluorescent probe. *Chem Phys Lipids* **58**:7–17.
211. Fucaloro AF, Forster LS, Campbell MK. 1984. Fluorescence quenching of indole by dimethylformamide. *Photochem Photobiol* **39**:503–506.
212. Swadesh JK, Mui PW, Scheraga HA. 1987. Thermodynamics of the quenching of tyrosyl fluorescence by dithiothreitol. *Biochemistry* **26**:5761–5769.
213. Valentino MR, Boyd MK. 1995. Ether quenching of singlet excited 9-arylxanthyl cations. *J Photochem Photobiol* **89**:7–12.
214. Medinger T, Wilkinson F. 1965. Mechanism of fluorescence quenching in solution, I: quenching of bromobenzene. *Trans Faraday Soc* **61**:620–630.
215. Ahmad A, Durocher G. 1981. How hydrogen bonding of carbazole to ethanol affects its fluorescence quenching rate by electron acceptor quencher molecules. *Photochem Photobiol* **34**:573–578.
216. Bowen EJ, Metcalf WS. 1951. The quenching of anthracene fluorescence. *Proc Roy Soc London* **206A**:437–447.
217. Schmidt R, Janssen W, Brauer H-D. 1989. Pressure effect on quenching of perylene fluorescence by halonaphthalenes. *J Phys Chem* **93**:466–468.
218. Encinas MV, Rubio MA, Lissi E. 1983. Quenching and photobleaching of excited polycyclic aromatic hydrocarbons by carbon tetrachloride and chloroform in micellar systems. *Photochem Photobiol* **37**(2):125–130.
219. Behera PK, Mukherjee T, Mishra AK. 1995. Quenching of substituted naphthalenes fluorescence by chloromethanes. *J Luminesc* **65**: 137–142.
220. Behera PK, Mishra AK. 1993. Static and dynamic model for 1-naphthol fluorescence quenching by carbon tetrachloride in dioxane-acetonitrile mixtures. *J Photochem Photobiol A: Chem* **71**:115–118.
221. Behera PK, Mukherjee T, Mishra AK. 1995. Simultaneous presence of static and dynamic component in the fluorescence quenching for substituted naphthalene-CCl_4 system. *J Luminesc* **65**:131–136.
222. Zhang J, Roek DP, Chateauneuf JE, Brennecke JF. 1997. A steady-state and time-resolved fluorescence study of quenching reactions of anthracene and 1,2-benzanthracene by carbon tetrabromide and bromoethane in supercritical carbon dioxide. *J Amer Chem Soc* **119**:9980–9991.
223. Tucker SA, Cretella LE, Waris R, Street KW, Acree WE, Fetzer JC. 1990. Polycyclic aromatic hydrocarbon solute probes, VI: effect of

dissolved oxygen and halogenated solvents on the emission spectra of select probe molecules. *Appl Spectrosc* **44**(2):269–273.
224. Wiczk WM, Latowski T. 1992. The effect of temperature on the fluorescence quenching of perylene by tetrachloromethane in mixtures with cyclohexane and benzene. *Z Naturforsch A* **47**:533–535.
225. Wiczk WM, Latowski T. 1986. Photophysical and photochemical studies of polycyclic aromatic hydrocarbons in solutions containing tetrachloromethane, I: fluorescence quenching of anthracene by tetrachloromethane and its complexes with benzene, p-xylene and mesitylene. *Z Naturforsch A* **41**:761–766.
226. Goswami D, Sarpal RS, Dogra SK. 1991. Fluorescence quenching of few aromatic amines by chlorinated methanes. *Bull Chem Soc Jpn* **64**:3137–3141.
227. Takahashi T, Kikuchi K, Kokubun H. 1980. Quenching of excited 2,5-diphenyloxazole by CCl_4. *J Photochem* **14**:67–76.
228. Bonesi SM, Erra-Balsells R. 2000. Outer-sphere electron transfer from carbazoles to halomethanes: reduction potentials of halomethanes measured by fluorescence quenching experiments. *J Chem Soc Perkin Trans* **2**:1583–1595.
229. Canuel C, Badre S, Groenzin H, Berheide M, Mullins OC. 2003. Diffusional fluorescence quenching of aromatic hydrocarbons. *Appl Spectrosc* **57**(5):538–544.
230. Alford PC, Cureton CG, Lampert RA, Phillips D. 1983. Fluorescence quenching of tertiary amines by halocarbons. *Chem Phys* **76**:103–109.
231. Lopez MM, Kosk-Kosicka D. 1998. Spectroscopic analysis of halothane binding to the plasma membrane Ca^{2+}-ATPase. *Biophys J* **74**: 974–980.
232. Eckenhoff RG, Tanner JW. 1998. Differential halothane binding and effects on serum albumin and myoglobin. *Biophys J* **75**:477–483.
233. Cavatorta P, Favilla R, Mazzini A. 1979. Fluorescence quenching of tryptophan and related compounds by hydrogen peroxide. *Biochim Biophys Acta* **578**:541–546.
234. Khwaja HA, Semeluk GP, Unger I. 1984. Quenching of the singlet and triplet state of benzene in condensed phase. *Can J Chem* **62**:1487–1491.
235. Washington K, Sarasua MM, Koehler LS, Koehler KA, Schultz JA, Pedersen LG, Hiskey RG. 1984. Utilization of heavy-atom effect quenching of pyrene fluorescence to determine the intramembrane distribution of halothane. *Photochem Photobiol* **40**(6):693–701.
236. Mae M, Wach A, Najbar J. 1991. Solvent effects on the fluorescence quenching of anthracene by iodide ions. *Chem Phys Lett* **176**(2): 167–172.
237. Fraiji LK, Hayes DM, Werner TC. 1992. Static and dynamic fluorescence quenching experiments for the physical chemistry laboratory. *J Chem Educ* **69**:424–428.
238. Vos R, Engelborghs Y. 1994. A fluorescence study of tryptophan–histidine interactions in the peptide alantin and in solution. *Photochem Photobiol* **60**(1):24–32.
239. Nakashima K, Tanida S, Miyamoto T, Hashimoto S. 1998. Photoinduced electron transfer from indolic compounds to 1-pyrenemethanol in polystyrene latex dispersions. *J Photochem Photobiol A: Chem* **117**:111–117.
240. Novaira AI, Avila V, Montich GG, Previtali CM. 2001. Fluorescence quenching of anthracene by indole derivatives in phospholipid bilayers. *J Photochem Photobiol B: Biol* **60**:25–31.
241. Marmé N, Knemeyer J-P, Sauer M, Wolfrum J. 2003. Inter- and Intramolecular fluorescence quenching of organic dyes by tryptophan. *Bioconjugate Chem* **14**:1122–1139.
242. Lakowicz JR, Anderson CJ. 1980. Permeability of lipid bilayers to methylmercuric chloride: quantification by fluorescence quenching of a carbazole-labeled phospholipid. *Chem–Biol Interact* **30**:309–323.
243. Holmes AS, Suhling K, Birch DJS. 1993. Fluorescence quenching by metal ions in lipid bilayers. *Biophys Chem* **48**:193–204.
244. Birch DJS, Suhling K, Holmes AS, Salthammer T, Imhof RE. 1993. Metal ion quenching of perylene fluorescence in lipid bilayers. *Pure Appl Chem* **65**(8):1687–1692.
245. Sawicki E, Stanley TW, Elbert WC. 1964. Quenchofluorometric analysis for fluoranthenic hydrocarbons in the presence of other types of aromatic hydrocarbon. *Talanta* **11**:1433–1441.
246. Dreeskamp H, Koch E, Zander M. 1975. On the fluorescence quenching of polycyclic aromatic hydrocarbons by nitromethane. *Z Naturforsch A* **30**:1311–1314.
247. Pandey S, Fletcher KA, Powell JR, McHale MER, Kauppila A-SM, Acree WE, Fetzer JC, Dai W, Harvey RG. 1997. Spectrochemical investigations of fluorescence quenching agents, 5: effect of surfactants on the ability of nitromethane to selectively quench fluorescence emission of alternant PAHs. *Spectrosc Acta Part A* **53**:165–172.
248. Pandey S, Acree WE, Cho BP, Fetzer JC. 1997. Spectroscopic properties of polycyclic aromatic compounds, 6: the nitromethane selective quenching rule visited in aqueous micellar zwitterionic surfactant solvent media. *Talanta* **44**:413–421.
249. Acree WE, Pandey S, Tucker SA. 1997. Solvent-modulated fluorescence behavior and photophysical properties of polycyclic aromatic hydrocarbons dissolved in fluid solution. *Curr Top Solution Chem* **2**:1–27.
250. Tucker SA, Acree WE, Tanga MJ, Tokita S, Hiruta K, Langhals H. 1992. Spectroscopic properties of polycyclic aromatic compounds: examination of nitromethane as a selective fluorescence quenching agent for alternant polycyclic aromatic nitrogen hetero-atom derivatives. *Appl Spectrosc* **46**(2):229–235.
251. Yang RH, Wang KM, Xiao D, Luo K, Yang XH. 2000. A renewable liquid drop sensor for di- or trinitrophenol based on fluorescence quenching of 3,3',5,5'-tetramethylbenzidine dihydrocholride. *Analyst* **125**: 877–882.
252. Wentzell PD, Nair SS, Guy RD. 2001. Three-way analysis of fluorescence spectra of polycyclic aromatic hydrocarbons with quenching by nitromethane. *Anal Chem* **73**:1408–1415.
253. Patra D, Mishra AK. 2001. Fluorescence quenching of benzo[k]fluoranthene in poly(vinyl alcohol) film: a possible optical sensor for nitro aromatic compounds. *Sens Actuators B* **80**:278–282.
254. Goodpaster JV, McGuffin VL. 2001. Fluorescence quenching as an indirect detection method for nitrated explosives. *Anal Chem* **73**: 2004–2011.
255. Ellison EH, Thomas JK. 2001. Enhanced quenching of anthracene fluorescence by nitroalkanes in zeolite X and Y. *Langmuir* **17**:2446–2454.
256. Goodpaster JV, Harrison JF, McGuffin VL. 2002. Ab initio study of selective fluorescence quenching of polycyclic aromatic hydrocarbons. *J Phys Chem A* **106**:10645–10654.

257. Koivusalo M, Alvesalo J, Virtanen JA, Somerharju P. 2004. Partitioning of pyrene-labeled phosphor- and sphingolipids between ordered and disordered bilayer domains. *Biophys J* **86**:923–935.
258. Bieri VG, Wallach DFH. 1975. Fluorescence quenching in lecithin: cholesterol liposomes by paramagnetic lipid analogues: introduction of new probe approach. *Biochim Biophys Acta* **389**:413–427.
259. Encinas MV, Lissi EA, Alvarez J. 1994. Fluorescence quenching of pyrene derivatives by nitroxides microheterogeneous systems. *Photochem Photobiol* **59**(1):30–34.
260. Matko J, Ohki K, Edidin M. 1992. Luminescence quenching by nitroxide spin labels in aqueous solution: studies on the mechanism of quenching. *Biochemistry* **31**:703–711.
261. Fayed TA, Grampp G, Landgraf M. 1999. Fluorescence quenching of aromatic hydrocarbons by nitroxide radicals: a mechanismatic study. *Int J Photoenergy* **1**:1–4.
262. Green JA, Singer LA, Parks JH. 1973. Fluorescence quenching by the stable free radical di-t-butylnitroxide. *J Chem Phys* **58**(7):2690–2659.
263. Lozinsky E, Martin VV, Berezina TA, Shames AI, Weis AL, Likhtenshtein GI. 1999. Dual fluorophore-nitroxide probes for analysis of vitamin C in biological liquids. *J Biochem Biophys Methods* **38**:29–42.
264. Kalai T, Hideg E, Jeko J, Hideg K. 2003. Synthesis of paramagnetic BODIPY dyes as new double (spin and fluorescence) sensors. *Tetrahedron Lett* **44**:8497–8499.
265. Grenier S, Dutta AK, Salesse C. 1998. Evaluation of membrane penetration depth utilizing fluorescence quenching by doxylated fatty acids. *Langmuir* **14**:4643–4649.
266. Szajdzinska-Pietek E, Wolszczak M. 1998. Quenching of excited states or pyrene derivatives by amphiphilic nitroxide radicals in cationic micellar solutions: dynamics and location of the guest molecules in the aggregates. *J Photochem Photobiol A: Chem* **112**:245–249.
267. Jones PF, Siegel S. 1971. Quenching of naphthalene luminescence by oxygen and nitric oxide. *J Chem Phys* **54**(8):3360–3366.
268. Denicola A, Batthyány C, Lissi E, Freeman BA, Rubbo H, Radi R. 2002. Diffusion of nitric oxide into low-density lipoprotein. *J Biol Chem* **277**(2):932–936.
269. Harper J, Sailor MJ. 1996. Detection of nitric oxide and nitrogen dioxide with photoluminescent porous silicon. *Anal Chem* **68**:3713–3717.
270. Denicola A, Souza JM, Radi R, Lissi E. 1996. Nitric oxide diffusion in membranes determined by fluorescence quenching. *Arch Biochem Biophys* **328**(1):208–212.
271. Ware WR, Holmes JD, Arnold DR. 1974. Exciplex photophysics, II: fluorescence quenching of substituted anthracenes by substituted 1,1-diphenylethylenes. *J Am Chem Soc* **96**:7861–7864.
272. Labianca DA, Taylor GN, Hammond GS. 1972. Structure-reactivity factors in the quenching of fluorescence from naphthalenes by conjugated dienes. *J Am Chem Soc* **94**(11):3679–3683.
273. Encinas MV, Guzman E, Lissi EA. 1983. Intramicellar aromatic hydrocarbon fluorescence quenching by olefins. *J Phys Chem* **87**: 4770–4772.
274. Abuin EB, Lissi EA. 1993. Quenching rate constants in aqueous solution: influence of the hydrophobic effect. *J Photochem Photobiol* **71**:263–267.
275. Chang SLP, Schuster DI. 1987. Fluorescence quenching of 9,10-dicyanoanthracene by dienes and alkenes. *J Phys Chem* **91**:3644–3649.
276. Eriksen J, Foote CS. 1978. Electron-transfer fluorescence quenching and exciplexes of cyano-substituted anthracenes. *J Phys Chem* **82**: 2659–2662.
277. Cioni P. 2000. Oxygen and acrylamide quenching of protein phosphorescence: correlation with protein dynamics. *Biophys Chem* **87**: 15–24.
278. Jameson DM, Gratton E, Weber G, Alpert B. 1984. Oxygen distribution and migration within $MB^{DES\ FE}$ and $HB^{DES\ FE}$. *Biophys J* **45**: 795–803.
279. Canuel C, Badre S, Groenzin H, Berheide M, Mullins OC. 2003. Diffusional fluorescence quenching of aromatic hydrocarbons. *Appl Spectrosc* **57**(5):538–544.
280. Gouterman M. 1997. Oxygen quenching of luminescence of pressure sensitive paint for wind tunnel research. *J Chem Educ* **74**(6): 697–702.
281. Camyshan SV, Gritsan NP, Korolev VV, Bazhin NM. 1990. Quenching of the luminescence of organic compounds by oxygen in glassy matrices. *Chem Phys* **142**:59–68.
282. Kikuchi K, Sato C, Watabe M, Ikeda H, Takahashi Y, Miyashi T. 1993. New aspects on fluorescence quenching by molecular oxygen. *J Am Chem Soc* **115**:5180–5184.
283. Vaughan WM, Weber G. 1970. Oxygen quenching of pyrenebutyric acid fluorescence in water: a dynamic probe of the microenvironment. *Biochemistry* **9**:464–473.
284. Abuin EB, Lissi EA. 1991. Diffusion and concentration of oxygen in microheterogeneous systems: evaluation from luminescence quenching data. *Prog React Kinet* **16**:1–33.
285. Parasassi T, Gratton E. 1992. Packing of phospholipid vesicles studies by oxygen quenching of laurdan fluorescence. *J Fluoresc* **2**(3): 167–174.
286. Lu X, Winnik MA. 2001. Luminescence quenching in polymer/filler nanocomposite films using in oxygen sensors. *Chem Mater* **13**: 3449–3463.
287. Okamoto M. 2001. Temperature dependence of the nearly diffusion-controlled fluorescence quenching by oxygen of 9,10-dimethylanthracene in liquid solution. *Phys Chem Chem Phys* **3**:3696–3700.
288. Okamoto M, Wada O, Tanaka F, Hirayama S. 2001. Fluorescence quenching by oxygen of 9,10-dimethylanthracene in liquid and supercritical carbon dioxide. *J Phys Chem* **105**:566–572.
289. Poulsen L, Zebger I, Klinger M, Eldrup M, Sommer-Larsen P, Ogilby PR. 2003. Oxygen diffusion in copolymers of ethylene and norbornene. *Macromolecules* **36**:7189–7198.
290. Brunori M, Cutruzzolà F, Savino C, Travaglini-Allocatelli C, Vallone B, Gibson QH. 1999. Structural dynamics of ligand diffusion in the protein matrix: a study on a new myoglobin mutant Y(B10) Q(E7) R(E10). *Biophys J* **76**:1259–1269.
291. Encinas MV, Lissi EA. 1983. Intramicellar quenching of 2,3-dimethylnaphthalene fluorescence by peroxides and hydroperoxides. *Photochem Photobiol* **37**(3):251–255.
292. Holmes LG, Robbins FM. 1974. Quenching of tryptophyl fluorescence in proteins by N'-methylnicotinamide chloride. *Photochem Photobiol* **19**:361–366.

293. Mao C, Tucker SA. 2002. High-performance liquid chromatographic separation of polycyclic aromatic hydrocarbons using pyridinium chloride as a selective fluorescence quencher to aid detection. *J Chromtogr A* **966**:53–61.
294. Diaz X, Abuin E, Lissi E. 2003. Quenching of BSA intrinsic fluorescence by alkylpyridinium cations its relationship to surfactant-protein association. *J Photochem Photobiol A: Chem* **155**:157–162.
295. Strom C, Hansson P, Jonsson B, Soderman O. 2000. Size of cationic surfactant micelles at the silica–water interface: a fluorescent probe study. *Langmuir* **16**:2469–2474.
296. Saha SK, Krishnamoorthy G, Dogra SK. 1999. Fluorescence quenching of 2-aminofluorene by cetylpyridinium chloride, iodide ion and acrylamide in non-ionic micelles: tweens. *J Photochem Photobiol A: Chem* **121**:191–198.
297. Martin MM, Ware WR. 1978. Fluorescence quenching of carbazole by pyridine and substituted pyridines: radiationless processes in the carbazole-amine hydrogen bonded complex. *J Phys Chem* **82**(26): 2770–2776.
298. Dreeskamp H, Laufer A, Zander M. 1983. Löschung der perylen-fluoreszenz durch Ag^{+}-ionen. *Z Naturforsch A* **38**:698–700.
299. Badley RA. 1975. The location of protein in serum lipoproteins: a fluorescence quenching study. *Biochim Biophys Acta* **379**:517–528.
300. Eftink MR, Ghiron CA. 1984. Indole fluorescence quenching studies on proteins and model systems: use of the inefficient quencher succinimide. *Biochemistry* **23**:3891–3899.
301. Razek TMA, Miller MJ, Hassan SSM, Arnold MA. 1999. Optical sensor for sulfur dioxide based on fluorescence quenching. *Talanta* **50**:491–498.
302. Moore H-PH, Raftery MA. 1980. Direct spectroscopic studies of cation translocation by *Torpedo* acetylcholine receptor on a time scale of physiological relevance. *Proc Natl Acad Sci USA* **77**(8): 4509–4513.
303. Mac M, Najbar J, Phillips D, Smith TA. 1992. Solvent dielectric relaxation properties and the external heavy atom effect in the time-resolved fluorescence quenching of anthracene by potassium iodide and potassium thiocyanate in methanol and ethanol. *J Chem Soc Faraday Trans* **88**(20):3001–3005.
304. Carrigan S, Doucette S, Jones C, Marzzacco CJ, Halpern AM. 1996. The fluorescence quenching of 5,6-benzoquinoline and its conjugate acid by Cl^{-}, Br^{-}, SCN^{-} and I^{-} ions. *J Photochem Photobiol A: Chem* **99**:29–35.
305. Horrochs AR, Kearvell A, Tickle K, Wilkinson F. 1966. Mechanism of fluorescence quenching in solution, II: quenching by xenon and intersystem crossing efficiencies. *Trans Faraday Soc* **62**:3393–3399.
306. Thulborn KR, Sawyer WH. 1978. Properties and the locations of a set of fluorescent probes sensitive to the fluidity gradient of the lipid bilayer. *Biochim Biophys Acta* **511**:125–140.
307. Ware WR, Andre JC. 1980. The influence of diffusion fluorescence quenching. In *Time-resolved fluorescence spectroscopy in biochemistry and biology*, pp. 363–392. Ed RB Cundall, R Dale. Plenum Press, New York.
308. Nelson G, Warner IM. 1990. Fluorescence quenching studies of cyclodextrin complexes of pyrene and naphthalene in the presence of alcohols. *J Phys Chem* **94**:576–581.
309. Peviani C, Hillen W, Ettner N, Lami H, Doglia SM, Piemont E, Ellouze C, Chabbert M. 1995. Spectroscopic investigation of tet repressor tryptophan-43 upon specific and nonspecific DNA binding. *Biochemistry* **34**:13007–13015.

PROBLEMS

P8.1. *Interpretation of Apparent Bimolecular Quenching Constants*: Calculate the apparent bimolecular quenching constant of 2-anthroyloxypalmitate (2-AP) for quenching by copper or dimethylaniline (Figure 8.71). Assume the unquenched lifetime is 10 ns. Interpret these values with respect to the maximum value of k_q possible in aqueous solution.

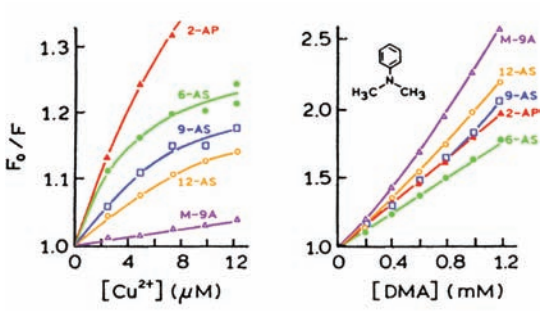

Figure 8.71. Quenching of the anthroyloxy probes by a water-soluble quencher, Cu^{2+}, and by a lipid-soluble quencher, dimethylaniline (DMA). Revised and reprinted from [306]. Copyright © 1978, Elsevier Science.

P8.2. *Oxygen Bimolecular Quenching Constant in a Membrane*: Use the data in Figure 8.72 to calculate k_q for oxygen quenching of pyrene in DMPC vesicles.

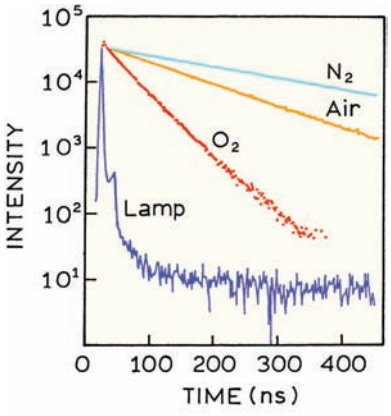

Figure 8.72. Intensity decays of pyrene in dimyristoyl phosphatidylcholine (DMPC) vesicles at 25°C, equilibrated with various partial pressure of oxygen. Revised and reprinted with permission from [58]. Copyright © 1975, Rockefeller University Press.

P8.3. *Quenching in the Presence of Cyclodextrins*: Figure 8.73 shows iodide quenching of naphthalene with 3 mM β-cyclodextrin. Figure 8.74 shows iodide quenching of naphthalene with 1% v/v benzyl alcohol with increasing amounts of β-CD. Assume the unquenched lifetime of naphthalene is 45 ns. Explain the results.

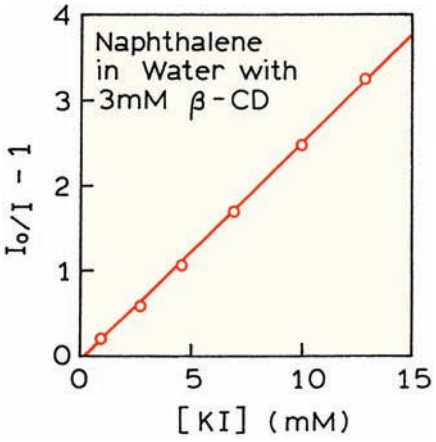

Figure 8.73. Quenching of naphthalene by iodide in the presence of 3.00 mM β-cyclodextrin. Revised and reprinted with permission from [308]. Copyright © 1990, American Chemical Society.

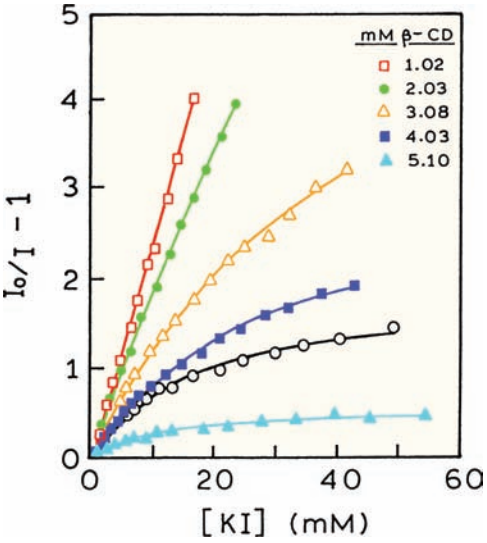

Figure 8.74. Quenching of naphthalene by iodide in the presence of benzyl alcohol (1% V/V) at various η-CD concentrations. Revised and reprinted with permission from [308]. Copyright © 1990, American Chemical Society.

P8.4. *Separation of Static and Dynamic Quenching of Acridone by Iodide*:[176] The following data were obtained for quenching of acridone in water at 26C° KNO_2 is used to maintain a constant ionic strength, and does not quench the fluorescence of acridone.

M KI	M KNO_2	F_0/F
0.0	1.10	1.0
0.04	1.06	4.64
0.10	1.00	10.59
0.20	0.90	23.0
0.30	0.80	37.2
0.50	0.60	68.6
0.80	0.30	137.0

A. Construct a Stern-Volmer plot.
B. Determine the dynamic (K_D) and static (K_S) quenching constants. Use the quadratic equation to obtain K_D and K_S from the slope and intercept of a plot of K_{app} versus [Q].
C. Calculate the observed bimolecular quenching constant. The unquenched lifetime τ_0 = 17.6 ns.
D. Calculate the diffusion limited bimolecular quenching constant, and the quenching efficiency. The diffusion constant of KI in water is 2.065 x 10^{-5} cm^2/s for 1 M KI (*Handbook of Chemistry and Physics*, 55th Edition).
E. Comment on the magnitude of the sphere of action and the static quenching constant, with regard to the nature of the complex.

P8.5. *Separation of Static and Dynamic Quenching*: The following table lists the fluorescence lifetimes and relative quantum yield of 10-methylacridinium chloride (MAC) in the presence of adenosine monophosphate (AMP).[18]

[AMP] (mM)	τ (ns)	Intensity
0	32.9	1.0
1.75	26.0	0.714
3.50	21.9	0.556
5.25	18.9	0.426
7.00	17.0	0.333

A. Is the quenching dynamic, static, or both?
B. What is (are) the quenching constant(s)?
C. What is the association constant for MAC-AMP complex?
D. Comment on the magnitude of the static quenching constant.
E. Assume the MAC–AMP complex is completely nonfluorescent, and complex formation shifts the absorption spectrum of MAC. Will the corrected excitation spectrum of MAC, in the presence of nonsaturating amounts of AMP, be comparable to the absorption spectrum of MAC or the MAC-AMP complex?

P8.6. *Effects of Dissolved Oxygen on Fluorescence Intensities and Lifetimes*: Oxygen is known to dissolve in aqueous and organic solutions, and is a collisional quencher of fluorescence. Assume your measurements are accurate to 3%. What are the lifetimes above which dissolved oxygen from the atmosphere will result in changes in the fluorescence intensities or lifetimes that are outside your accuracy limits? Indicate these lifetimes for both aqueous and ethanolic solutions. The oxygen solubility in water is 0.001275 M for a partial pressure of one atmosphere. Oxygen is fivefold more soluble in ethanol than in water. The following information is needed to answer this question:

k_q (in water) = 1 x 10^{10} M^{-1} s^{-1}

k_q (in ethanol) = 2 x 10^{10} M^{-1} s^{-1}

P8.7. *Intramolecular Complex Formation by Flavin-Adenine Dinucleotide (FAD)*: FAD fluorescence is quenched by both static complex formation between the flavin and adenine rings, and by collisions between these two moieties. Flavin mononucleotide (FMN) is similar to FAD except that it lacks the adenine ring. Use the following data for FAD and FMN to calculate the fraction complexed (f) and the collisional deactivation rate (k) of the flavin by the adenine ring. Q is the relative quantum yield. Note that the deactivation rate is in s^{-1}:

τ (FMN) = 4.6 ns

τ (FAD) = 2.4 ns

Q (FMN) = 1.0 (assumed unity)

Q (FAD) = 0.09

P8.8. *Quenching of Protein Fluorescence: Determination of the Fraction of the Total Fluorescence Accessible to Iodide*: Assume a protein contains four identical subunits, each containing two tryptophan residues. The following data are obtained in the presence of iodide.

[I^-] M	Fluorescence intensity
0.00	1.0
0.01	0.926
0.03	0.828
0.05	0.767
0.10	0.682
0.20	0.611
0.40	0.563

A. What fraction of the total tryptophan fluorescence is accessible to quenching? Which property of the Stern-Volmer plots does indicate an inaccessible fraction?

B. Assume all the tryptophans have equal quantum yields and lifetimes (5 ns). How many tryptophan residues are accessible to quenching?

C. What are the bimolecular quenching constants for the accessible and inaccessible residues?

D. Assume you could selectively excite the accessible tryptophans by excitation at 300 nm. Draw the predicted Stern-Volmer and modified Stern-Volmer plots for the accessible and the inaccessible residues.

P8.9. *Quenching of Endonuclease III*: Figure 8.75 shows the effect of a 19-mer of poly(dAdT) on the intrinsic tryptophan emission of Endo III. Explain the data in terms of the structure of Endo III (Figure 8.15). Is it the quenching collisional or static? Assume the unquenched decay time is 5 ns. The concentration of Endo III is 0.8 µm.

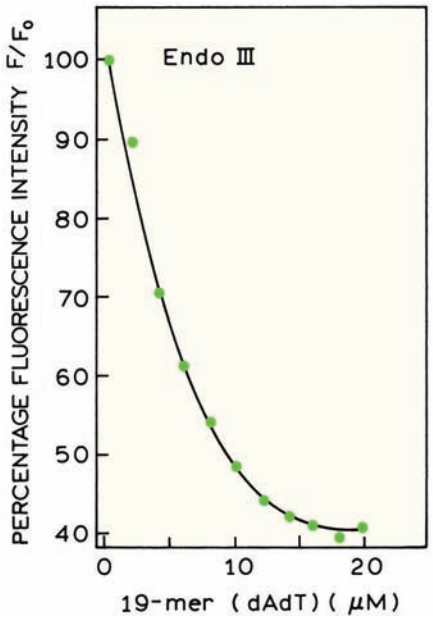

Figure 8.75. Fluorescence intensity of Endo III with increasing concentrations of a 19-mer of poly(dAdT). Revised and reprinted with permission from [42]. Copyright © 1995, American Chemical Society.

P8.10. *Quenching of the Tet Repressor F75*: Figure 8.76 shows the emission spectra of the W75F mutant of the tet repressor in the absence and presence of bound operator. Explain the extent of quenching. Predict the extent of quenching for the wild-type protein.

P8.11. *Intramolecular Quenching*: Figure 8.67 showed intensity decay data for DBO with a quencher collision rate of 9 x 10^6 s^{-1}. Calculate the decrease in DBO intensity due to guanine quenching. Also calculate the relative intensity (F/F_0) expected for a fluorophore with a lifetime of 2 ns or 2 ms.

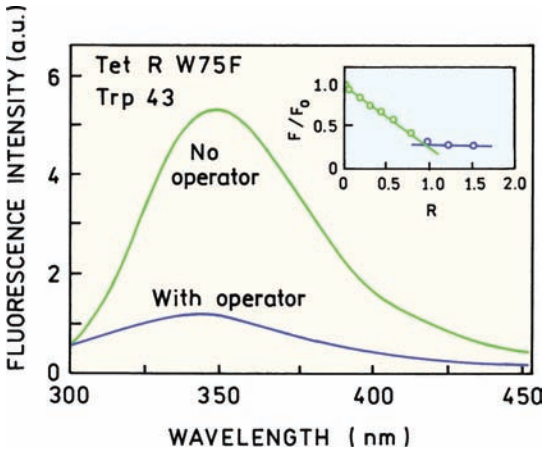

Figure 8.76. Emission spectra of Trp 43 in tet repressor W75F in the absence and presence of a 76-bp operator. In the insert the concentration of Tet R dimer is 1 μM and the ratio refers to the molar ratio of operator to dimer. Revised and reprinted with permission from [309]. Copyright © 1995, American Chemical Society.